

**HUNTINGTON'S DISEASE STUDIES AT THE INTERFACE OF CHEMISTRY,
PHYSICS, AND BIOLOGY**

by

Kenneth W Drombosky Jr

B.S. in Biochemistry, Duquesne University, 2011

Submitted to the Graduate Faculty of
the School of Medicine in partial fulfillment
of the requirements for the degree of
PhD in Molecular Pharmacology

University of Pittsburgh

2016

UNIVERSITY OF PITTSBURGH

SCHOOL OF MEDICINE

This dissertation was presented

by

Kenneth W Drombosky Jr

It was defended on

March 14, 2016

and approved by

Michael Palladino, PhD, Professor

Donald DeFranco, PhD, Professor

Tija Jacob, PhD, Assistant Professor

Patrick Thibodeau, PhD, Assistant Professor

Dissertation Advisor: Ron Wetzel, PhD, Professor

Copyright © by Kenneth W Drombosky Jr

2016

HUNTINGTON'S DISEASE STUDIES AT THE INTERFACE OF CHEMISTRY, PHYSICS, AND BIOLOGY

Kenneth W Drombosky, PhD

University of Pittsburgh, 2016

Huntington's disease (HD) is a uniformly fatal genetic disease causing progressive degeneration of the central nervous system in approximately 250,000 people worldwide. Unlike other neurodegenerative diseases, such as Alzheimer's and Parkinson's disease, HD is explicitly caused by a single genetic defect – a CAG codon expansion in the *huntingtin* gene, which codes for polyglutamine (polyQ) in the protein huntingtin (htt). People carrying 40 or more CAG/glutamine repeats will develop HD by early adulthood, while those with 36 or less are unaffected. Despite this discovery over two decades ago, there are still no treatments to cure, prevent, or delay the underlying progression of HD.

The physical state of the huntingtin “exon1” fragment responsible for triggering HD pathology (amyloid aggregates, non- β oligomers, or monomers) is a controversial roadblock that limits therapeutic discovery. Previous attempts to determine the toxic species have recently been identified as flawed or inconclusive. Herein, we describe mutated htt-exon1 analogs containing only 22-24 glutamine residues that deliver atypical aggregation: a “hyper-amyloid” analog that – despite its short glutamine repeat lengths – aggregates into amyloid fibrils comparable to pathogenic huntingtin, and “hypo-amyloid” analogs whose aggregation stops at the non- β oligomer stage. Hyper-amyloid htt-exon1 produces inclusions, cytotoxicity in rat neurons, and decreased lifespans with movement deficits in flies. Neurons and flies expressing hypo-amyloid

htt-exon1 alone have no detectable HD phenotype. Our data strongly supports a toxic amyloid hypothesis, and we find no evidence of a toxic non- β oligomer.

Furthermore, the non-toxic hypo-amyloid analogs are also able to inhibit amyloid formation of pathogenic repeat length htt-exon1. Co-expression of hypo-amyloid htt-exon1 with pathogenic htt-exon1 reduces aggregation *in vitro*, inhibits toxicity in neuron cultures, and rescues behavioral and lifespan HD phenotypes in flies. These exciting results offer novel, rationally designed approaches to HD therapeutics.

TABLE OF CONTENTS

LIST OF ABBREVIATIONS	XV
ACKNOWLEDGEMENTS	XVII
1.0 INTRODUCTION.....	1
1.1 AMYLOID DISEASES.....	1
1.2 HUNTINGTON'S DISEASE.....	3
1.3 MECHANISM OF MUTANT HUNTINGTIN TOXICITY.....	7
1.3.1 Biological Function of Wild Type Huntingtin.....	7
1.3.2 The Toxic Amyloid Hypothesis.....	9
1.3.3 The Toxic Oligomer Hypotheses.....	12
1.3.4 The Toxic Monomer Hypothesis.....	14
1.3.5 Alternative Hypotheses.....	16
1.4 POLYGLUTAMINE REPEAT DISORDERS	17
1.4.1 DNA Repeat Diseases.....	17
1.4.2 Polyglutamine Repeat Disorders	19
1.4.3 Simple Polyglutamine Models.....	21
1.4.3.1 Rationale for Simple PolyQ Models.....	21
1.4.3.2 Simple PolyQ as a Model	22
1.4.4 Role of the Huntingtin N-Terminus in Aggregation.....	24

1.4.5	Role of the Huntingtin C-Terminus in Aggregation	27
1.4.6	Huntingtin Exon1 and Full Length Huntingtin as models	27
1.4.7	Role of β -hairpin Structure in Nucleation	29
1.5	MODEL SYSTEMS OF HUNTINGTON'S DISEASE	32
1.5.1	Monitoring Polyglutamine Aggregation <i>in vitro</i>	32
1.5.2	<i>In vivo</i> Models.....	33
1.5.2.1	Cell Culture Models.....	33
1.5.2.2	Primary Neurons	34
1.5.2.3	<i>Drosophila</i> as a tool to study neurodegeneration.....	35
1.5.2.4	Other animal models of Huntington's Disease.....	37
1.6	CURRENT THERAPEUTIC APPROACHES	38
1.6.1	Small Molecular inhibitors of polyglutamine aggregation.....	38
1.6.2	Small Molecules to Target Biological Pathways.....	40
1.6.3	Huntingtin Lowering Strategies.....	42
1.6.4	Peptide Based Inhibitors of Aggregation	44
1.7	MATERIALS AND METHODS.....	47
2.0	THE ROLE OF BETA-STRUCTURE IN NUCLEATION AND AGGREGATION OF HUNTINGTIN	51
2.1	INTRODUCTION	51
2.2	RESULTS.....	54
2.2.1	Design of a β -hairpin peptide compatible with htt-exon1	54
2.2.2	β -hairpin enhanced huntingtin fragments aggregate through a htt ^{NT} -mediated mechanism.....	64

2.2.3	htt ^{NT} Q ₂₂ P ₁₀ K ₂ -βHP seeds can recruit huntingtin into amyloid fibrils	68
2.3	DISCUSSION.....	69
3.0	DESIGNING HUNTINGTIN AMYLOID INHIBITORS THAT STOP HUNTINGTIN AGGREGATION AT NON-BETA OLIGOMERS.....	73
3.1	INTRODUCTION.....	73
3.2	RESULTS.....	76
3.2.1	Rational design of a competitive peptide-based inhibitor of nucleation ...	76
3.2.2	Glutamine to Proline substitutions block amyloidogenesis.....	78
3.2.3	Hypo-Amyloid huntingtin analogs as proof-of-principal polyQ aggregation inhibitors.....	81
3.3	DISCUSSION.....	86
4.0	VALIDATING & TRANSLATING BIOPHYSICAL OBSERVATIONS IN CELL MODELS.....	90
4.1	INTRODUCTION.....	90
4.2	RESULTS.....	92
4.2.1	Transient Transfection of the β-Hairpin Enhanced htt Analogs in PC12 cells	92
4.2.2	β-Hairpin Enhanced Huntingtin Analogs are toxic in primary rat cortical neurons. Oligomeric huntingtin analogs are well tolerated and rescue htt-ex1-Q ₄ associated toxicity.....	95
4.3	DISCUSSION.....	103
5.0	<i>DROSOPHILA</i> AS A MODEL OF NEURODEGENERATION.....	107
5.1	INTRODUCTION.....	107

5.2	RESULTS	108
5.2.1	Constructing a <i>Drosophila</i> HD model	108
5.2.2	Hyper-amyloid huntingtin analogs, and not hypo-amyloid analogs, have locomotor and lifespan defects.....	112
5.2.3	Hypo-amyloid huntingtin analogs rescue htt-ex1-Q ₉₄ associated toxicity	115
5.3	DISCUSSION	117
6.0	CONCLUSIONS	122
6.1	EVIDENCE SUPPORTING A BETA-STRUCTURED AMYLOID HUNTINGTIN TOXIC SPECIES	122
6.2	EVIDENCE SUPPORTING A SOLUBLE NON-BETA, NON-AMYLOID HUNTINGTIN TOXIC SPECIES	125
6.3	THE POTENTIAL OF TARGETING AGGREGATION FOR DISEASE-MODIFYING THERAPIES	128
	BIBLIOGRAPHY	133

LIST OF TABLES

Table 1: Protein Sequences described in this study	xx
--	----

LIST OF FIGURES

Figure 1: Sedimentation Analysis of Simple PolyQ Peptides.	57
Figure 2: Concentration Dependence of Aggregation for the β HP peptide.....	60
Figure 3: Time Squared Plot of β HP Aggregation..	60
Figure 4: Log-Log Plot of Simple PolyQ and htt-ex1 ^{P10} peptides.....	61
Figure 5: FTIR Traces of Simple PolyQ Peptides..	63
Figure 6: Electron Microscopy Images of Simple PolyQ Peptides.	63
Figure 7: Sedimentation Analysis of htt-ex1 ^{P10} Peptides.	65
Figure 8: FTIR Traces of htt-ex1 ^{P10} Peptides.	65
Figure 9: Electron Microscopy Images of htt-ex1 ^{P10} Peptides.	66
Figure 10: Circular Dichroism Traces of the htt-ex1 ^{P10} - β HP Peptide.	67
Figure 11: Overlay of Circular Dichroism and Sedimentation Analysis Kinetics for htt-ex1 ^{P10} - β HP..	68
Figure 12: Seeded Elongation of htt-ex1 ^{P10} -Q ₂₅	69
Figure 13: Sedimentation Analysis of Hypo-Amyloid Peptides.	78
Figure 14: Sedimentation Analysis of htt-ex1 ^{P10} Hypo-Amyloid Peptides	79
Figure 15: Circular Dichroism Traces of htt-ex1 ^{P10} - β HP-P ²	80
Figure 16: Electron Microscopy Images of Hypo-Amyloid htt-ex1 ^{P10} Peptides.....	80

Figure 17: Sedimentation Analysis of Hypo-Amyloid Inhibition 10:20.	82
Figure 18: Sedimentation Analysis of Hypo-Amyloid Inhibition 10:10.	82
Figure 19: Sedimentation Analysis of Hypo-Amyloid Inhibition 10:5.	83
Figure 20: Electron Microscopy Images of the Hypo-Amyloid Inhibited Reaction.	83
Figure 21: Co-Aggregation of the Hypo-Amyloid Peptides with its target htt-ex1 ^{P10} -Q ₃₇	84
Figure 22: Lack of Inhibition or Co-Aggregation Between without htt ^{NT}	85
Figure 23: Stronger β HP Motifs Correlate with Stronger Inhibition.	86
Figure 24: Percentage of PC12 Cells with Visible Puncta.	93
Figure 25: Percentage of Expressing Neurons Positive for Puncta.	97
Figure 26: Representative confocal images from Figure 25 used in puncta quantification.	98
Figure 27: Viability of Neurons at DIV14.	100
Figure 28: Viability of Neurons at DIV21.	101
Figure 29: Example Line Trace Between htt-ex1-Q ₉₄ -EGFP and mCherry.	102
Figure 30: Example Line Trace Between htt-ex1-Q ₉₄ -EGFP and htt-ex1- β HP-P ² -mCherry.	103
Figure 31: Rapid Iterative Negative Geotaxis (RING) Assay Testing Locomotor Function.	113
Figure 32: Lifespan Analysis of <i>Drosophila</i> . Survival curves of flies aged at 29 °C after eclosion.	114
Figure 33: Lifespan Rescue Analysis of Rescue HD <i>Drosophila</i>	116
Figure 34: Locomotor Rescue of Rescue HD <i>Drosophila</i>	117

LIST OF SCHEMES

Scheme 1: General Aggregation Mechanisms of Huntingtin	xix
Scheme 2: <i>Drosophila</i> mating scheme	111
Scheme 3: Representation of the Toxic Species of Huntingtin	128

EQUATIONS

Equation 1: Eaton-Ferrone Kinetics Model of Nucleation	23
Equation 2: Eaton-Ferrone Simple PolyQ Nucleation Model	57
Equation 3: t^2 Plot	58
Equation 4: log-log Plot	59

LIST OF ABBREVIATIONS

Abbreviations

HD – Huntington’s Disease

htt – Huntingtin (protein)

mhtt – mutant Huntingtin (protein)

htt-ex1 – Huntingtin exon 1

htt^{NT} – Huntingtin N-Terminal 17 amino acids

N17 – Huntingtin N-Terminal 17 amino acids

polyQ - polyglutamine

SCA – Spinocerebellar Ataxia

SBMA - Spinal Bulbar Muscular Atrophy

DRPLA - dentatorubral pallidoluysia natrophy

CNS – Central Nervous System

CD – Circular Dichroism

FTIR – Fouriter Transform Infrared Red Spectroscopy

ATM – Atomic Force Microscopy

EM – Electron Microscopy

NGF – Neuron Growth Factor

RING - Rapid Negative Geotaxis Assay

DM1 – myotonic dystrophy type 1

DM2 – myotonic dystrophy type 2

FXS – Fragile X Syndrome

ACKNOWLEDGEMENTS

Ron Wetzel for countless meetings, discussions, emails, and for all of your patience and mentorship through my graduate career.

Thesis Committee:

Michael Palladino, Don DeFranco, Tija Jacob, and Patrick Thibodeau for their thoughtful discussions, patience, and guidance.

Ron Wetzel Lab:

Sascha Rode – For your tireless work in driving the *in vitro* section and for numerous discussions about project ideas and directions.

Karunakar Kar – Whose original work in β -hairpin architecture inspired this work, for your technical expertise and training in many of the structural biology instruments needed for this project, and for your words of wisdom.

Irene Arduini – For having the patience to mentor me in cell culture, microscopy, and getting started on the biological side of this work.

Ravi Kodali – For general discussions about this work and for technical assistance with FTIR and EM.

Drosophila collaboration:

Michael Palladino – For graciously welcoming me into his lab, spending significant amounts of time in helping with project design, and for teaching me about the *Drosophila* animal model.

Bart Roland – For technical assistance and always being around to discuss findings.

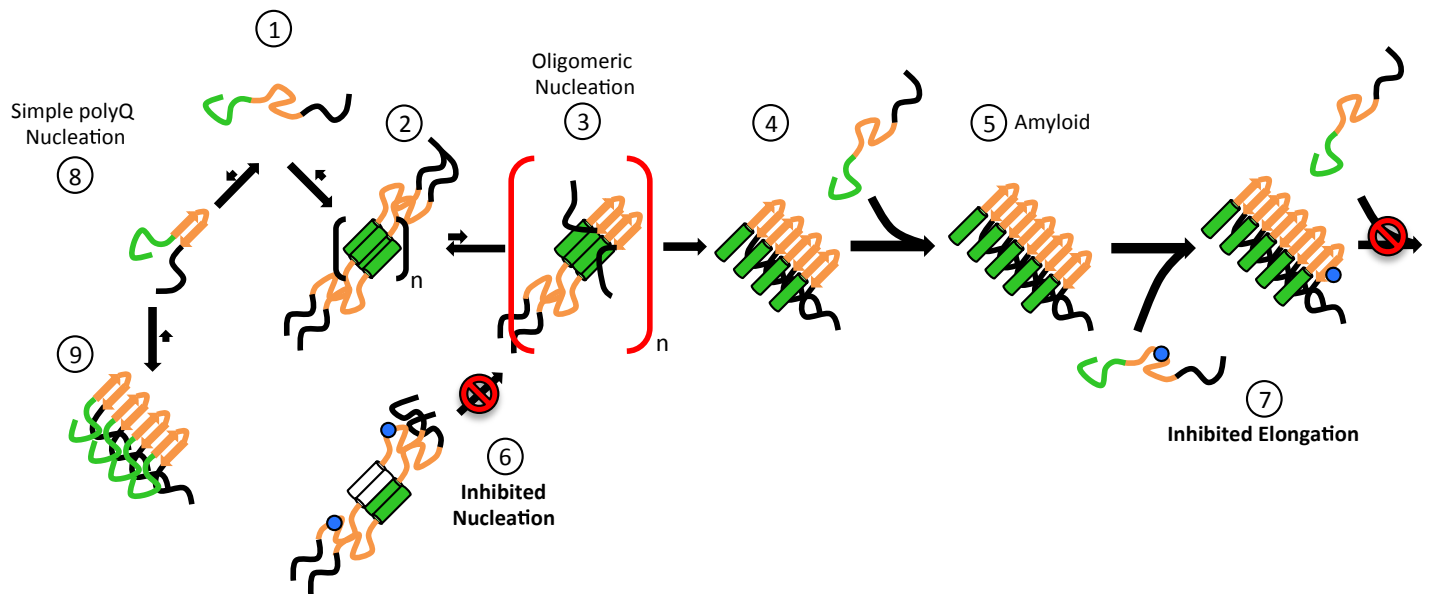
Atif Towheed – For technical assistance and for convincing me that *Drosophila* was an excellent model system for this project.

Primary neuron collaboration:

Tija Jacob – For graciously welcoming me into her lab, personal mentorship, and teaching me how to design and drive data using primary neuron models.

Megan Brady & Nick Graff – for their technical assistance in preparing rat primary neurons, for helping teach me proper primary neuron culture, and for being patient as I learned in their laboratory.

To the PIND, Pharmacology, and Structural Biology departments, which helped foster a collaborative project.



Scheme 1: General Aggregation Mechanisms of Huntingtin. (1) Htt-ex1 monomers are composed of three intrinsically disordered segments (htt^{NT} , green; polyQ, orange; proline rich domain, black) that are capable of two distinct, but similar amyloid nucleation pathways. The first pathway follows a two-step process, where the first step is the rate limiting nucleation of aggregation *via* an inter- or intra-molecular rearrangement of polyQ into a critical nucleus structure (8), which is able to initiate rapid elongation of amyloid *via* monomer additions to the growing fibril (9). Alternatively, and if htt -ex1 has a functional htt^{NT} domain, htt -ex1 monomers can self-assemble into α -helical rich bundle formations (2). In the oligomeric phase, the local concentration of polyQ is artificially increased, accelerating nucleation of aggregation (3) to generate β -sheet rich fibril formation (4) that elongates *via* monomer addition (5). One strategy to limit nucleation is the initial presence of htt^{NT} -containing peptides, which can compete for initial oligomer formation and limit the artificial increase in local polyQ concentration (6). Alternatively, the elongation mechanisms of aggregation can be inhibited with Pro-interrupted polyQ tracts that can add to htt -ex1 fibrils and block further additions (7).

1.0 INTRODUCTION

1.1 AMYLOID DISEASES

Protein misfolding, particularly protein misfolding into β -sheet rich amyloid, is increasingly being recognized as a hallmark of over 50 diseases ¹, many of which are becoming more common as the average life expectancy increases ² and as the obesity endemic leads to new cases of type II diabetes ³. A number of metastable proteins that are prone to misfolding into amyloid also have neurodegenerative phenotypes. Alzheimer's disease involves the aggregation of the amyloid- β peptide, which is a cleavage product of the amyloid precursor protein (APP), into β -sheet rich amyloid plaques ⁴. In Parkinson's disease, α -synuclein forms insoluble fibrils to form molecular pathologies characterized by Lewy bodies ⁵. Huntingtin and other expanded polyglutamine-containing proteins also aggregate into amyloid fibrils *in vitro* ⁶, in model organisms ⁷, and in human brains ⁸. Although less prevalent in humans, the conversion of α -helical rich prion protein (PrP^C) into insoluble β -structured PrP^{Sc} to cause spongiform encephalopathies is a classical example of infectious proteinopathy ^{9,10}.

Amyloid diseases are not restricted to simply the CNS and neurodegeneration, but can affect the entire body. Immunoglobulin light chain can aggregate into amyloid causing amyloid light chain amyloidosis, a condition typically affecting the heart ¹¹. In type II diabetes, increased cosecretion of insulin and pro-IAPP results in granule formation that can seed aggregation of

IAPP (amylin)¹². This process may be partially responsible for the loss of islet β -cells in type II diabetes¹².

Of the amyloid associated diseases, prion diseases are currently the only protein misfolding disease labeled as infectious. There are a number of documented cases supporting the spread of prion, such as in the disease Kuru, where transmission of the infectious prion particle is passed through ritualistic cannibalism¹³. Similarly, Creutzfeldt-Jakob disease can be acquired by the ingestion of contaminated meat containing scrapie prions¹⁴⁻¹⁷ or by blood transfusions with affected patients¹⁸. This transmissible phenotype between humans has not been documented for HD or other neurodegenerative diseases, but recent work suggests that infectivity may be possible: patients treated with pituitary-derived growth hormone contaminated with A β seeds were recently identified as being significantly more likely to develop vascular A β pathology typical of early onset Alzheimer's disease¹⁹. Indeed, because of the recurring similarities between prions and protein misfolding diseases in neurodegeneration, many neurodegenerative diseases are being reinvestigated as being potentially prion-like in their mechanisms of transmission and toxicity. Although the misfolded protein in many of these diseases has been clearly identified, the mechanism by which amyloid generates toxicity is unclear. The primary sequences and cellular roles between different amyloid causing diseases are distinct from one other, with the only commonality being their inherent capacity to aggregate into insoluble amyloid, which involves a cross β -sheet quaternary structure and a dehydrated hydrophobic core^{20,21}. Cross seeding of amyloid structure between different proteins is possible, but requires sufficient primary sequence and structural homology between the seed and the soluble protein. For example, amyloid proteins that are too dissimilar, such as IAPP relative to A β , show poor cross seeding²².

Because of these striking similarities between amyloid formation and toxicity, many researchers have proposed a common toxic amyloid hypothesis, though some evidence may also point to other aggregated protein conformations or a misfolded toxic monomer (Section 1.3). Isolating the monomeric, oligomeric, and amyloid species of these proteins and identifying their individual toxic contribution is not yet technologically feasible, due to such factors as the tendency of the metastable monomeric and oligomeric forms to ultimately transition to a thermodynamically stable amyloid, and the challenge of detecting and quantifying various aggregates states *in vivo* in real time.

1.2 HUNTINGTON'S DISEASE

George Huntington first described Huntington's disease (HD) in detail in 1872²³. It wasn't until 1993 that the affected gene, huntingtin, was found at chromosome 4p16.3²⁴. Therefore, unlike Alzheimer's disease, Parkinson's disease, Amyotrophic Lateral Sclerosis and several other neurodegenerative diseases, HD is a monogenetic disorder. This makes diagnosis, prediction of disease progression, the generation of model organisms, and many other clinical aspects of HD relatively less difficult compared to AD and other neurodegenerative diseases. HD, which affects approximately 1 in 7,300 people in Western populations²⁵, is therefore a prime candidate to model both neurodegeneration as well as amyloid diseases as a whole.

In unaffected persons, the huntingtin gene *HTT* contains a variable CAG repeat domain of 6-35 repeats. CAG repeats of 36-39 coincide with a potential risk of developing HD, while CAG repeats ≥ 40 are highly penetrant. The CAG codon repeat is unstable and prone to expansion, particularly during meiotic transmission whose instability increases with increasing

CAG repeat length ²⁶. Therefore, parents with 35-39 CAG repeats that do not experience HD may pass on a fully penetrant copy of *HTT* to their offspring. CAG repeats above 40 correlate with earlier onset of disease and more severe symptoms ²⁶. A single copy of the mutant *HTT* gene is sufficient to cause HD, though it is unclear if a second copy of mutant *HTT* worsens disease. This autosomal dominant inheritance pattern suggests a toxic gain-of-function disease, as opposed to other recessive loss-of-function monogenetic diseases, such as Cystic Fibrosis or Fragile X Syndrome ²⁷⁻²⁹. The nature of how huntingtin gains toxic function, potentially through a conformational change in the protein, is discussed in greater detail in Section 1.3.

HD patients experience a number of locomotor, cognitive, and behavioral defects affecting the CNS, as well as the entire body, that categorically progresses with age. Onset and clinical diagnosis of HD typically occurs in adulthood, where latent pre-manifest and prodromal symptoms become more pronounced. Following clinical diagnosis and the onset of locomotor dysfunction, progression of the disease is uniformly fatal with a median survival of 18 years after initial motor impairment ³⁰. Core symptoms of HD include, most notably, a progressive degeneration of locomotor control leading to spastic movements termed chorea, cognitive impairment, and behavioral abnormalities. MRI and CT scans confirm progressive neurodegeneration evident by striatal atrophy, particularly medium GABAergic neurons of the striatum, as well as atrophy in the cortex, caudate, and basal ganglia ^{31,32}. For reasons that are not yet clear, the cerebellum and brain stem are relatively spared. This can be partially explained by the differential expression levels of mhtt in different brain regions, differing vulnerabilities between varying neuronal populations, or altered binding partners between different cell types. For example, the striatal-enriched GTPase Rhes is thought to bind to and SUMOylate mhtt,

altering its toxicity. Ectopic expression of GTPase Rhes in the cerebellum of HD mice leads to loss of balance, caspase 3 activation, and lesions within the cerebellum³³.

The *HTT* gene encodes a 3,144 amino acid protein whose wild type function is largely unknown. A smaller fragment of huntingtin, htt-exon1, is produced through a number of proteolytic cleavage events³⁴ or by alternative splicing^{35,36}. Htt-exon1 is approximately 100 amino acids long and contains three sequence domains: the huntingtin N-terminus (htt^{NT}) of 17 amino acids, a CAG repeat polyQ segment of variable length, and a 51 amino acid proline rich domain (PRD). Expression of polyQ-expanded htt-exon1 fragment is both sufficient and necessary to cause HD-like phenotypes in model organisms⁷. However, the mechanistic details of how a polyQ-expanded htt-exon1 causes disease is highly debated. Neither the molecular form of htt that causes toxicity, nor its primary cellular targets leading to HD symptoms, are known with certainty. Monomeric, oligomeric, and amyloid protein conformations have all been proposed as toxic species and are discussed in more detail in Section 1.3.1 through 1.3.4.

Oligomer formation of htt-exon1 is visible biochemically by separation in SDS-free gels with large pore sizes, such as Agarose Gel Electrophoresis for Resolving Aggregates (AGERA)³⁷, by microscopy methods such as fluorescence correlation spectroscopy (Sahoo 2016 Manuscript Submitted), by biophysical methods such as analytical ultracentrifugation (AUC)³⁸, and by electron microscopy³⁹. Conversely, large aggregates with fibrillary substructures formed by expanded polyQ versions of huntingtin are evident *in vitro*⁶, in model organisms⁷, and in HD patient brain tissues⁴⁰. These aggregates can range from >100,000,000 molecule conglomerates⁴¹ to the more recently identified smaller aggregates of <100,000 huntingtin fragments⁴²⁻⁴⁴. Mirroring the polyQ repeat length threshold of disease in humans, longer polyQ repeat lengths *in vitro* correlate with more efficient nucleation of aggregation and faster overall kinetics to

amyloid formation ⁴⁵. Indeed, the idea of prion-like transmission and propagation of amyloid aggregates *in vivo* is gaining favorability. Mature polyQ amyloid aggregates are capable of seeding the aggregation of other metastable polyQ-containing proteins. This is reminiscent of prion diseases, and may include a cell-to-cell infectious remission, also seen in prion disease ⁴⁶. Additional evidence in favor of a toxic amyloid is the toxicity associated with delivering preformed polyQ aggregates to mammalian cells in culture ⁴⁷.

Molecular pathogenesis of huntingtin includes a myriad of dysfunctional biochemical pathways, some of which are tied to the proposed functions of wild type huntingtin, including: ER stress ⁴⁸, changes in basal chaperone function ⁴⁹, changes in chromatin architecture ⁵⁰, alterations in the ubiquitin-proteasome system ⁵¹, autophagy dysregulation ⁵², transcriptional anomalies ⁵³, mitochondrial impairment ^{54,55}, synaptic dysfunction ⁵⁶, and many others. Additionally, huntingtin shuttles between the cytoplasm and the nucleus, serves a role in the development of the CNS, influences the release of brain-derived neurotrophic factor (BDNF), and potentially has a wild type role in autophagy ⁵⁷, all of which may be linked to a potential loss-of-function pathogenesis as huntingtin is sequestered into insoluble amyloid. The roles of these pathways and their contribution to disease progression – whether they are symptoms or primary drivers of disease – is unknown. Nevertheless, these pathways represent some of the better candidates for potential disease modifying drug interventions, discussed in Section 1.6. Despite intense efforts, there are no treatments to slow or prevent disease progression.

Because of HD's monogenetic nature, there are several well-defined clinical outcomes, including qualitative rating scales such as the Unified Huntington's Disease Rating Scale (UHDRS) and biochemical assays to monitor brain-specific proteins in the CNS, such as soluble huntingtin or cytokines ^{58,59}. Neuroimaging *via* structural MRI can sensitively measure caudate

atrophy and give feedback on how drug interventions may delay brain atrophy on a relatively short timescale of 6-18 months^{31,32}. A combination of the monogenetic nature of the disease, research into the mechanism of amyloid aggregation, identification of key pathways involved in the cellular response to mhtt, and well-defined clinical outcomes will hopefully accelerate future drug discovery.

1.3 MECHANISM OF MUTANT HUNTINGTIN TOXICITY

1.3.1 Biological Function of Wild Type Huntingtin

The huntingtin gene *HTT*, like several of the polyQ-expanded diseases, is largely known for its role in causing disease and is sparsely studied for its wild type function. Wild type huntingtin, as well as several of the other polyQ-expanded proteins, does not have a well-defined cellular function, though there are several clues suggesting a highly conserved role in the development and maintenance of the CNS and other organ systems. Huntingtin is expressed ubiquitously, but is found at higher concentrations in CNS neurons⁶⁰. The huntingtin protein and its expression patterns are highly conserved from human to mouse to *Drosophila* to the lowly sea urchin. Huntingtin knockout mouse models are embryonically lethal during the initial stages of CNS development, solidifying its important role in the developing brain⁶¹⁻⁶³. These huntingtin knockout mice exhibit poor neuronal growth and ultimately die during embryonic day 8.5, coinciding with gastrulation and formation of the nervous system⁶⁴⁻⁶⁶. Huntingtin continues to play an active role in the maintenance of the adult brain. Inactivation of huntingtin in the adult

mouse brain can be accomplished using a Cre/*loxP*-mediated recombination, generating a null allele where the *loxP*-modified *Hdh* allele was. Expression of *cre* can be driven to postnatal mouse forebrain by the promoter of the gene *Camk2a* (the α -subunit of calcium/calmodulin-dependent protein kinase II) ^{67,68}. Inactivation of huntingtin in a mouse adult brain leads to neurodegeneration, memory problems, and sterility in males, which is due to an unclear role of huntingtin in spermatogenesis ⁶². In this study (as is common within the field), huntingtin was only examined within the context of the brain, testis, and ovaries because of its obvious expression patterns in these organs. More recent studies indicate that huntingtin – either mhtt or endogenous WT huntingtin – may play active roles outside of the brain, such as in the heart and skeletal muscles ⁶⁹⁻⁷¹. Many proposed methods to genetically suppress mutant huntingtin, some of which are planned to enter clinical trials, may also suppress expression of the non-pathogenic allele ⁷². Because complete knockout of *HTT* is also toxic, it's therefore critical that researchers proceed with caution when considering lowering both pathogenic and non-pathogenic huntingtin alleles in humans.

Another hint of huntingtin's wild type function is the identification of HEAT repeat domains ^{73,74}. In other proteins, such as protein phosphatase 2A and the yeast kinase TOR1, HEAT repeats are responsible for mediating protein-protein interactions ⁷³. Given the relatively large size of the full-length huntingtin protein (~350 kDa) and the fact that huntingtin interacts promiscuously in Co-IPs ⁷⁵, wild type huntingtin's function may be as a scaffolding protein. Coinciding with the promiscuous nature of scaffolding proteins, in a stringent proteomics study by Shirasaki *et al.*, full-length huntingtin isolated from wild-type mouse brain was found to interact with 576 different proteins encompassing a multitude of networks: proteostasis, pre-synaptic function, post-synaptic function, calcium signaling/mitochondria, actin cytoskeleton,

and aging ⁷⁵. More recently, huntingtin was proposed to have an Atg11-like function in selective autophagy, again consistent with a scaffold protein function ⁵⁷. These data include structural homology between the C-terminal domain of full-length huntingtin and Atg8/11, *via* the presence of a WXXL domain, also known as a LC3-interacting region (consensus sequence W/F/Y-X-X-L/I/V/F). Full-length htt coimmunoprecipitates with known Atg11 interactors, such as LCB3 (mammalian homolog of Atg8) and GABA receptor-associated proteins (GABARAPL1), in a WXXL-dependent manner. Although the function of wild type huntingtin remains unclear, its ability to cause disease in a polyQ-dependent fashion remains a central tenet of the field - much of the time and resources have been spent focusing on the disease-causing aspects of polyQ expanded huntingtin.

1.3.2 The Toxic Amyloid Hypothesis

Despite decades of groundbreaking research, a precise mechanism by which polyQ expansion in the huntingtin protein causes neurodegeneration remains elusive. The development of an effective therapy for slowing, preventing, or reversing Huntington's disease will require a better and more detailed mechanism of how huntingtin exerts its toxicity. Exemplifying this is the fact that non-hypothesis driven drug screens have systematically failed to find a disease-modifying therapy, though there are certainly several drugs to manage symptoms (Section 1.6.1). There are several proposed hypotheses of how mutant huntingtin protein achieves its toxic gain-of-function: a toxic misfolded monomer, a toxic oligomeric species of which several have been proposed, large soluble aggregates, mature insoluble aggregates, inclusion bodies, and more. This thesis work aims to test several of these, most notably the toxic amyloid hypothesis and toxic oligomer hypothesis.

The toxic amyloid hypothesis states that the process of amyloid formation (including the presence of amyloid itself) represents the toxic factor in HD. This model gained early traction from simple observations of post-mortem human HD brains, which have large intracellular inclusion bodies containing insoluble protein material⁴⁰. The levels of insoluble protein deposits correlates with severity and progression of the disease. Historically, in particular with other amyloid diseases, dyes to detect amyloid, such as Congo Red, have been used to identify and histologically score amyloid inclusion formation in post-mortem brains. Animal models expressing polyQ expanded huntingtin also reveal a similar pattern of nuclear huntingtin aggregation using antibodies and neuron death⁷.

The pathological repeat length of disease in humans, which begins around 37 glutamines in HD, is roughly mirrored by a similar repeat-length dependence of aggregation *in vitro*⁷⁶. The predicted time to aggregate into amyloid for a simple polyQ peptide in PBS at 1 nM with 23-25 glutamine repeats is 100,000 - 1,000,000,000 years; far too slow to be physiologically relevant. However, polyQ repeats of 26-37 are calculated to aggregate on the order of 10-100 years, roughly the age of onset of HD and well within a humans' average lifespan⁷⁷. The propensity of simple polyQ sequences to aggregate *in vitro* with increasing polyQ repeats correlates well with cellular aggregation and cell death in many of the polyQ diseases. Even simple expanded polyQ peptides, which lack protein context, can cause disease. For instance, flies expressing expanded polyQ peptides have similar neurodegenerative phenotypes as mhtt flies⁷⁸. Complementing this, pre-formed simple polyQ aggregates added to PC12 cell culture media are toxic on their own⁴⁷. Additional biophysical evidence comes from mathematical modeling, which maintains that disease onset and progression rates are consistent with a nucleation-dependent aggregation process^{79,80}. The correlation between an expanded polyQ sequence's ability to aggregate into

amyloid *in vitro* and *in vivo* and its toxicity would appear to be overwhelmingly in support of the toxic amyloid hypothesis.

Contesting the toxic amyloid hypothesis, several *in vitro* studies using live-cell tracking in primary neuron culture systems demonstrated that inclusion body formation is potentially a cellular protection mechanism: cultured striatal neurons that form intracellular inclusions have better odds of survival than neurons that failed to do so^{81,82}. This research suggested that inclusion body formation best predicts improved survival and leads to decreased level of mutant huntingtin elsewhere, which they believe to be the toxic species. While this research suggests that one form of large aggregates, cytoplasmic inclusion bodies, are less toxic than thought, some research groups have over-interpreted this to mean that all aggregated species are non-toxic. This has caused many researchers in the field to pursue other potential toxic species, such as a soluble toxic oligomer or misfolded monomer, discussed in the next Sections.

Recently, inclusion bodies were found to have their own toxicity associated with them, and are not as benign as previously believed⁸³. To further address this, Moerner's laboratory confirmed the suspicion that not all huntingtin aggregates are sequestered into the handful of bright large inclusion bodies seen by standard fluorescence microscopy methods⁴²⁻⁴⁴. By photobleaching the fluorescence signal from excessively bright inclusion bodies and using super-resolution microscopy techniques, smaller aggregates of <1,000,000 monomers become visible, which appear to take on amyloid-like morphologies. These smaller and relatively less bright aggregates were previously obscured in the soluble signal; in many studies, cells containing these small aggregates may have been erroneously labeled as soluble monomeric or oligomeric populations. Other sensitive techniques, such as fluorescence correlation spectroscopy, can detect small diffusible aggregates in cell lysates and in live cells⁸⁴ (Sahoo 2015 Manuscript

Submitted). These results reignite the possibility that aggregated proteins, such as amyloid, protofibrils or other relatively large β -sheet rich aggregates, can participate in causing cell death. This is a particularly salient point if these smaller aggregates have not yet been targeted by the protein quality control mechanisms of the cell.

Ultimately, to date, the field is not unified on the mechanism of how polyQ expanded huntingtin causes Huntington's disease, nor is there a consensus on the nature of the toxic species. Further work defining the contribution and mechanism of huntingtin amyloid to HD pathology is crucial to developing effective hypothesis driven therapies.

1.3.3 The Toxic Oligomer Hypotheses

More recently, alternative hypotheses have been developed in order to explain the toxic effects of mutant huntingtin, namely the toxic oligomer hypothesis, which states that some non-amyloid, soluble oligomer of huntingtin is the toxic species⁸⁵⁻⁸⁹. A number of key experiments question the direct correlation between amyloid aggregation and toxicity. Small molecules that enhance autophagy and the clearance of large aggregates in cells do not rescue HD phenotype in animals⁹⁰. Primary cultured rat neurons that successfully form large inclusion bodies survive longer than those without inclusion body formation⁸¹. Other experiments correlate the apparent timing of different huntingtin species with cellular markers of toxicity, such as ER stress⁹¹. The serendipitously developed "shortstop" form of human huntingtin exon1, which is truncated at amino acid 117, forms widespread inclusions in transgenic mice, but no neurodegeneration or behavioral defects⁸⁷. However, later studies demonstrated that expanded shortstop is less

capable of forming amyloid than htt-exon1, which was interpreted to mean that oligomers are toxic⁸⁶. All together, a number of groups have proposed that the formation of large inclusion bodies leads to a lower toxic cellular protective response^{92,93}.

Altogether, this has led many research groups to study the role of soluble non-amyloid oligomers in HD pathogenesis. Takahashi *et al.* found that mhtt fragments that increased levels of oligomerization correlated with increased cytotoxicity, however, this study utilized split-GFP constructs to report dimerization, which may act to promote oligomerization independent of or in concert with htt⁹⁴. Split-GFP proteins have their own affinity to bind to one another and form a fluorescently active reporter GFP protein – this process may very likely accelerate the oligomerization of the huntingtin proteins they are fused to. Other studies incorporate the serendipitously discovered huntingtin shortstop, which is a 117-amino acid fragment of huntingtin that forms aggregates in mice, but is non-toxic⁸⁷. Shortstop oligomeric species are not recognized by the antibody 3B5H10, which is claimed to detect a toxic conformation of polyglutamine in htt fragments⁸⁶.

A possible mechanism of oligomer toxicity is the inhibition of endoplasmic reticulum-associated degradation (ERAD), which induces ER stress before the formation of visible inclusions⁹⁵. Another paper found that oligomeric mutant huntingtin accumulates in the nucleus and can inhibit transcription factors, such as TATA-binding protein and CREB-binding protein⁹⁶.

However, many of these studies rely on the correlative timing of molecular events or rely on the lack of appearance of bright inclusion bodies to determine whether or not aggregation into amyloid has taken place. Subsequent reexamination of cells expressing mhtt-ex1 using super-resolution microscopy has shown that a multitude of small, previously undetected amyloid-like

aggregates exist outside of inclusion bodies, further reigniting this complex problem⁴²⁻⁴⁴ (Sahoo 2016 Manuscript Submitted). These relatively small, fibrillar aggregates are not readily visible within the resolution limits of confocal microscopy and were previously categorized as part of the soluble non-amyloid portion of htt-ex1 in the cell. Previous interpretations of a toxic oligomer that relied on the absence of massive inclusion bodies or assumed a homogeneous mixture of huntingtin conformers *in vivo* need to be thoroughly re-evaluated in light of this new evidence.

1.3.4 The Toxic Monomer Hypothesis

Support for a toxic misfolded monomer comes from a number of experiments. First is evidence purporting that chemically synthesized polyQ peptides can exist as a stable β -sheet monomeric form⁹⁷; however, these results were likely an artifact from the peptide synthesis process, which can introduce pre-aggregated contaminants that can rapidly seed further aggregation of the soluble portion. Chemically synthesized polyQ peptides that have undergone rigorous disaggregation protocols show an initial state of random structure for simple polyQ peptides^{98,99}.

Further support for the toxic monomer hypothesis stems from work using antibodies to correlate the presence of huntingtin epitopes with toxic folding events. Preferential binding of the 1C2 antibody to soluble expanded polyQ sequences was initially thought to be due to conformational changes within the monomeric form of expanded polyQ huntingtin, which could represent a toxic species¹⁰⁰. Additionally, the antibody 3B5H10 recognizes a species of huntingtin protein that predicts neuronal death¹⁰¹. However, a linear lattice model^{98,102,103} explains how these antibodies bind with additional affinity and stoichiometry as the number of

epitope regions increases in expanded polyQ sequences. Thus, MW1 and other similar polyQ antibodies likely do not recognize a distinct conformation of the monomer or oligomer, but bind to the additional available polyQ epitopes with increased avidity.

A number of independent studies using varied techniques find no evidence for a significantly populated structured huntingtin monomer in water. Firstly, fluorescence correlation spectroscopy studies *in vitro* and in cells demonstrate that polyQ-expanded huntingtin rapidly forms oligomers, with little detectable monomer (Sahoo 2016 Manuscript Submitted). Secondly, studies using solution NMR^{104,105} or circular dichroism^{106,107} to monitor crude secondary structure show that expanded polyQ sequences adopt a random structure in aqueous solution and only gain β -structure as it aggregates into amyloid^{102,107}. In fact, even with the addition of the β -hairpin enhancing motifs, the effect on the monomer structure in solution is not detectable by circular dichroism (CD), a measure of ensemble protein secondary structure¹⁰⁸. Thirdly, the amide functional group in glutamine provides ample opportunity for H-bonding. Previous papers using fluorescence correlation spectroscopy report that water is a poor solvent for polyglutamine, which forms a collapsed compact coil, brought on by glutamine side chain amides H-bonding to the main chain amide groups¹⁰⁹. Fourthly, the equilibrium constant between unstructured monomer and a structured nucleus in simple polyQ peptides ranges from 10^{-10} to 10^{-15} depending on polyQ repeat length^{77,108}. Therefore, the population of soluble huntingtin in this nucleus form is infinitesimally small, making it a poor candidate for a toxic species. However, an unstructured toxic monomer may come about from an increased affinity of expanded polyQ huntingtin to bind partners with higher affinity^{98,110}.

1.3.5 Alternative Hypotheses

In addition to the toxic aggregate, toxic oligomer, and toxic monomer hypotheses in HD, there are several alternative mechanisms of toxicity. However, to date it remains difficult to tease out which toxic events are primary, and which are secondary symptoms. Whatever the toxic mechanism may be, the inevitable result is a global cellular crisis that obscures primary and secondary toxic events; mitochondrial dysfunction, impaired axon transport, altered transcription and DNA methylation, synaptic and neurotransmitter dysfunction, and pro-apoptotic signaling all precede eventual cell death.

A loss-of-function phenotype has also been proposed. Adult HD KO mice and *Drosophila* have impaired neurological function, including motor phenotypes and reduced lifespan^{62,111}. However, a loss-of-function phenotype can also be rationalized as the dominant gain-of-function of mutant huntingtin's capacity to recruit soluble huntingtin into a growing amyloid fibril.

Aggregated mutant htt may be able to sequester other polyQ-containing proteins into a growing amyloid aggregate. Aggregation of polyQ or A β proteins may also be capable of promiscuously co-aggregating with other dissimilar proteins^{75,112,113}. Huntingtin aggregates have been found to co-immunoprecipitate with other meta-stable proteins that contain short, normally benign polyQ repeat lengths ($Q > 7$)¹¹⁴. These large aggregates may act as a sink to sequester other soluble proteins into the growing amyloid, causing a synchronous loss-of-function from dozens of proteins.

Similar to the recruitment hypothesis, large amyloid aggregates may also act as a sink of heat shock proteins. DNAJB/HSP40¹¹⁵⁻¹¹⁷, HSP70^{117,118}, HSF-1^{50,119}, TRiC^{120,121}, α B-crystallin^{122,123}, CHIP¹²⁴ and other heat shock response proteins are protective in cell and some

animal models of HD. This makes logical sense, as heat shock response proteins capable of interacting with misfolded mhtt may be capable of catalyzing the refolding of misfolded mhtt or facilitating the degradation of misfolded mhtt. However, if an excess of misfolded mhtt places an excessive demand on the heat shock response system, cellular protein quality control may suffer. Recent work has demonstrated that inclusion bodies precede the appearance of diffusible sub-diffraction amyloid-like species in cells, suggesting that inclusion bodies of mhtt stress the heat shock response system past a certain breaking point, where the cell's heat shock response system is no longer able to maintain the solubility of other metastable proteins⁴². Additionally, the steady state heat shock protein response is dampened in HD animal models, which are unable to launch an appropriate heat shock protein response even when given HSF1 activating compounds⁵⁰. This may be due to a number of factors, including sequestering a limited number of important molecules from the ubiquitin proteasome system, restructured chromatin⁵⁰, or by inhibiting clatherin-mediated endocytosis by sequestering chaperones¹²⁵.

1.4 POLYGLUTAMINE REPEAT DISORDERS

1.4.1 DNA Repeat Diseases

Fragile X syndrome (FXS) is a genetically inherited disease that causes cognitive disability in about 1 in 3,600 males and 1 in 6,000 females¹²⁶ making it the most prevalent trinucleotide repeat disorder. Because this developmental disorder is linked to the X chromosome, it particularly affects boys. The culprit of FXS is a trinucleotide repeat expansion of CGG in the *Fragile X mental retardation 1 (FMR1)* gene¹²⁷, where unaffected individuals carry less than 45

CGG repeats while Fragile X patients may carry 200 or more CGG repeats. This mutation results in a loss-of-function of the fragile X mental retardation protein (FMRP), which is involved in the transport of RNAs along neuronal dendrites required for synaptic maturation ¹²⁸.

A variety of other triplet repeat expansions cause disease in both an autosomal recessive and dominant fashion. A GAA expansion in the *FXN* gene results in Friedreich's ataxia ¹²⁹. The GAA expansion, which is located in a non-coding intron, reduces mRNA and protein levels of the *FXN* gene, leading to a deficiency of the mitochondrial protein frataxin ¹³⁰. Conversely a CTG triplet repeat in the *DMPK* gene, which codes for myotonic dystrophy protein kinase expressed in skeletal muscle, results in the autosomal dominantly inherited disease myotonic dystrophy type 1 (DM1), which causes a more severe disease with increased CTG repeats ¹³¹. The CTG trinucleotide repeat expansion in DM1, similar to Friedreich's ataxia, is located in a non-protein-coding intron sequence. However, this CTG repeat is linked to an RNA toxic gain-of-function. The resulting CUG-containing RNA transcripts interfere with RNA-protein interactions ¹³²⁻¹³⁶. Furthermore, not all DNA expansion diseases are trinucleotide; myotonic dystrophy type 2 (DM2) is caused by a tetranucleotide expansion of CCTG in the *ZNF9* gene and is also a toxic RNA gain-of-function disease ¹³¹, but is considerably more rare.

Other trinucleotide repeat disorders involve expansion of a repeat of the CAG codon in exons, which codes for the amino acid glutamine. Genetic instability of CAG repeats trend toward an increase in total CAG repeat during meiotic transmission ²⁶. Curiously, the CAA codon, which also codes for glutamine, is not associated with DNA expansion or disease. *In vitro*, pure CAG repeats are more prone to expansion than pure CAA repeats or mixed CAA/CAG repeats ¹³⁷. Mixed CAA/CAG repeats are also associated with a lower rate of trinucleotide expansion in human versus pure CAG repeats *in vivo* ¹³⁸⁻¹⁴⁰. The preference for

CAG expansion over other trinucleotides is not completely understood, but may result from a number of factors, including imperfect base excision and other aberrant DNA repair mechanisms (which allow the formation of loop structures stabilized by CAG repeats) and subsequent loop incorporation, nucleotide excision repair, and polymerase slippage^{141–143}. For instance, one lab found that certain histone deacetylase complexes, such as Hda1, promote the expansion of CTG•CAG codons specifically¹⁴⁴, while others have implicated a role of imperfect 3' to 5' exonuclease proofreading of DNA polymerase III in *E. coli*¹⁴⁵. Strand “slippage” of DNA may be more likely to occur in multiple CAG repeats, as opposed to other codon repeats, as a result of stable hairpin formation¹⁴⁶, which can be mitigated by CAA insertions¹⁴⁷. Furthermore, expansion of the CAG repeat in an RNA transcript may alter RNA splicing, resulting in a htt-exon1 splice form³⁵. Uncovering the mechanism of CAG repeat expansion may lead to new ways of preventing expansion of the *HTT* gene from parents to offspring.

1.4.2 Polyglutamine Repeat Disorders

To date, there are at least ten diseases linked to a polyglutamine repeat expansion^{26,148–150}: Huntington’s Disease, spinocerebellar ataxia (SCA) type 1, 2, 6, 7, and 17, Machado-Joseph disease (SCA3), spinal bulbar muscular atrophy (SBMA), and dentatorubral pallidoluysia atrophy (DRPLA). All ten diseases are autosomal dominantly inherited, suggesting a common gain-of-toxic-function associated with the expanded polyQ/CAG repeats. This type of inheritance pattern is expected for a dominant gain-of-function prion or prion-like mechanism

(similar to PrP^{Sc}) of disease and contrasts with many genetic loss-of-function diseases, such as recessively inherited cystic fibrosis, sickle cell anemia, or fragile X syndrome.

One key symptom of expanded polyQ-containing proteins is the accumulation of large, insoluble, protein aggregates in the CNS and other tissues. Aggregation of the defective polyQ-expanded protein has been observed *in vitro* or *in vivo* for SCA 1^{151,152}, SCA 2^{153,154}, SCA 3^{122,155–158}, SCA 6¹⁵⁹, SCA 7^{160–162}, SMBA¹⁶³, SCA 17¹⁶⁴, and DRPLA^{165–167}. A significant amount of attention has been paid to Huntington's disease, which readily forms amyloid *in vitro*⁶ and in animal models^{7,168,169}. Large insoluble aggregates are also found in post-mortem human HD patient brain tissue⁴⁰. In each polyQ disease, there are characteristic neurodegenerative patterns involving neuronal dysfunction and subsequent loss of neurons in the CNS, which have varying regional differences between diseases. Despite elucidating the mutant polyQ/CAG repeat expansion responsible for Huntington's disease over two decades ago²⁴, the precise mechanism by which expanded polyQ sequences grant toxic-gain-of-function remains uncertain (Discussed in Section 1.3). The lack of a detailed mechanism of toxicity has greatly hampered hypothesis-driven therapeutic design.

The expression profiles and wild type functions of the polyQ-expanded proteins all have some level of RNA transcription and protein expression within the CNS⁶⁰. Beyond this, their roles in the CNS are varied or largely unknown. For instance, TATA-box binding protein (SCA17) is a general transcription factor that is evolutionarily highly conserved and ubiquitously expressed throughout the human body⁶⁰. Another transcription factor, the androgen nuclear receptor partially responsible for sexual dimorphism, is also affected by polyQ expansion resulting in SBMA^{170,171}. However, the affected gene of SCA6, *CACNA1A*, encodes a subunit of a P/Q voltage-dependent calcium channel Cav2.1¹⁷² and Ataxin 3 is a deubiquitinating enzyme

¹⁷³. Many of the other polyQ disease proteins, such as several of the ataxin proteins, have very poorly understood wild type function. Additionally, the endogenous function of polyQ domains in general and what kind of evolutionary advantage they bestow, if any, is also unclear.

1.4.3 Simple Polyglutamine Models

1.4.3.1 Rationale for Simple PolyQ Models As previously discussed, a wide range of seemingly unrelated proteins are affected by polyQ repeat expansion: the androgen receptor (Spinobulbar muscular atrophy), the $Ca_v2.1$ P/Q voltage-dependent calcium channel (Spinocerebellar ataxia type 6), the TATA-binding protein (Spinocerebellar ataxia type 17), huntingtin (Huntington's Disease), and six others. The lowest common denominator between these proteins is their polyQ domains, which causes neurodegenerative phenotypes in a repeat length dependent manner. In each instance, expanded polyQ domains also gain a propensity to aggregate into amyloid *in vitro*, *in vivo*, and in human patients ⁶⁻⁸. Additionally, expanded polyQ domains alone aggregate and are toxic when expressed in *C. elegans* ¹⁷⁴, *Drosophila* ⁷⁸, when simple polyQ aggregates are delivered to cell culture media ⁴⁷, and when CAG repeats are inserted into phosphoribosyltransferase (HPRT), which is not associated with any of the ten CAG repeat diseases ¹⁷⁵. Collectively, these data point toward a common and central role of aggregation of expanded polyQ domains in the toxic gain-of-function of each disease.

Studying the lowest common denominator, the expanded polyQ sequence, is therefore an attractive research pursuit; the properties of expanded polyQ sequences may represent a universal mechanism of aggregation and toxicity. Therefore, mechanisms of simple polyQ

aggregation are immediately relevant and therapeutics targeting simple polyQ aggregation and toxicity could prove beneficial to the polyQ repeat diseases.

Additionally, the effect that protein context (N- and C-terminal flanking sequences, expression profiles, etc.) has on expanded polyQ domains can be best understood in the context of how “naked” polyQ peptides behave. For instance, in some polyQ diseases, N- and C-terminal flanking sequences alter the aggregation mechanism of the associated polyQ domain, such as the Josephin domain of Ataxin 3^{155,156} and the htt^{NT} segment of huntingtin¹⁷⁶, which undergoes a more complex intermediate oligomer formation step^{39,176} (Section 1.4.4).

Finally, the polyQ repeat-length dependence of disease and aggregation *in vivo* is mirrored by simple polyQ repeat-length aggregation kinetics *in vitro*^{77,107}. Simple polyQ peptides recapitulate a portion of the aggregation pathway by forming similar final β -sheet rich amyloid-like structures by FTIR and EM¹⁷⁶. The final aggregates have their own toxicity associated with them, and can bestow toxicity when delivered to cell media⁴⁷, or when expressed in *Drosophila*⁷⁸.

1.4.3.2 Simple PolyQ as a Model The fibril elongation reaction of simple polyQ peptides, which undergo a single nucleation step, can be mathematically modeled to initial aggregation kinetics by applying the Eaton-Ferrone model^{22,107,177,178}, represented by the Equation 1, where K_n^* is the equilibrium constant of nucleation, k_+^2 is the aggregate elongation constant (11,400 liters/mol*s)¹⁷⁷, t is time in seconds, and C is the initial monomer concentration.

Equation 1: Eaton-Ferrone Kinetics Model of Nucleation

$$\Delta = \frac{1}{2} (k_+^2)(K_{n^*})(C^{(n^*+2)})(t^2)$$

Information about the nucleation and elongation processes can be obtained by plotting the decay in monomer concentration for early reaction time points versus t^2 to yield a slope of $(1/2)(K_{n^*})(k_+^2)(C^{n^*+2})$, which is a representation of the initial reaction rate. A plot of the log of this rate versus the log of the starting concentration, for a series of reactions at different starting concentrations, yields a slope equal to $n^* + 2$. Using this model, nucleus size n^* , nucleus equilibrium constant k_{n^*} , and the Gibbs free energy of nucleus formation ΔG_{n^*} can be calculated experimentally^{108,177}. The Eaton-Ferrone model of aggregation provides descriptive features of aggregation phenomenon that follow a simple single-step nucleation. Not only are these parameters important for describing the behavior and mechanism of polyQ aggregation, but also can be used to diagnose how future aggregation inhibitors affect the aggregation mechanism.

In HD, the age of onset decreases as polyQ repeat length increases. *In vitro*, the kinetics of nucleation and aggregation are enhanced as polyQ repeat length increases. PolyQ peptides with as few as 8-10 glutamine repeats may be capable of aggregating into β -rich amyloid-like structures *in vitro*^{38,76,179}, albeit extremely slowly. These short polyQ peptides likely aggregate too slowly to escape protein quality control mechanisms *in vivo*. PolyQ peptides with fewer than 25 glutamine repeats receive an enhancement to aggregation kinetics with each additional glutamine repeat; however, after 25 glutamine repeats, additional glutamines drastically enhance aggregation by altering the mechanism of aggregation. Kar *et al.* found that longer simple polyQ peptides ($Q \geq 25$) nucleate aggregation efficiently with a monomeric nucleus, $n^* = 1$ (a single

molecule is required for nucleation, likely through intramolecular rearrangement), while shorter polyQ peptides have an inefficient tetrameric nucleus of $n^* = 4$ (four molecules required to initiate and template amyloid aggregation)⁷⁷. The enhancement of nucleation efficiency results in a substantial boost in kinetics of nucleation between $Q \leq 23$ and $Q \geq 25$, which can be rationalized as the generic difference in kinetics between inter- versus intra-molecular reactions.

The initial nucleation event is extremely rare, even for expanded polyQ sequences, resulting in a lag-phase in the kinetics profile, followed by a rapid elongation phase. Even expanded $K_2Q_{47}K_2$ has a tremendously small portion of monomers exploring the nucleus state at any given time in solution ($K_{n^*} = 2.6 * 10^{-9}$). The rate limiting lag-phase can be bypassed if pre-formed polyQ aggregates are added to soluble polyQ peptides, resulting in seeded elongation. Addition of pre-formed aggregate seeds eliminates the energy barrier in the formation of the initial nucleation event, thus removing the lag-phase and proceeding directly to the rapid elongation phase. This process is relevant to disease, as seeding elongation may occur *in vivo* as part of a prion-like transmission and propagation of mutant huntingtin¹⁸⁰⁻¹⁸². Simple polyQ models may be useful to screen for or validate molecules that block seeding competency, that dampen nucleation formation, or limit polyQ elongation efficiency.

1.4.4 Role of the Huntingtin N-Terminus in Aggregation

The aggregation prone polyQ domains of each polyQ disease are flanked by N- and C-terminal amino acids that vary between proteins. In huntingtin, the disease-causing polyQ core is flanked by a short N-terminal 17 amino acids (htt^{NT} or N17) and a C-terminal poly-proline/proline-rich region. Addition of the 17 amino acid htt^{NT} region has a drastic enhancing effect on the

aggregation kinetics of polyQ by altering its aggregation mechanism^{176,183}. Htt^{NT}-polyQ peptides still retain their polyQ repeat length dependence of aggregation kinetics and final β -sheet rich amyloid product, but also introduce an intermediate step of oligomer formation¹⁷⁶.

When htt^{NT}-polyQ peptides are initially solubilized as monomers, they are largely unstructured by CD^{107,184}. Upon incubation, htt^{NT} alters the mechanism of polyQ aggregation by introducing intermediate oligomer formation. These oligomers are detectible by EM³⁹, AUC analysis³⁸, biochemical assays^{37,185}, and FCS (Sahoo 2016 Manuscript Submitted). Even htt^{NT} alone forms homo- α -oligomers in a concentration dependent manner³⁸ that are pelletable by ultracentrifugation¹⁸⁶. α -helical secondary structure of htt^{NT} is also predicted by computational modeling¹⁸⁷ and can be detected by CD in htt^{NT}-polyQ peptides at higher concentration before their transition into β -sheet rich aggregates³⁸. Disrupting α -helical propensity of htt^{NT} by strategic alanine substitutions or serine 13/16 phosphorylation¹⁸⁸ reduces nucleation efficiency, presumably by making htt^{NT}-mediated nucleation within the oligomer inoperable and forcing nucleation to occur through the slower simple polyQ nucleation mechanism (Scheme 1).

Another piece of evidence supporting the role of htt^{NT}-mediated oligomer formation is varied resistance to trypsin digest: htt^{NT} is sensitive to trypsin digest in both monomeric (to residues 6, 9, and 15) and amyloid huntingtin (to residue 6), but resistant to trypsin digest in the oligomeric state^{176,188}. This further suggests that htt^{NT} is buried and is playing an active role in oligomer formation, consistent with a coiled-coil domain.

In simple polyQ peptide aggregation, there is only a single nucleating step, which can be modeled mathematically^{107,178}. The intermediate oligomers formed by htt^{NT}-containing polyQ peptides change the mechanism of nucleation of aggregation; there is not yet a mathematical model for this more complex aggregation pathway. Applying the Eaton-Ferrone model to htt^{NT}-

polyQ aggregation kinetics results in non-real values, such as a critical nucleus size of -1 for htt^{NT}-Q₃₀-P₆ in contrast to $n^* = 1$ for K₂Q₃₀K₂¹⁸³. Such non-real values cannot be directly interpreted, but nonetheless provide a consistent signature for peptides following a nucleation mechanism featuring an intermediate oligomer. This allows identification of this more complex mechanism by carrying out the standard analysis of initial aggregation rate vs. initial concentration.

The model of htt^{NT}-mediated oligomerization as an accessory to polyQ aggregation is further supported by htt^{NT} based inhibitors of aggregation. A synthetic peptide comprised of only the htt^{NT} region (17 amino acids) can kinetically compete with htt^{NT}-polyQ monomers for oligomeric bundle formation¹⁸⁹. Because the synthetic htt^{NT} inhibitor does not bring with it an associated polyQ sequence, the mixed α -helix rich oligomers statistically contain fewer polyQ strands per oligomer. The polyQ domains effectively dilute and slow the rate limiting nucleation step in a stoichiometry-dependent fashion. However, htt^{NT} peptides require super-stoichiometric ratios to achieve significant delays in target htt^{NT}-polyQ aggregation. Even at high ratios, the thermodynamic driving force of amyloid formation eventually overcomes these inhibitory effects¹⁸⁹. Nonetheless, in the cell environment where multiple kinetic pathways of aggregation exist, even a modest acceleration to aggregation kinetics may be sufficient for proteins to misfold fast enough to escape the protein quality control mechanisms and have significant cellular consequences. In addition, further research addressing the mechanisms of nucleation inhibition could yield more potent aggregation inhibitors with greater therapeutic potential.

1.4.5 Role of the Huntingtin C-Terminus in Aggregation

The C-terminus portion of htt-exon1 immediately following the polyQ domain is a poly-proline/proline rich domain (PRD), which is a total of 51 amino acids in length and consists of two unbroken P₁₀ and P₁₁ segments. The exact role of the C-terminal PRD is unknown, but may have co-evolved alongside the growing polyQ domain to limit its aggregation potential. The proline-rich tail can adopt a poly-proline type II structure¹⁹⁰ and in some cases may interact with the htt^{NT} helix of shorter polyQ repeat peptides^{191,192}. In some experiments, the PRD has a modest affect in delaying polyQ aggregation¹⁹³, but does not change the overall aggregation mechanism in the way that the N-terminal htt^{NT} domain does.

Synthetic huntingtin peptides that include the entire PRD, which are significantly more difficult to synthesize, behave similarly to peptides with truncated poly-proline sequences, such as P₁₀, and follow the same two step aggregation mechanism¹⁹⁴. For these reasons, the Wetzel laboratory uses abbreviated htt-exon1 constructs (htt-ex1^{P10}; Table 1).

1.4.6 Huntingtin Exon1 and Full Length Huntingtin as models

The huntingtin gene is comprised of 31 exons yielding a protein of just over 3100 amino acids or around 350 kDa. The disease-causing portion of huntingtin, the polyQ repeat, is limited to the extreme N-terminus of the first exon starting after only 17 amino acids into the sequence (AKA the N17 domain or htt^{NT}). Flanking sequences between all of the polyQ diseases have no obvious commonality; however, flanking sequences may play an accessory role in protein aggregation kinetics, thermodynamics, and toxicity of each disease protein. For example, htt^{NT} in cis with

polyQ sequences greatly accelerates nucleation of aggregation by promoting an alternative mechanism of nucleation *via* the formation of α -helical-like bundles^{38,176,183,186,188} (Schematic 1). Conversely, htt^{NT} in trans with polyQ delays amyloid nucleation by competing for mixed oligomers¹⁸⁹.

Huntingtin inclusions in post-mortem HD brains are not the entire full-length huntingtin protein, but rather a short fragment representing roughly the first exon. Antibodies recognizing the N-terminal regions (CCAG53b: AA 18-40; HP1: AA 80-113) stain HD neurons with an intranuclear inclusion pattern, while antibodies against the C-terminal portion of full-length huntingtin (P2: AA 1187-1207; HF1: AA 1981-2110) gives a granular cytoplasmic stain¹⁹⁵. These data highly suggest that a protein fragment corresponding to roughly the first exon of htt is produced in HD patients, and that this N-terminal fragment (which contains the pathogenic expanded polyQ sequence) is aggregation prone. How this fragment is produced is not yet understood. A number of caspase and calpain cleavage sites exist between amino acids 469 to 586, which could result in the cleavage product of roughly the first exon of huntingtin³⁴. In *Drosophila*, expression of any of these potential fragments (ranging from 469-586 AA in length, including a 90 and 108 AA truncated htt peptide) is toxic, with a true htt-exon1 fragment of AA 586 being the most severe in *Drosophila*¹⁹⁶. Additionally, new evidence indicates a portion of this abbreviated huntingtin could be generated through alternative splicing of the first exon³⁵. Finally, the full-length protein of huntingtin is not required to generate HD symptoms in animal models. Expressing just mhtt-exon1 is both sufficient and necessary to cause HD⁷.

Htt-exon1 is commonly used as the model protein in HD for several reasons: modeling all 3,000+ amino acids of full-length huntingtin is technologically difficult, the disease-causing sequence is contained to the first exon^{7,195}, the first exon alone is both necessary and sufficient

to cause disease ⁷, and an exon1 fragment is generated endogenously in HD patients and animal models ^{35,195}. Full-length huntingtin animal models have also been constructed ^{168,197}, and their disease phenotypes are less severe and appear later in life than htt-ex1 models, likely because full-length expression requires an extra step to generate the more toxic htt-exon1 fragment.

In order to characterize how the huntingtin exon1-like fragments behave biophysically, synthetic and recombinantly expressed proteins can be used. Producing huntingtin protein through recombinant protein expression methods requires the use of an N-terminal solubilizing tag, such as GST, to help solubilize the poorly behaved expanded polyQ sequence ⁶. Subsequent cleavage of the GST tag results in residual amino acids that are non-native to the huntingtin protein and may affect huntingtin's ability to aggregate *in vitro*. Current chemical synthetic approaches allow better control of the primary amino acid sequence, particularly of the htt^{NT} domain; however, more recent advances in recombinantly expressed proteins have a cleavage site that leaves the htt^{NT} intact at the Met residue ²¹, which would be cleaved with a subsequent acetylation if expressed *in vivo* ¹⁹⁸. Chemical synthesis comes with its own limitations, such as a limit to the absolute amino acid length, making full length htt-exon1 extremely challenging and full-length htt not yet possible. Because of these various limitations, the Wetzel laboratory uses synthetic huntingtin analogs to model polyQ and/or huntingtin aggregation *in vitro* and htt-ex1 expression in cells and animal models.

1.4.7 Role of β -hairpin Structure in Nucleation

Work by Chen *et al.*, and later Kar *et al.* uncovered an intramolecular monomeric nucleation event in simple polyQ peptides with sufficient polyQ repeat length ($Q \geq 26$) ^{77,107}. The structure

of this nucleating event was unknown, but was thought to contain either a β -turn or β -arc element for a number of reasons: monomeric nucleation should by definition contain an intramolecular fold, polyQ-containing peptides gain β -sheet character by circular dichroism as aggregation progresses¹⁰⁷, FTIR signatures of the final aggregates are dominated by β -sheet signal^{38,77}, magical angle spinning solid-state NMR studies reveal an interdigitated β -hairpin core of the final fibrils²¹, β -sheet layering is seen by time-resolved fluorescence decay¹⁹⁹, and finally, only β -hairpins can form dimers with sufficient lifetimes to be able to act as key intermediates during amyloid nucleation²⁰⁰.

Due to technological limitations and the extremely rare nature of nucleation of aggregation, the nucleus structure cannot be detected or characterized directly. As an indirect probe into the structure of the nucleus, Kar *et al.* employed a series of substitutions installed into a polyQ peptide to enhance a β -hairpin fold¹⁰⁸. These alterations consist of: (1) coulombic interactions (two N-terminal negatively charged aspartic acid residues and two C-terminal positively charged lysine residues), (2) l-proline-glycine turns, which do not necessarily promote, but are compliant with a turn structure, (3) the stronger d-proline-glycine turn, which does independently promote turn formation, (4) a cysteine disulfide bond across the N- and C-terminus, (5) tryptophan zipper motifs, which rely on edge-edge stacking of two aromatic tryptophans, as well as additional hydrogen bonding, and (6) various combinations and permutations of these motifs, such as the tryptophan zipper motif plus a d-proline-glycine turn. All of these substitutions (except for the weakly β -hairpin promoting l-proline-glycine substitution), when installed into a K₂Q₂₃K₂ simple polyQ peptide, significantly enhanced the overall aggregation kinetics. EM of the aggregates showed typical amyloid-like ribbon structures of the final aggregates seen in other simple polyQ aggregates while FTIR of the final aggregates

had β -sheet signature banding at 1604-1606 cm^{-1} for glutamine N-H bending, 1625-1628 cm^{-1} for β -sheet, and 1656-1658 cm^{-1} for glutamine C=O stretching¹⁰⁸. Circular dichroism of these analogs mirrored the same time-dependent shift from random gross secondary structure to becoming β -sheet dominated, indicating that the monomeric ensemble does not gain appreciable β -structure in spite of the β -hairpin enhancing motifs. These results suggest that installation of β -hairpin encouraging motifs enhances, but does not alter, the aggregation pathway of simple polyQ peptides. These motifs achieve this by promoting the intramolecular folding required for nucleus formation, providing strong indirect evidence that polyQ nucleation of amyloid involves β -hairpin structure.

Applying the Eaton-Ferrone model to these peptides reveals that β -hairpin enhanced peptides, despite their short absolute polyQ repeat length, have a decrease in critical nucleus size previously only seen with expanded polyQ repeat lengths⁷⁷. All of the β -hairpin enhanced peptides tested, which should have a nucleus size of $n^* = 4$ due to their short polyQ repeat length, had a decrease of nucleus size to a monomeric $n^* = 1$. The decrease in nucleus size is indicative of a more efficient intramolecular nucleation event granted by installation of these β -hairpin motifs. As a result, the time spent in the lag phase, which is directly related to nucleation formation, is greatly shortened¹⁰⁸. Thus, by installing motifs that enhance intramolecular β -sheet folding, Kar *et al.* demonstrated that a β -hairpin structure plays a role in efficient nucleation of amyloid aggregation for simple (i.e. without confounding effects of flanking sequences) polyglutamine peptides.

Together, these results indicate that enhancing β -hairpin formation mimics the biophysical characteristics of expanded polyQ *in vitro*. This insight into the mechanism of aggregation of polyglutamine may lead to better designed therapeutic approaches that are

capable of targeting the nucleation event to prevent aggregation and potential subsequent toxicity.

1.5 MODEL SYSTEMS OF HUNTINGTON'S DISEASE

1.5.1 Monitoring Polyglutamine Aggregation *in vitro*

HD patient brains initially hinted at an aggregated state of huntingtin being the culprit of HD ¹⁹⁵. Indeed, the first HD mouse model, which was constructed in 1996, mimicked the characteristic protein aggregation and intranuclear neuronal inclusion formation seen in human HD patients ⁷. Shortly after, polyglutamine aggregation was first observed *in vitro* using a cleavable GST solubilizing tag fused to huntingtin exon-1, which found a concentration and polyQ repeat length dependence of aggregation ⁶. Electron micrographs and filter retardation assays were utilized to show a high molecular weight, SDS-insoluble amyloid aggregate reminiscent of scrapie prions and β -amyloid fibrils in Alzheimer's disease. Since then, a plethora of *in vitro* systems have been constructed to conveniently and accurately model the protein aggregation aspect of HD. Atomic force microscopy ^{201–203}, dynamic light scattering ⁹⁹, circular dichroism ¹⁰⁷, and more recently super-resolution microscopy ⁴³ and fluorescence correlation microscopy ⁸⁴ (Sahoo 2016 Manuscript Submitted) are all viable tools for quantitatively monitoring the aggregation process in real or near real time. Indirect biochemical methods of monitoring aggregation kinetics use rigorous disaggregation techniques coupled with centrifugation and HPLC to monitor loss of soluble protein ⁹⁹. Data derived from the kinetics of aggregation can be modeled using the Eaton-

Ferrone model to determine nucleus size n^* , nucleus equilibrium constant k_{n^*} , and Gibbs free energy of nucleus formation ΔG_{n^*} experimentally. Highly sensitive high throughput assays of this process allow for rapid screening of aggregation modifiers that is not possible with cell based methods. Advances in the understand of the biophysical mechanisms of huntingtin aggregation and how aggregation generates toxicity (i.e. whether there is a single “toxic species”) will help guide more sophisticated screening methods to identify aggregation and disease modifying drugs.

1.5.2 *In vivo* Models

1.5.2.1 Cell Culture Models A wide variety of immortalized HD cell lines exist to study huntingtin aggregation and cell toxicity. Historically, PC12 cells, derived from a pheochromocytoma of a rat adrenal medulla, were used as a convenient cell model for HD. PC12 cells are neuro-endocrine in origin and can be differentiated into neuron-like dopamine-synthesizing cells with the addition of nerve growth factor (NGF)²⁰⁴. These differentiated PC12 cells become post-mitotic, release vesicles containing dopamine, and form axonal branches. PC12 cells therefore offer a convenient cell model system without requiring primary neuron cultures. Stably inducible cell lines expressing WT human htt-Q₂₅-exon1-EGFP or pathogenic htt-Q₉₇-exon1-EGFP are readily available, easily cultured, and can be useful to screen for aggregation inhibitors in the context of a mammalian cell. Cell lines expressing mhtt have a polyQ repeat length and time dependence to inclusion formation, which appear to be perinuclear²⁰⁵. PC12 cells have also been an excellent cell culture system to study how structural limitations of a polyQ protein affects its ability to aggregate and cause toxicity²⁰⁶. However, PC12 cells

have recently come under scrutiny, as they do not wholly mimic the nuclear inclusions found in human HD neurons and are not as sensitive to the toxic effects of mutant huntingtin as primary neurons²⁰⁷. Other cell lines, such as SH-SY5Y²⁰⁸, derived from a human neuroblastoma, or SThdhQ111/111, derived from HD knock-in mouse striatal neurons, offer similar benefits in terms of ease of use and robust cytoplasmic aggregation. Unfortunately, as with PC12 cell lines, most non-primary neurons exhibit minimal toxic effects when expressing mhtt (cell death, caspase activation, etc.) and may only be useful to quickly screen for general cytoplasmic aggregation modifiers.

1.5.2.2 Primary Neurons Primary cortical, hypothalamic, or striatal neurons from rats or mice offer a more appropriate and sensitive cell culture model than immortalized cell lines. In human HD, the striatum and cortex are burdened with a heavy huntingtin aggregate load and selective neurodegenerative loss²⁰⁹. Rat²¹⁰ and mouse models expressing mutant human huntingtin, such as the R6/2 or YAC128, also mimic the spatio-temporal sensitivity of cortical and striatal neurons to mutant huntingtin^{7,168}. Therefore, these regions are of interest when designing *ex-vivo* cell culture models.

Embryonic rat primary cortical neurons can be robustly transfected and recapitulate valuable mutant huntingtin disease phenotypes, such as inclusion body formation⁸¹, intranuclear aggregation, and cell death²¹¹. Cell death and aggregate formation in primary neuron cultures often mirrors neuron loss and behavioral abnormalities in animal models. Primary cortical neurons have also been useful for screening small molecule inhibitors of aggregation²¹² and to study the role of wild type huntingtin⁵⁷.

In human HD, selective loss of medium GABAergic striatal neurons of the striatum is associated with the first brain regions to undergo massive neurodegeneration, followed by cortical neurons in the prefrontal cortex. This neuron-specific sensitivity is also seen in rat primary neurons: striatal and cortical neurons are both sensitive to mutant huntingtin toxicity, while striatal neurons have a modestly higher risk of death ²¹¹. Thus, primary neurons offer a sensitive and physiologically relevant cell culture method to monitor aggregation and neuron viability.

1.5.2.3 *Drosophila* as a tool to study neurodegeneration *Drosophila* provide a unique approach to modeling neurodegenerative diseases. *Drosophila* have been extensively utilized as a genetic model, including one of the first complete genome sequencing of any animal ²¹³. As such, the *Drosophila* model comes with a uniquely extensive molecular and genetic toolbox. Unlike many other model organisms, dozens of *Drosophila* lines have been engineered for site-specific ΦC31 integrase-mediated transgenesis ²¹⁴. This technology allows for non-random integration of a gene-of-interest into a variety of established gene *loci*. In combination with exhaustively characterized Gal4 lines ^{215,216} and a UAS-promoter sequence ²¹⁷, spatio-temporal expression of a gene of interest with minimal disruption to the genome can be achieved relatively easily. Together, these technologies give rise to the Gal4-UAS expression system, which is widely used to generate transgenic *Drosophila* ²¹⁸.

In addition to their ease and precision of transgenesis, *Drosophila* models also provide several robust endpoints for monitoring neurodegeneration. Many of the cells in the compound eye, such as the photoreceptor cell, are neuronal in origin and play supporting roles in the structure and health of the eye ²¹⁹. Degeneration of the structure, organization, and pigmentation

of the compound eye correlates well with CNS degeneration ²²⁰. Additionally, the eye is not necessary for the viability of the animal, so lethal compounds can be studied (or *vice versa*, compounds can be screened as modifiers of extremely toxic diseases). Therefore, eye morphology and depigmentation of the eye can be used as an indirect measure to quickly screen for neurodegeneration. This process is commonly used to screen for small molecule drugs and RNAs that modify disease states, which can be further studied more in depth in *Drosophila* or in other models ^{221–223}.

Drosophila also mirror the shortened lifespan ^{224,225}, dysfunctional locomotion ²²⁶, and histological pathologies seen in human HD patients ²²³. Therefore, *Drosophila* provide an optimal balance between robustness of endpoints and the power to study multiple transgenic lines in a cost and time efficient manner. HD *Drosophila* lines constructed by other labs tend to include greater than 100 glutamine repeats, which decreases median *Drosophila* lifespan to 20–45 days (down from ~65–80 days for wild type at 25 C or 29 C) ^{224,225}. The severe lifespan decrease associated with highly expanded polyQ mhtt strongly mirrors the shortened lifespan seen in juvenile HD patients.

In addition to lifespan studies, *Drosophila* behavioral defects can be monitored as a function of age. Locomotion decline can be measured by a Rapid Negative Geotaxis Assay (RING), which challenges flies to climb an arbitrary vertical distance in some amount of time ²²⁶. As flies age or develop locomotor defects, they are less capable of completing the climbing challenge. This assay is of particular significance to locomotor diseases, and is regularly employed when studying HD in flies.

Dozens of *Drosophila* HD models have already been constructed using a knock-in of the mutant human huntingtin gene. Full-length huntingtin ¹⁹⁷, htt-exon1 thru 12 ²²⁵, htt-exon-1 ^{222,223},

and truncated htt-exon-1^{196,224,227-230} have all been constructed with variations of N- and C-terminal fluorescent proteins and polyQ lengths ranging from 0 to 150+. These models differ in the fluorescent protein used (if any), the location of the gene insertion, expression level, and CAG/polyQ repeat length, though many of the different HD lines show a similar severity of HD phenotype between comparable CAG repeats. Additionally, other polyQ *Drosophila* models, such as Spinocerebellar ataxia type 1 (SCA1, ATXN1)^{152,231} and expanded polyQ peptides without protein context⁷⁸, all mirror the neurodegenerative phenotypes seen in human pathologies.

Therefore, *Drosophila* provide a convenient model to rapidly and thoroughly examine neurodegenerative phenotypes. They offer a strong compromise between ease of use, statistical power, and powerful genetic tools, while still having a complex CNS network capable of testing more sophisticated behavioral outcomes.

1.5.2.4 Other animal models of Huntington's Disease Other than *Drosophila*, mice and *C. elegans* have also been used to model Huntington's disease extensively. Mice have been historically useful in determining that polyQ-expanded htt-exon1 alone is sufficient and necessary to generate HD⁷. Both full-length and htt-exon1 HD mice exhibit reduced brain and body mass, hind-limb clasping, aggregate formation in the CNS, reduced balance *via* rota-rod performance, and premature death. Additionally, full-length polyQ-expanded htt-exon1 also generates a similar protein fragment, either through alternative splicing³⁵ or proteasomal cleavage³⁴. Mice expressing the htt-exon1 fragment appear to have accelerated disease onset, but this is difficult to directly compare between mice of different backgrounds, polyQ repeat lengths, and expression levels. Unfortunately, mice are costly, take years to develop new lines,

and can take months to years to run experiments. Even existing lines require a large time and financial commitment to achieve sufficient statistical power.

In contrast to mice, *C. elegans* are quick to develop and can be readily manipulated. Adult *C. elegans* contain a simple and well-defined set of exactly 302 neurons making up their nervous system. This simplifies some complications of studying neurodegeneration, but the nervous system of *C. Elegans* may not have the complex interconnectivity needed to accurately model a human brain. Despite this limitation, *C. Elegans* have been useful in studying the heat shock protein response to aggregated polyQ proteins^{232,233} and provide a convenient model to quickly screen for HD modulating drugs.

1.6 CURRENT THERAPEUTIC APPROACHES

1.6.1 Small Molecular inhibitors of polyglutamine aggregation

Dozens of disease-modifying small molecules have shown promise pre-clinically in cell and animal models. Several have advanced into human clinical trials, but currently no drug therapy has been approved by the FDA to slow, delay, or prevent the progression of HD in humans. Most therapies have instead failed to show efficacy in Phase III²³⁴.

Methylene Blue, a dye originally used to visualize amyloid aggregates, shows promise as a disease-modifying drug. Methylene Blue is already FDA approved for treating methemoglobinemia and can cross the blood-brain barrier. Recent findings in cells, *Drosophila*, and R6/2 HD mice show that Methylene Blue can decrease mhtt oligomer size as well as

decrease the accumulation of large insoluble mhtt aggregates²¹². Methylene Blue also increases lifespan in HD *Drosophila* and R6/2 mice, but only when given before symptoms appear²¹². In clinical trials, Methylene Blue showed promise after successfully completing a Phase IIb clinical trial for mild to moderate Alzheimer's Disease, slowing AD progression by 81% over one year²³⁵. Subsequent trials (conducted under TauRx Therapeutics) have not been filed. A newer Methylene Blue analog LMTXTM is currently being tested in other tauopathies in Phase II trials.

C2-8 is a polyQ aggregation inhibitor first identified in a yeast screen²³⁶. In mice, C2-8 was shown to inhibit mhtt polyQ aggregation in transiently transfected mammalian cells and R6/2 brain slice cultures²³⁷. C2-8 also has a dose-dependent rescue of neurodegeneration using a *Drosophila* photoreceptor assay²³⁶. Furthermore, in R6/2 mice, C2-8 is non-toxic, orally available, crosses the blood-brain barrier, and reduced mhtt aggregate size²³⁷. An independent study confirmed that C2-8 crosses the blood-brain barrier, is well tolerated, and reduced mhtt nuclear aggregate size²³⁸. However, C2-8 had no benefit to lifespan, Rotarod performance, hang-wire tests, or striatal pathology in mice. No further work or clinical trials have since been published on C2-8. The unfortunate results of C2-8's failures are similar with several other compounds, such as the benzothiazole aggregation inhibitor riluzole, which reduces mhtt aggregate burden in R6/2 brain slices, but is ineffective when administered to mice²³⁹.

There are several reasons why anti-aggregation small molecules seem promising during *in vitro* screens but are not effective *in vivo*. For instance, drugs may inhibit aggregation at high concentrations *in vitro*, but may not be able to achieve those concentrations *in vivo* due to toxicity, lifetime, and bioavailability. Secondly, because these screens are not mechanistic based, many of the anti-aggregation small molecules found have generic colloidal activity, which have not been successful *in vivo*²⁴⁰, or simply redirect aggregation to other non-amyloid pathways,

which do not provide therapeutic effect *in vivo*²⁴¹. Third, several screens also suffered from flawed screening protocols. Protocols using recombinantly expressed htt-exon1, such as htt-exon1 produced by the cleavage of htt-exon1 from a solubilizing GST tag⁴⁵, would mutilate a significant portion of the htt^{NT} domain. Thus, these screens were not capable of identifying anti-aggregation inhibitors that go through an htt^{NT}-based aggregation mechanism. There is therefore a need to develop a better understanding of the aggregation pathways of huntingtin and what role different huntingtin aggregates play in causing neurodegeneration. In this way, more sophisticated screening methods could be developed that better address a relevant toxic species of huntingtin.

1.6.2 Small Molecules to Target Biological Pathways

As an alternative approach to identifying anti-aggregation compounds, other groups are targeting biological pathways whose augmentation or manipulation may lead to a better cellular response to toxic mutant huntingtin.

FTY720 is a sphingosine analog that acts on four sphingosine-1-phosphate receptors^{242,243} and is a current treatment for multiple sclerosis²⁴⁴. FTY720 shows good blood-brain barrier penetration²⁴⁵, where it acts to increase BDNF production and reduce NMDA excitotoxicity²⁴⁶. This type of activity may have a therapeutic effect in other neurodegenerative diseases. In HD R6/2 mice, FTY720 shows only a modest increase in lifespan and ladder tasks when given before disease onset²⁴⁷. FTY720 has not yet entered clinical trials.

Several lines of evidence suggest copper, zinc, and other metals may play a role in neurodegenerative diseases, including HD^{248–250}. Whether altered metal accumulation plays a

primary or secondary role in neurodegeneration is unclear. PBT2, a second-generation metal protein-attenuating compound, acts to restore copper and zinc ion homeostasis. Reach2HD ran a Phase II trial of PBT2 showing safety and tolerability, but failed to meet seven out of eight of its secondary outcomes (for which it was not statistically powered for). The only secondary outcome met, a reduction in brain atrophy, involved only two brain scans from placebo and drug patients. The efficacy of PBT2 and other metal chelators to ameliorate HD in humans remains to be seen.

Transglutaminase can cross-link huntingtin protein and trigger aggregation^{251,252}, and may therefore be involved in the etiology of HD. Cysteamine, which is a competitive inhibitor of transglutaminase, may be able to ameliorate this process. Cysteamine is already FDA approved to break up cysteine crystals in the kidney for nephropathic cystinosis patients²⁵³. Cysteamine prolongs survival in HD mice^{254,255} and is also neuroprotective in R6/2²⁵⁶ and YAC128 HD mice models²⁵⁷. A recent phase II trial at 450-1800 mg/day showed good tolerability, but no significant differences in the Unified Huntington's Disease Rating Scale (UHDRS), cognitive, behavioral, or functional tests. However, the study was unpowered to test HD outcomes, lasting only 16 weeks with 16 patients. Raptor Pharmaceuticals is conducting a Phase II/III trials with cysteamine (RP103). After 3 years, RP103 showed a 58% slower progression of Total Motor Score worsening. While promising, these results used non-pre-specified subgroups that were stratified post-hoc, not controlled for concomitant medications, and should therefore be interpreted cautiously.

Several other drugs are currently being tested for safety and tolerability in Phase II trials, with secondary efficacy outcomes. Phosphodiesterase 10A (PDE10A) hydrolyzes the secondary messengers cyclic adenosine monophosphate and cyclic guanosine monophosphate

predominantly in medium spiny neurons of the striatum²⁵⁸ and may play a role in the changed neurotransmission seen in HD^{259,260}. PDE10A inhibition partially ameliorates striatal pathology in R6/2 HD mice²⁶¹. Omeros (OMS824) and Pfizer (PF-02545920) are testing such inhibitors, but Omeros suspended a Phase II trial in humans for safety concerns from parallel pre-clinical studies in rats, where adverse observations were seen in rats receiving OMS824 dosing several times higher than that measured in humans.

Deep brain stimulation provides beneficial outcomes in some Parkinson's disease patient's symptoms and may also work to help manage chorea symptoms in HD^{262,263}. Deep brain stimulation in HD is being addressed in a small Phase II trial to assess UHDRS-TMS primary endpoints (clinical trial NCT00902889 at clinicaltrials.gov).

Many small molecule drugs have been systematically screened as potential therapies in HD, but none have been found. Many promising leads, such as Antinomycin D identified from a 11,000 natural product extract screen²⁶⁴, PGL-135 identified from a 184,000 small molecule screen^{239,265}, screens identifying hits from the NINDS NIH Custom Collection of 1,040 compounds²⁰⁷, screens targeting autophagy^{266,267}, and many others have all been fruitless. While there is still continued research developing small molecule modifiers of HD, it is important to also continue hypotheses-driven therapeutic approaches in parallel with designing more sophisticated screening methods.

1.6.3 Huntingtin Lowering Strategies

Because Huntingtin is an autosomal dominant genetic disease, many groups have hypothesized that reducing or eliminating huntingtin expression of the mutant allele will prevent or reverse disease. Work by Dr. Reits shows that mhtt aggregates can be cleared, albeit painstakingly, from

the cell when mhtt expression is turned off. In this system, disease progression is reversed^{268,269}. This gives hope to mhtt lowering strategies that likely will be given to post-symptomatic patients.

Early studies using RNA interference (RNAi) showed improved phenotypes in HD mouse models as mutant htt levels were lowered²⁷⁰⁻²⁷². Many other research groups later contributed to this work by designing improved AAV-mediated delivery systems, modifying RNAi to enhance their half-life, and improvements to allele-selectivity^{273,274}. Although this avenue is promising, allele-selectivity may play a critical role in maintaining a healthy CNS. Complete reduction of wild type htt leads to progressive neurodegeneration and other CNS pathologies^{62,275}, but a partial reduction of 25-35% had no adverse effects in mice after 9 months of treatment²⁷⁶.

DNA editing strategies may also become a viable option. Deletion of the aberrant mhtt gene can be achieved *via* specifically engineered zinc finger nucleases²⁷⁷. Zinc fingers can be engineered as sequence-specific endonucleases that induce double strand breaks of the target gene loci^{278,279}. Zinc finger repressors targeting mhtt already have exciting preliminary results in an R6/2 HD mouse model²⁸⁰, but will still likely require the same allele-specific approaches as RNAi designs. Additionally, recent advances in CRISPR/Cas9 offer a potentially more powerful gene-editing tool. Use of the CRISPR/Cas9 technology has generated some preliminary results of homologous recombination rates up to 12% in an induced pluripotent stem cell HD model²⁸¹. Advances in these systems may prove efficient enough to one day silence the mhtt gene.

1.6.4 Peptide Based Inhibitors of Aggregation

If mutant huntingtin gains toxicity as a symptom of aggregation into amyloid, then identifying anti-aggregation strategies is a logical step in generating HD therapeutics that treat the underlying cause of HD onset and progression. Despite a large amount of resources being spent on the high-throughput drug screens of small molecules, no viable drug candidate has been found^{238,239}; targeting protein-protein interactions using small <500 Da molecules to interrupt large featureless surfaces may prove a Sisyphean task. That is, small molecules, which are unable to make sufficient non-covalent interactions with their target, may be inherently poor aggregation inhibitors. One alternative strategy to small molecule screening is designing hypothesis-driven aggregation modifiers of larger peptidomimetic molecules, which could be capable of making a sufficient number of contacts with mhtt in order to influence its aggregation properties.

A number of peptides and proteins have shown anti-polyQ aggregation activity, though their mechanism of action is unclear. P42 is peptide comprised of 23 amino acids from the huntingtin protein (amino acid sequence: AASSGVSTPG SAGHDIITEQ PRS) that decreases aggregate burden by filtertrap assay and partially rescues HD *Drosophila* phenotype²⁸². The peptide QBP1 (amino acid sequence: SNWKWWPGIF D) was found in a phage display search for amino acid sequences that bind polyQ and inhibits aggregation *in vitro* with an IC₅₀ of around 5 μM^{283,284}. As with P42, the mechanism by which QBP1 inhibits aggregation is unknown and this lack of knowledge limits the potential to develop more potent inhibitors. Neither of these inhibitors has been independently reported to achieve efficacy in a pre-clinical setting. Other peptides have a proposed mechanism of inhibition, such as bivalent suppressors developed by Kazantsev *et al.*, which rescues HD phenotype in *Drosophila*²⁸⁵.

Several other protein screens found polyQ aggregation inhibitors that also contain a polyQ domain. Many yeast proteins found to suppress htt103Q toxicity in proteome-wide screens are other glutamine- and asparagine-rich prion-like proteins ^{286,287}. Other polyQ-containing proteins, such as histone deacetylase 4 ^{288,289}, glycine threonine serine repeat protein, nuclear polyadenylated RNA-binding protein 3, and minichromosome maintenance protein 1 ²⁹⁰ also modulate mhtt aggregation and toxicity. These results reveal that polyQ and other prion-like domains can interact with and modulate each other. A better understanding of how this processes works could lead to new therapeutic avenues, which may have more success at inhibiting polyQ aggregation than small molecules.

Modified polyQ peptides have shown some promise in inhibiting polyQ aggregation *in vitro*. Polyglutamine peptides with N-methylation of either the backbone or the side chain amides are inhibitors of polyglutamine aggregation ²⁹¹. Of these, the most potent inhibitors were those that left a portion of the polyQ chain intact with occasional side chain glutamine amide methylations. Further work in simple polyQ peptide inhibitors comes from Kar *et al.*, who confirmed that a number of chemical modifications inhibit polyQ aggregation both in *cis* and in *trans* (Kar *et al.* Manuscript Submitted). These modifications include main chain amide methylation and substituting L-glutamine for D-glutamine. Other non-chemical modifications, such as glutamine to proline substitutions, can also inhibit polyQ aggregation, particularly elongation, both in *cis* and in *trans* ²⁹². Thakur demonstrated that these polyQ inhibitors could participate in the dock (an initial reversible binding) and lock (completion of the elongation cycle) mechanism on the growing end of amyloid, but block subsequent steps by essentially crippling the surface of the growing end. Elongation is therefore blocked until the inhibitor eventually dissociates. Although these inhibitors primarily target the elongation mechanism, they

may also inhibit nucleation of aggregation, due to the nucleus requiring some level of elongation to become stable enough to sustain itself¹⁷⁸. This work exemplifies the importance of how peptiomimetics may be able to make sufficient non-covalent interactions between the inhibitor and its target polyQ peptide, thus modifying mutant huntingtin's aggregation properties.

Beyond simple polyQ peptides, huntingtin's N-terminus (htt^{NT}) is also involved in the aggregation mechanism of huntingtin (Section 1.4.4). Taking advantage of this, Mishra *et al.* showed that htt^{NT} peptides are able to compete with htt^{NT}-Q₃₇P₁₀K₂ for oligomer formation¹⁸⁹. This process delays the nucleation of aggregation; however, this inhibitory effect is eventually overcome, even when superstoichiometric ratios of inhibitor are used. This is likely due to both the statistical likelihood of some mhtt oligomers forming without the htt^{NT} inhibitor and other inhibited mhtt peptides nucleating through the less efficient simple polyQ nucleation mechanism¹⁸³. Scrambled htt^{NT} sequences were less capable of inhibiting htt^{NT}-Q₃₇P₁₀K₂ aggregation; however, a few scrambled htt^{NT} sequences that retained an ability to form α -helical oligomers continued to exhibit inhibitory effects, strongly suggesting that htt^{NT}'s ability to compete for α -helical coiled coils is part of its mechanism of inhibition. Indeed, post-translational modifications to the htt^{NT} domain, such as phosphorylation of Ser13 or Ser16, limits nucleation and aggregation efficiency, presumably by disrupting the ability of htt^{NT} to form α -helical bundles^{188,189}.

Small peptides that offer a combination of the above strategies may be more effective inhibitors; for instance, linking a proline-interrupted polyQ elongation inhibitor (Kar 2016 Manuscript Submitted) with the htt^{NT} domain. This class of peptides could be able to both compete for α -helical tetramer formation and inhibit nucleation and also inhibit elongation of pre-formed growing amyloid fibrils¹⁸⁹. Whether or not these aggregation inhibitors can mitigate

HD progression *in vivo* remains to be seen. Peptidomimetics also pose a challenge of drug delivery; large peptides will not likely be able to passively diffuse through the blood brain barrier or pass through cell membranes. Advances in peptide delivery technologies will be vital to the feasibility of using peptidomimetics in the clinic. However, until those technologies are developed, peptidomimetics will remain as proof-of-principle research tools.

1.7 MATERIALS AND METHODS

Water (HPLC grade), acetonitrile (99.8% HPLC grade), formic acid, and HFIP (99.5%, spectrophotometric grade) were from Acros Organics. Trifluoroacetic acid (99.5%) was from Pierce and phosphate buffered saline from Invitrogen.

Peptide Synthesis and Preparation: All peptides were synthesized at the Small Scale Synthesis facility at the Keck Biotechnology Resource Laboratory of Yale University and supplied crude. All peptides were purified and disaggregated as previously described^{77,293}.

Sedimentation Assay: Following rigorous disaggregation, ultracentrifugation (100,000 rpm, 4 C, 2 hours), and passage through a 0.02 μm filter, samples were allowed to aggregate in PBS buffered water. At specific times, aliquots of the reaction were centrifuged (21,000 g, 4 C, 30 minutes), and the supernatant concentrations were measured using analytical HPLC based standard curves, as previously described⁹⁹. Nucleation analysis was carried out using the initial

rates from the sedimentation assay to generate concentration and t^2 plots, as previously described^{77,107,293}.

Electron Microscopy: Electron microscopy was conducted as described previously⁷⁷ in the Structural Biology Department's EM facility using a Tecnai T12 microscope (FEI) operating at 120 kV and 30,000× magnification and equipped with an UltraScan 1000 CCD camera (Gatan).

Fourier Transform Infrared Spectroscopy: Aggregates from end time points of each reaction were isolated and analyzed on an ABB Bomem FTIR instrument. A total of 400 scans were collected at room temperature with 4 cm^{-1} resolution. Residual buffer absorption was subtracted to yield second-derivative minima. PROTA software (Biotools, Inc.) was used to identify spectral components.

Circular Dichroism: Far-UV CD measurements were performed on a JASCO J-810 spectropolarimeter using a 1-mm path length cuvette. CD samples were prepared in parallel to sedimentation assays (10-30 μM). CD spectra were analyzed using the CONTINLL program from the CDPro package.

Statistical analysis. All sedimentation assays contain error bars representing standard error of the mean as technical replicates of $n = 3$; in some cases error bars are smaller than the datapoint symbols and so are not evident. Critical nucleus error is presented as a 95% confidence interval of the slope from log-log plots. Primary neuron toxicity and aggregation data error bars representing standard deviation, analyzed using one-way ANOVA multiple comparison's with Tukey's multiple comparisons test. Primary neuron colocalization analyzed using a Pearson's correlation. Drosophila survival was statistically analyzed using Log-rank Mantel-Cox test of Kaplan-Meier survival curves, *** = $p < 0.0001$. Drosophila locomotor activity error bars

representing standard error of the mean, analyzed using two-way ANOVA with Bonferroni's multiple comparisons test *** = $p < 0.01$. All statistical data was analyzed using GraphPad Prism software. At 80% power, 5% significance, assuming a standard deviation of 10 days, a sample size of 100 flies per condition was found to be sufficient to detect a change in mean lifespan of 4 days. The value of 10 days for lifespan standard deviation was estimated from previous survival curves of wild type and HD flies.

Primary Neurons. Rat Primary Cortical Neurons were isolated from E18 day pups. 2 million neurons were co-transfected with 1.5 + 1.5 μg DNA and plated with Gibco Neurobasal Medium (ThermoFisher #21103-049) + L-glutamine on poly-D lysine coated (100 μL at 0.1 mg/mL, overnight) glass bottom dishes (MatTek) for live imaging or glass coverslips. Because one of our cell models combines co-expression of a pathogenic htt-ex1 with an inhibitory htt-ex1 derivative, we performed co-transfections using vectors encoding EGFP or mCherry to standardize the number of transgenes and total DNA content. For viability assays, live neurons were imaged on a Nikon A1 Confocal Microscope (40x oil immersion lens at 2.0 zoom) at room temperature. Samples for confocal imaging were sequentially scanned with individual lasers (488, 561, and 640 nm) and appropriate emission band pass filters (500-550 and 575-625 nm) or long pass filter (650LP). 75 μL of fresh NucRed Dead 647 (ReadyProbes) in 1 mL imaging saline was added to neurons and incubated at 37 °C for 20 minutes. Neurons were imaged for the following 45 minutes. At least 50 neurons per condition were captured. For aggregate counting, neurons grown on coverslips were fixed in 4% paraformaldehyde and imaged using an Olympus Fluoview 1000 confocal microscope (60x oil immersion lens) at room temperature. Random fields were scored blind (>100 cells per condition over 3-5 independent experiments) for the

percentage of Map2 positive neurons also positive for EGFP or mCherry puncta. Images were analyzed using ImageJ software.

Drosophila. Huntingtin analogs were sub-cloned into identical pUAS plasmids containing a w^[+] marker and an AttB construct. Site-specific insertion was achieved using the AttP18 site on the X chromosome. *Genetic Services* performed the embryo injections. Flies were screened for the w^[+] marker and balanced over *FM0*. Flies were then mated to yield homozygous huntingtin alleles on either X chromosome, and *elav-Gal4* on the 2nd chromosome for expression. Upon eclosion, non-virgin female flies were selected and kept at 29 C in 12 hour light cycles, 16 flies per vial on standard fly food. Media was changed every other day and the number of live and dead flies was counted. A minimum of 100 flies per condition was tested.

Drosophila Behavioral Assay. Rapid Iterative Negative Geotaxis (RING) assay was performed at the indicated ages. Age-matched samples were transferred to fresh media-free vials and allowed 1 minute to acclimate. The flies were knocked down with gentle tapping and filmed. Height climbed after 8 seconds was recorded, with 5 vertical cm being the maximum. A minimum of 30 flies per condition was tested.

2.0 THE ROLE OF BETA-STRUCTURE IN NUCLEATION AND AGGREGATION OF HUNTINGTIN

2.1 INTRODUCTION

Huntington's disease (HD) is one of at least ten expanded CAG repeat diseases^{26,27,150,292}. The huntingtin protein (htt) totals around 3,200 amino acids and 350 kDa, but pathogenesis is contained to the first exon (htt-exon1), which contains the polyglutamine (polyQ) expansion^{107,179,294}. The N-terminal exon-1 accounts for ~3 % of the total huntingtin protein, and has been found as a cleaved product in transgenic animal models and human brains, which correlates with neuropathology^{8,40,195,295}, but may also be formed as a mis-spliced exon1³⁵. Htt-exon1 contains three sequence regions: the 17 amino acid N-terminus (htt^{NT}), followed by the disease causing polyQ sequence, and finally a poly-proline/proline-rich segment. Many of the polyQ diseases have a pathological repeat length threshold of 30+ glutamines in their encoded disease-specific proteins, though this varies between diseases. In SCA6, for instance, the threshold for disease is as few as 21-30 glutamine repeats²⁹⁶. In Huntington's disease, the repeat threshold begins at 36 glutamine repeats, and gains full penetrance by 40^{297,298}. Generally, a higher polyglutamine repeat length results in an increase of disease risk and decreased age of onset *in vivo* and increase aggregation kinetics *in vitro*^{6,26}. A detailed mechanism of how expanded polyQ tracts grant

huntingtin a toxic gain-of-function remains unclear and is one major hurdle limiting hypothesis-driven therapeutics.

Previous work from the Wetzel laboratory showed that simple polyQ peptides (primary sequence format $K_2Q_NK_2$) aggregate according to a nucleated growth polymerization mechanism⁷⁷. Kar *et al.* demonstrated that polyQ peptides with ≥ 26 polyQ repeats nucleate aggregation as a monomer, resulting in a substantial boost to nucleation efficiency and kinetics. Additionally, installing β -hairpin encouraging motifs in simple polyQ peptides also promotes monomeric nucleation, suggesting a role of β -hairpin architecture in nucleation¹⁰⁸. However, flanking sequences in polyQ proteins can alter the aggregation mechanism, which ultimately has a significant impact on aggregation kinetics^{38,176,188,189}. For example, the htt^{NT} region of huntingtin has a dramatic enhancing effect on the aggregation kinetics and toxicity of polyQ sequences¹⁷⁶. Htt^{NT} achieves this by introducing an intermediate oligomeric phase, which has a net result of accelerating huntingtin's aggregation mechanisms¹⁸³. The htt^{NT} segment mediates oligomerization and accelerates nucleation by forming homo-oligomers *via* α -helical-like bundles therefore bringing together their associated polyQ sequences and artificially increasing the local concentration of aggregation prone polyglutamine domains¹⁸³.

The detailed mechanism by which the htt^{NT} flanking sequence and its subsequent oligomerization accelerates nucleation of aggregation is poorly understood. This lack of a detailed mechanism limits the ability to design hypothesis driven inhibitors of nucleation. In order to indirectly probe the mechanism of nucleation, we employed a modified version of the previously described β -hairpin enhancing motifs¹⁰⁸. If β -hairpin architecture plays a role in htt-exon1 nucleation, we would expect htt-exon1 harboring β -hairpin encouraging motifs to have accelerated nucleation kinetics, similar to the results from simple polyQ peptides. However, if

nucleation occurs through a different process, a β -hairpin encouraging motifs may dampen or be neutral towards nucleation kinetics. A more detailed understanding of how htt-exon1 nucleates aggregation in the oligomer phase is crucial to designing target-based aggregation inhibitors.

Additionally, there is currently a robust debate over the major toxic species (Section 1.3). A number of toxic species have been proposed: misfolded monomer, tetramers, oligomers, spheroids, protofibrils, soluble β -rich aggregates, protofibrils, amyloid, and inclusion bodies. Studies attempting to identify the toxic species heavily rely on correlations between the appearance of huntingtin species and toxic events. However, one significant hurdle in identifying the toxic species is huntingtin's potential to rapidly generate a heterogeneous mixture of monomer, oligomer, and a diverse array of higher ordered species *in vitro* and *in vivo* (Sahoo 2015 Manuscript Submitted). Other recent studies identified the presence of small aggregates in what were previously thought of as a soluble monomer or oligomer pool in cells⁴²⁻⁴⁴. These recent findings bring the methodology of correlative studies into question and create new questions regarding the toxic conformational species of huntingtin. That is to say, it is entirely plausible that previously undetected small and diffuse amyloid-like aggregates could contribute significantly to toxicity; previous studies may be difficult to reinterpret in this new light, as traditional confocal microscopy could blur the distinction between monomer, oligomer, and diffuse aggregate.

As a means to circumvent these technological limitations, we have generated a series of huntingtin analogs capable of rapid fibril formation ("hyper-amyloid") or are incapable of forming amyloid and are blocked at the oligomeric phase ("hypo-amyloid") (Section 3.0). The hyper-amyloid analog, in spite of its short absolute polyQ repeat length, rapidly fibrillizes. The

toxicity profiles of these peptides may help shed light on whether inherent amyloidogenesis or oligomerization is responsible for HD phenotype.

In this study, we use chemically synthesized peptides to explore two separate but related issues. Firstly, we designed peptides that contain a β -hairpin enhancing motif in a polyQ sequence that is compatible with htt-exon1 flanking sequences. Previously studied motifs, such as an α -acetyl tryptophan zipper, could not incorporate N-terminal flanking sequences, which are crucial to huntingtin aggregation. By redesigning this structural element, we can now study what role, if any, β -hairpin motifs play in a htt-exon1 background. A clearer understanding of the nucleation events that take place in oligomeric htt-exon1 is critical to designing future inhibitors of nucleation and aggregation. Secondly, these new β -hairpin motifs no longer require special chemical modifications. This allows us the ability to use standard genetic tools to express the hyper-amyloid construct *in vivo* to test its associated toxicity. Any toxicity associated with the expression of a hyper-amyloid protein may help identify how polyQ sequences gain toxic function.

2.2 RESULTS

2.2.1 Design of a β -hairpin peptide compatible with htt-exon1

We previously described a series of simple polyQ peptides demonstrating a relationship between enhanced intramolecular β -hairpin formation and accelerated nucleation of aggregation¹⁰⁸. By installing these β -hairpin enhancing motifs, simple polyQ peptides formed efficient monomeric

nuclei (critical nucleus, $n^* = 1$), had reduced lag-phase kinetics, and accelerated overall kinetics of amyloid aggregation, despite a nominal polyQ repeat length. The most amyloid competent peptide, AcWQ₁₁pGQ₁₁WTGK₂, formed amyloid-like aggregates significantly faster than a K₂Q₃₇K₂ positive control. Based on these results, we reasoned that if similar motifs could be introduced into a htt-exon1 type background, we could address unresolved issues about the relative roles of polyQ repeat length and the presence of the htt^{NT} segment in controlling nucleation of amyloid formation. We also realized that if such sequences could be arranged to be compatible with ribosomal synthesis, we could address important questions about polyQ toxicity in HD using a novel approach.

To accomplish this, we modified AcWQ₁₁pGQ₁₁WTGK₂, a previously employed β -hairpin enhance peptide¹⁰⁸ (Table 1), by first altering the tryptophan zipper (trp-zip) by substituting the α -acetylated tryptophan with two small flexible glycines. Loss of the α -acetyl group is predicted to destabilize the capping ability of the trp-zip motif by ~ 4 kJ/mol²⁹⁹, but its removal is required to allow installation of the upstream htt^{NT} segment. Secondly, in order to make cellular expression possible, we replaced the previously employed _D-Pro-Gly β -turn with _L-Pro-Gly. Since _L-Pro-Gly does not actively enhance aggregation kinetics like _D-Pro-Gly, but rather is only relatively passively compatible with β -turns^{179,300,301}, it was not clear that the _L-Pro-Gly sequence would impart any aggregation rate enhancement. _L-Pro-Gly would also destabilize other secondary structures, such as an extended β -chain or α -helix. Together, the modified trp-zip and _L-Pro-Gly are predicted to theoretically stabilize a β -hairpin conformation approximately -2 to -3 kJ/mol²⁹⁹. This is roughly in line with other modifications, such disulfide bonds between the chain termini (-4 to -4.5 kJ/mol³⁰²), Coulombic effects at chain termini (-1.5 to -2.5 kJ/mol²⁹⁹), _L-Pro-Gly alone (-1.4 kJ/mol), and the stronger acetylated tryptophan zipper

(-6.9 kJ/mol)¹⁰⁸. Thus, the final product is a hyper-amyloid competent β -hairpin enhanced peptide that is also compatible with the endogenous htt flanking sequences and can feasibly be expressed *in vivo* using standard expression methods (“ β HP”; Table 1).

Furthermore, these motifs are unlikely to contribute to other secondary structures; proline, glycine, and tryptophan have relatively low propensities to directly participate in α -helix or β -sheet secondary structure^{303,304}. Therefore, if the true nucleus structure were other than a β -hairpin, the addition of these motifs would likely act to destabilize the nucleus and retard aggregation.

We first tested our *in vivo* compatible β -hairpin construct using a simple polyQ model (format $K_2Q_NK_2$). Negative control $K_2Q_{23}K_2$ aggregates with a long lag phase, even at relatively high concentrations of 130 μ M (Figure 1). Positive control $K_2Q_{37}K_2$ reaches $t_{1/2}$ at 140 hours at 15 μ M, while the β HP peptide aggregates with $t_{1/2} = 45$ hours at 18 μ M (sequence: KKGGWQ₁₁PGQ₁₁WTGKK, Table 1), despite only containing 22 total glutamines. Thus, β HP aggregates substantially faster than a comparable $K_2Q_{23}K_2$ and even somewhat faster than $K_2Q_{37}K_2$. The aggregation kinetics profile of the β HP peptide exhibits a shortened lag-phase, suggesting that nucleation of aggregation is relatively more efficient compared to $K_2Q_{23}K_2$ and even a peptide at the disease-repeat threshold, $K_2Q_{37}K_2$.

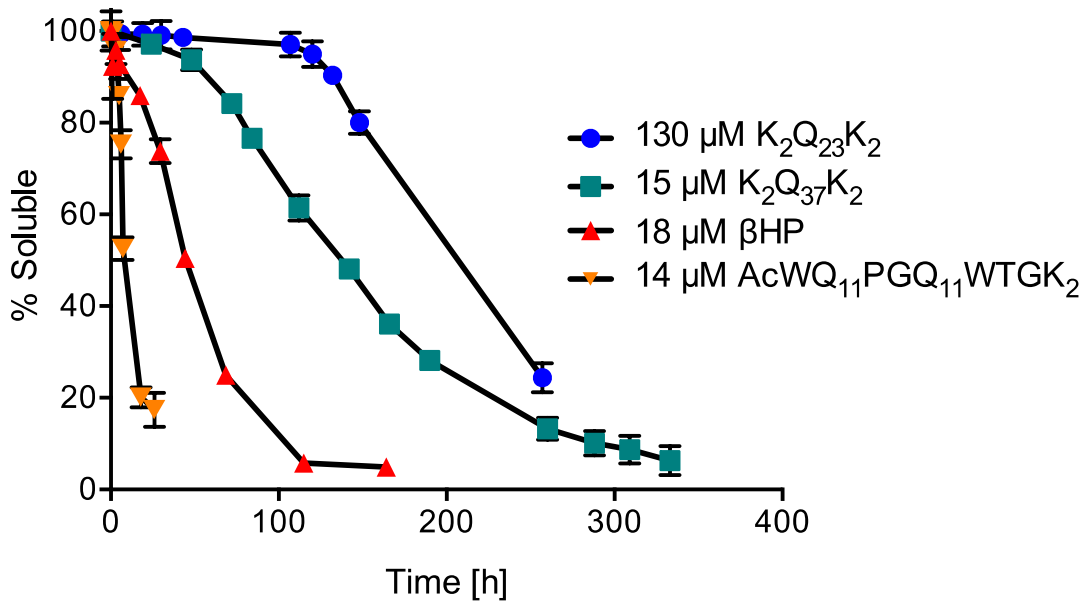


Figure 1: Sedimentation Analysis of Simple PolyQ Peptides. Time-dependent loss of monomeric peptide from solution upon incubation in PBS at 37 °C.

The initial aggregation kinetics of simple polyQ peptides can be mathematically modeled using an Eaton-Ferrone kinetics model given in Equation 2^{107,178}, where K_{n^*} is the equilibrium constant of nucleation, k_+^2 is the aggregation elongation constant (11,400 liters/mol*s)¹⁷⁷, t is time in seconds, C is the initial monomer concentration, and Δ is the molar concentration of the soluble fraction converted to insoluble aggregates at time t .

Equation 2: Eaton-Ferrone Simple PolyQ Nucleation Model

$$\Delta = \frac{1}{2} (k_+^2)(K_{n^*})(C^{(n^*+2)})(t^2)$$

Information about the nucleation and elongation process can be obtained by plotting the decay in soluble concentration Δ for early reaction time points (typically any data point with >85% remaining solubility) versus t^2 , which isolates a slope of m , given in Equation 3:

Equation 3: t^2 Plot

$$\Delta = \left[\frac{1}{2} (k_+^2) (K_{n^*}) (C^{(n^*+2)}) \right] * (t^2) + 0$$

$$y = \quad \quad \quad m \quad \quad \quad x + b$$

Equation 3 thus yields $\text{SlopeA} = 1/2(k_+^2)(K_{n^*})(C^{(n^*+2)})$, which contains the elongation constant k_+^2 , a known value, the equilibrium constant K_{n^*} , the initial monomer concentration C , a known value, and the critical nucleus size n^* . To isolate n^* from Equation 3, one can plot the log of the rate Δ versus the log of SlopeA for a series of reactions with varying starting concentrations (Equation 4). The slope of that resulting “log-log” plot equals $n^* + 2$ (i.e. if the slope of the log-log plot is 6, then $n^* = 4$, a tetramer). Equation 3 would be implemented for each reaction of varying starting concentration, resulting in a single data point per kinetic profile. A minimum of 3-5 points can be used to generate a line in the log-log plot. These steps are necessary in order to rearrange the Eaton-Ferrone nucleation kinetics model and isolate the nucleus size n^* .

Equation 4: log-log Plot

$$\log(\text{slope } A) = (n^* + 2) * \log(C) + \log[\frac{1}{2}(k_+^2)(K_{n^*})]$$
$$y = m x + b$$

In order to determine the critical nucleus size for β HP, we first characterized the concentration dependence of β HP aggregation at varying initial concentrations (Figure 2), then generated a t^2 plot from the early data points (Figure 3) and subsequent log-log plot (Figure 4) as previously described^{77,108,177,184}.

In a simple polyQ model, short polyQ repeats inefficiently form a tetrameric nucleus ($\text{polyQ} \leq 24$, $n^* = 4$), while longer polyQ repeats are monomeric ($\text{polyQ} > 26$, $n^* = 1$). Based purely on its modest absolute polyQ repeat length of 22, the β HP peptide is predicted to aggregate *via* an inefficient tetrameric nucleus ($n^* = 4$). Despite this, the β HP peptide efficiently builds a monomeric nucleus ($n^* = 1$), similar to pathogenic repeat lengths of polyQ (Figure 4).

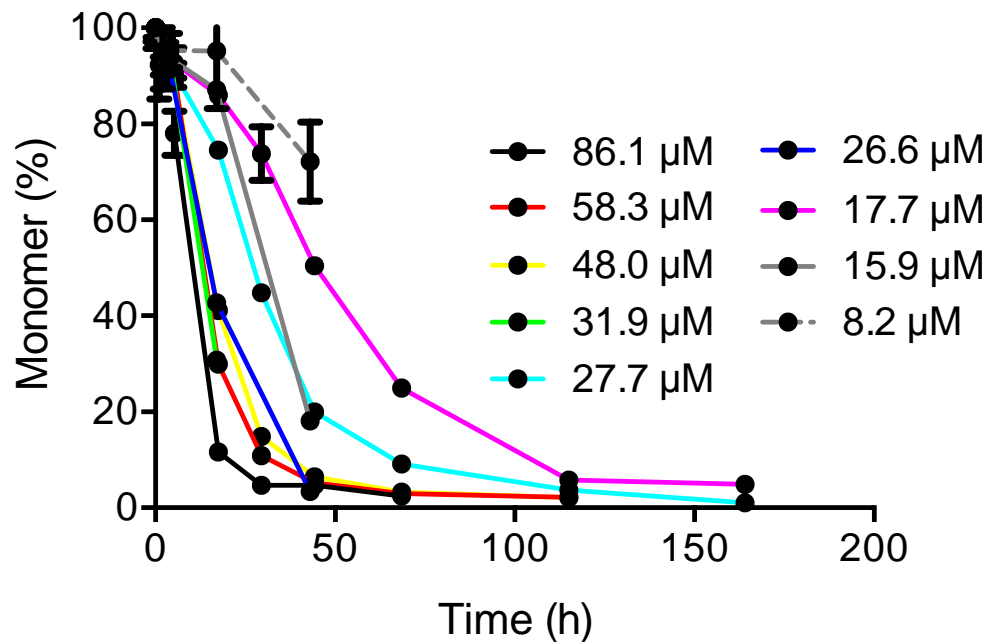


Figure 2: Concentration Dependence of Aggregation for the β HP peptide.

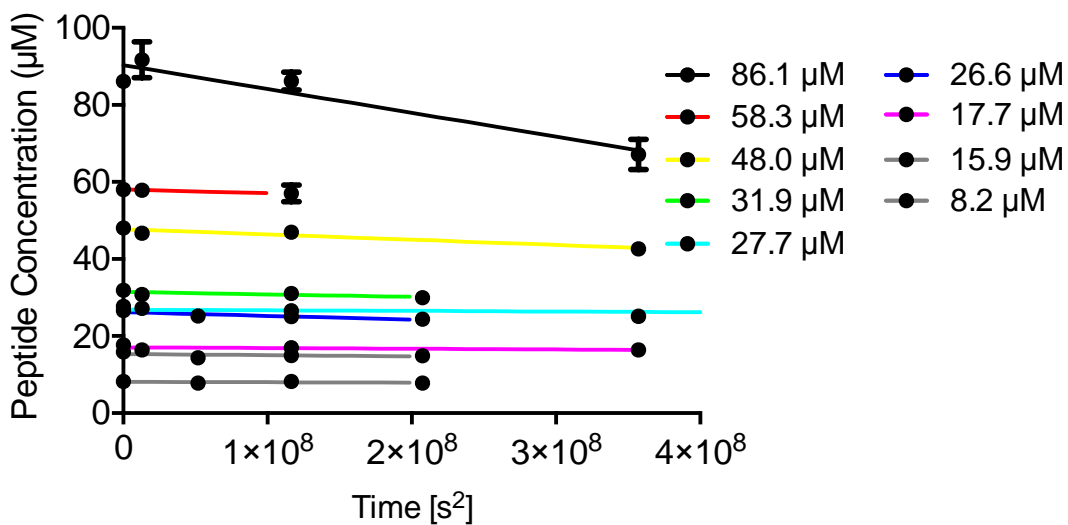


Figure 3: Time Squared Plot of β HP Aggregation. Time-squared plots using the initial aggregation rates from the concentration dependence plot above are necessary to generate the log-log dependence of initial rate on initial concentration.

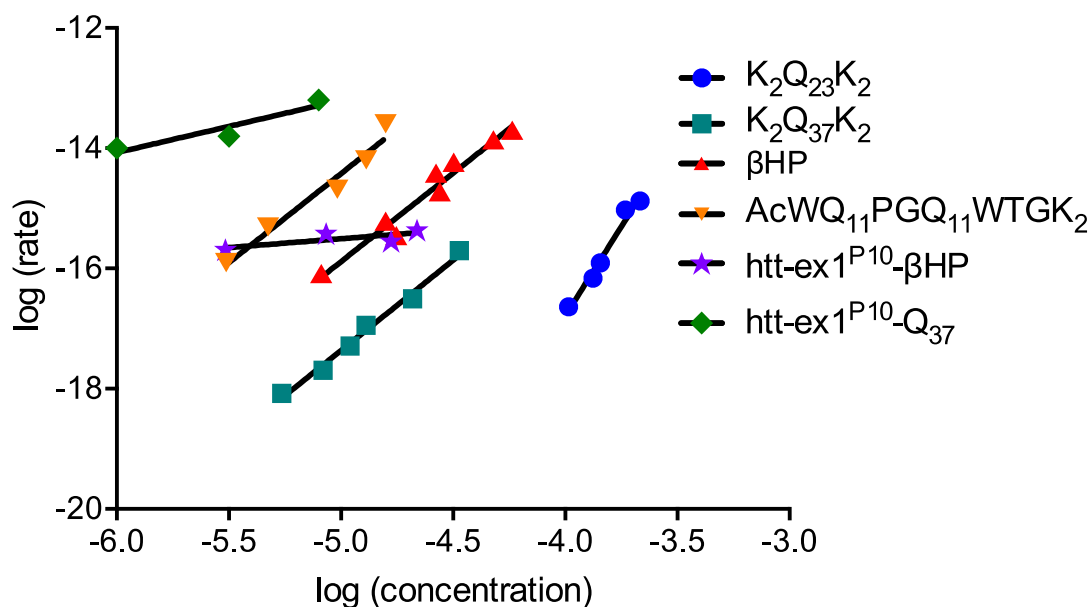


Figure 4: Log-Log Plot of Simple PolyQ and htt-ex1^{P10} peptides. Slopes and subsequent n* values for the various peptides are as follows: K₂Q₂₃K₂ (slope = 5.9 ± 0.5; n* = 4); K₂Q₃₇K₂ (slope = 3.0 ± 0.2; n* = 1); βHP (slope = 2.9 ± 0.3; n* = 1); AcWQ₁₁PGQ₁₁WTGK₂ (slope = 3.0 ± 0.3; n* = 1); htt-ex1^{P10}-βHP (slope = 0.3 ± 0.2); htt-ex1^{P10}-Q₃₇ (slope = 0.9 ± 0.3). Data for K₂Q₂₃K₂ and K₂Q₃₇K₂ are from reference ⁷⁷ and data from AcWQ₁₁PGQ₁₁WTGK₂ is from reference ¹⁰⁸.

$\Delta G_{\text{folding}}$, the Gibbs free energy associated with forming the nucleus of aggregation, is substantially more favorable in the βHP peptide than a comparable simple polyQ. $\Delta G_{\text{folding}}$ values were derived from log-log plots, as previously described ^{77,177,293}. Typical $\Delta G_{\text{folding}}$ values for proteins that spontaneously fold range from -10 to -60 kJ/mol, with the negative symbol corresponding to a favorable fold. For the K₂Q₄₇K₂ peptide, $\Delta G_{\text{folding}} = +12.2$ kJ/mol, emphasizing how tremendously unfavorable it is for simple polyQ peptides to initiate nucleation of aggregation ¹⁷⁷. In the βHP peptide, $\Delta G_{\text{folding}}$ is further stabilized to +10.5 kJ/mol, which roughly matches the theoretically predicted stabilization of 2-3 kJ/mol. Thus, spontaneously forming a nucleus for the βHP peptide is still an exceedingly rare and largely energetically

unfavorable event, but it is nonetheless substantially more favorable than for $K_2Q_{37}K_2$. Thus, the energy barrier of initiating amyloid aggregation is lowered for the β HP peptide compared to comparable polyQ peptides, or even some polyQ peptides with pathologically relevant repeat lengths.

It is important to note that these β -hairpin enhancing substitutions, while strongly enhancing aggregation by encouraging nucleation of aggregation, are not expected to appreciably form β -hairpin structured monomers. The change in the nucleation equilibrium constant between $K_2Q_{37}K_2$ and the β HP peptide is a shift from $K_{n^*} = \sim 10^{-12}$ to $K_{n^*} = \sim 10^{-10}$ (roughly 1 in 1,000,000,000,000 $K_2Q_{37}K_2$ molecules adopting a β -hairpin nucleating structure at any given time in solution, versus 1 in 10,000,000,000 for the β HP peptide). Therefore, the accelerated aggregation kinetics of β HP can be rationalized as an order of magnitude enhancement in nucleation efficiency compared to $K_2Q_{37}K_2$, but the absolute number of molecules adopting this structure remains vanishingly small.

The final aggregates of each peptide were characterized using Fourier Transform Infrared Spectroscopy (FTIR) and Electron Microscopy (EM). FTIR was used to ensure that the final aggregate of β HP contains the same “fingerprint” structural absorbencies at $\sim 1605\text{ cm}^{-1}$ (Gln side-chain N-H bending), $\sim 1625\text{-}1630\text{ cm}^{-1}$ (β -sheet), and $\sim 1654\text{-}1658\text{ cm}^{-1}$ (Gln side-chain C=O stretching). Indeed, the FTIR traces of the final β HP aggregate overlay with traces from $K_2Q_{23}K_2$ and $K_2Q_{37}K_2$ aggregates (Figure 5). Additionally, electron microscopy images of β HP aggregates show rigid amyloid-like structures (Figure 6a), which are comparable to $K_2Q_{23}K_2$ (Figure 6b) or $K_2Q_{37}K_2$ aggregates (Figure 6c).

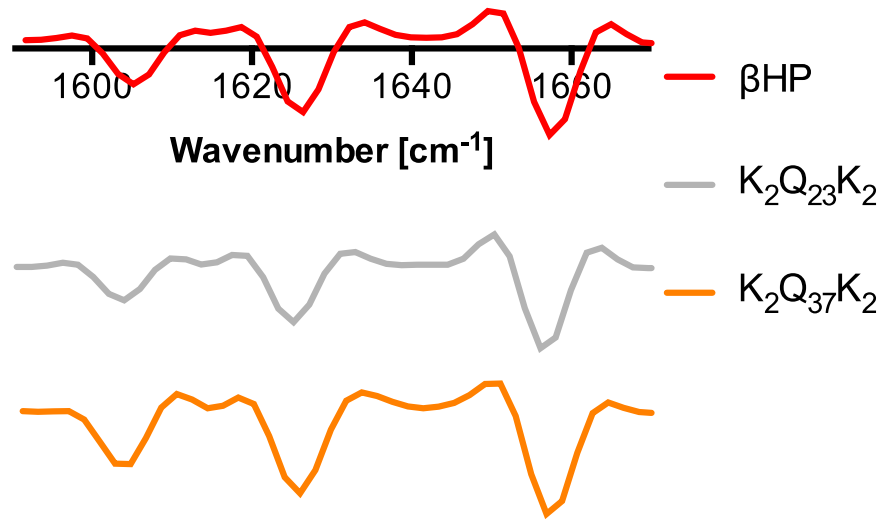


Figure 5: FTIR Traces of Simple PolyQ Peptides. Second derivative FTIR spectra was taken at the end of each aggregation reaction. Samples were centrifuged at 30,000 RPM for 30 minutes to isolate large aggregated pellets. The FTIR spectra are dominated by three signals at $\sim 1625\text{-}1630\text{ cm}^{-1}$ (β -sheet), $\sim 1605\text{ cm}^{-1}$ (Gln side-chain N-H bending) and $\sim 1654\text{-}1658\text{ cm}^{-1}$ (Gln side-chain C=O stretching).

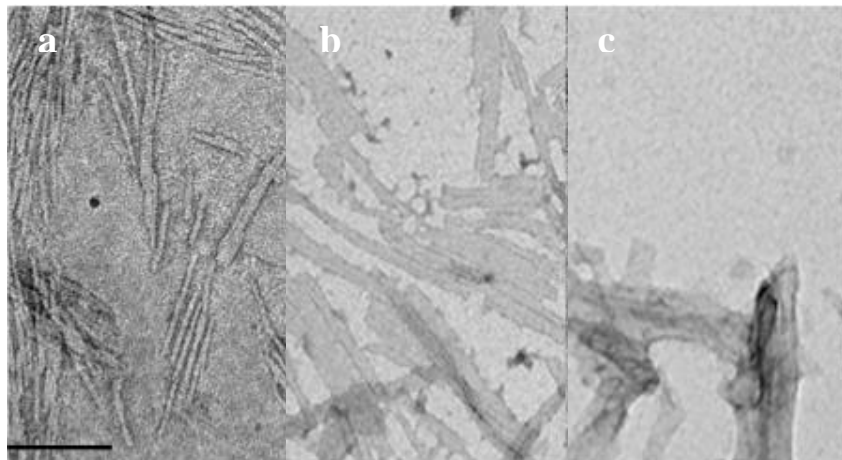


Figure 6: Electron Microscopy Images of Simple PolyQ Peptides. Bar = 50 nm (a) β HP (b) $K_2Q_{23}K_2$ (c) $K_2Q_{37}K_2$

2.2.2 β -hairpin enhanced huntingtin fragments aggregate through a htt^{NT}-mediated mechanism

The htt^{NT} (also referred to as N17) domain is implicated in accelerating huntingtin amyloid formation by first mediating oligomer formation *via* homo- α -helical like bundles^{38,176,305}. This nucleation pathway is distinct from the simple polyQ mediated nucleation (Schematic 1). Given the primary role of the htt^{NT} sequence to alter the aggregation mechanism and enhance nucleation of aggregation, it was unclear whether installing the β -hairpin enhancing architectures into a htt-ex1 background would produce any aggregation rate effect at all. If a rate effect were to be observed, it is also unclear if the β -hairpin enhancing motifs would cooperate with the htt^{NT} mediated nucleation pathway, or prefer the simple polyQ mediated nucleation pathway. To test this, we incorporated both the endogenous htt^{NT} 17 amino acids with a truncated C-terminal P₁₀K₂ segment (htt-ex1^{P10}, Table 1), as previously described¹⁹⁴.

We found that htt-ex1^{P10}- β HP, which contains only 22 total glutamines, aggregates faster than a comparable htt^{NT}-ex1^{P10}-Q₂₅, and even slightly faster than a positive control htt^{NT}-ex1^{P10}-Q₃₇ (Figure 7). Due to its complex aggregation mechanism, there is currently no known mathematical model to determine the critical nucleus size of htt^{NT}-containing polyQ peptides. Erroneously applying the Eaton-Ferrone model, which successfully models simple polyQ nucleation, to htt^{NT}-containing peptides consistently returns non-real values. Both htt-ex1^{P10}- β HP and htt-ex1^{P10}-Q₃₇ return the same signature non-real values ($n^* = -1$), indicating that β -hairpin motifs are no longer aggregating *via* simple a polyQ mediated mechanism, and likely cooperate with an htt^{NT}-mediated nucleation event (Figure 4). FTIR traces of the final aggregates show the same signature peaks between htt-ex1^{P10}- β HP and htt-ex1^{P10}-Q₃₇ (Figure 8).

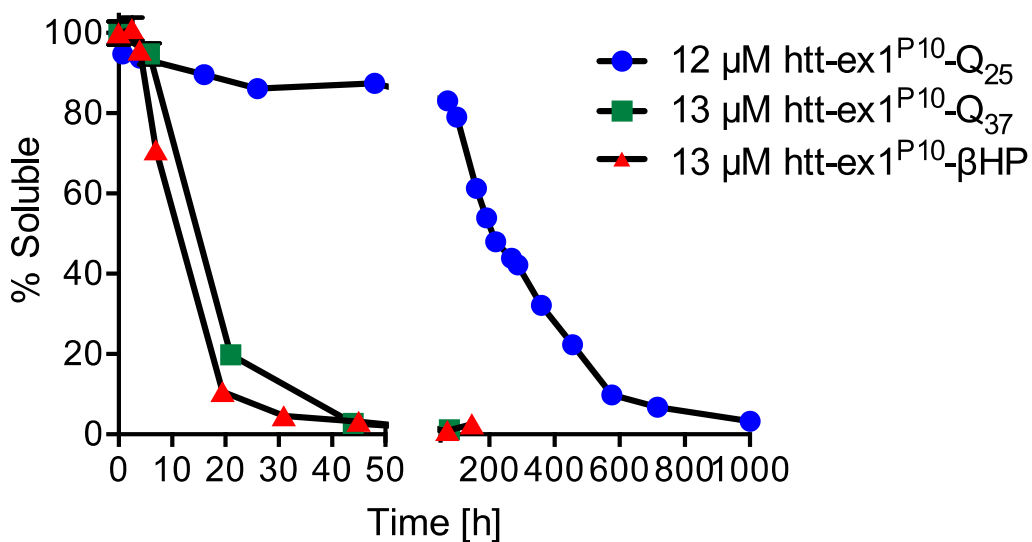


Figure 7: Sedimentation Analysis of htt-ex1^{P10} Peptides. Time-dependent loss of monomeric peptide from solution upon incubation in PBS at 37 °C.

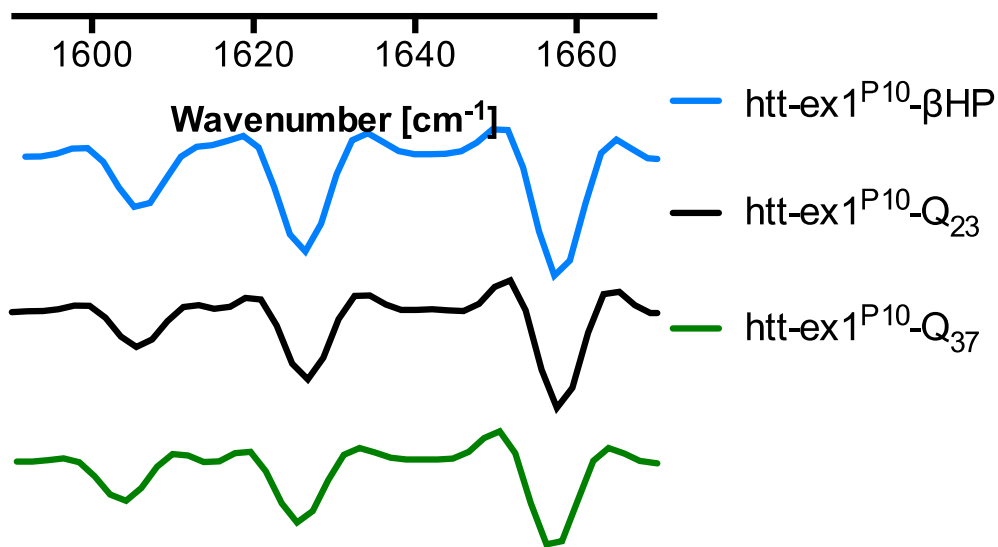


Figure 8: FTIR Traces of htt-ex1^{P10} Peptides. Second derivative FTIR spectra was taken at the end of each aggregation reaction. Samples were centrifuged at 30,000 RPM for 30 minutes to isolate large aggregates pellets. The FTIR spectra are dominated by three signals at ~1625-1630 cm⁻¹ (β-sheet), ~1605 cm⁻¹ (Gln side-chain N-H bending) and ~1654-1658 cm⁻¹ (Gln side-chain C=O stretching). The α-helix peak from the htt^{NT} segment is obscured by the Gln band.

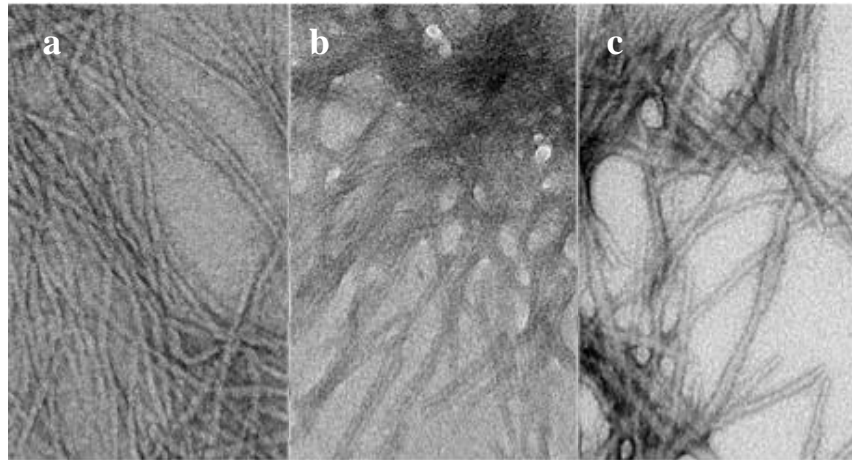


Figure 9: Electron Microscopy Images of htt-ex1^{P10} Peptides. (a) htt-ex1^{P10}-βHP (b) htt-ex1^{P10}-Q₂₅ (c) (b) htt-ex1^{P10}-Q₃₇.

EM images of the final aggregates illustrate morphologically similar amyloid fibrils for htt-ex1^{P10}-βHP (Figure 9a), htt-ex1^{P10}-Q₂₅ (Figure 9b) and htt-ex1^{P10}-Q₃₇ (Figure 9c). A circular dichroism trace of htt-ex1^{P10}-βHP, which measures gross ensemble secondary structure, confirms that the initial monomeric ensemble is randomly structured and only gains appreciable β-sheet character upon aggregating (Figure 10). Typical huntingtin fragment peptides transition from random compact coil (204 nm minimum) to β-sheet (217 nm minimum and ~200 nm maximum) as they aggregate into amyloid fibrils^{38,107}. CD signatures obtained from htt-ex1^{P10}-βHP aggregation reactions show the same transition from random compact coil to β-sheet (Figure 10). Plotting the change in absorption at 204 nm as a function of time, the transformation from random coil to β-sheet follows the same kinetics as aggregation from the HPLC-based sedimentation assay (Figure 11).

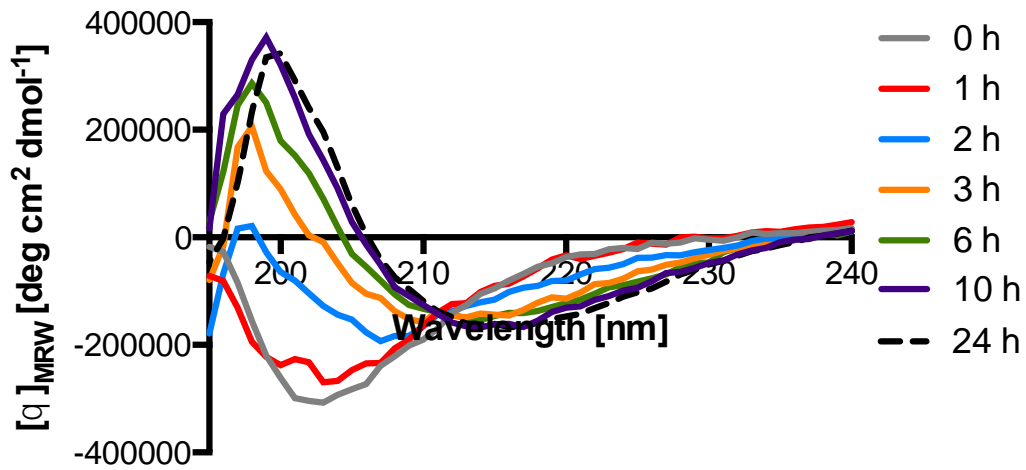


Figure 10: Circular Dichroism Traces of the htt-ex1^{P10}-βHP Peptide. Time-dependent far-UV CD was analyzed in a 1 mm path-length cuvette using the same freshly disaggregated monomeric solution in parallel to sedimentation assays. CD time course was done in Tris buffer (50 mM Tris-Cl pH 7.5, 150 mM NaCl) at 37 °C. 32 μM htt-ex1^{P10}-βHP shows a time-dependent transition from initial random coil structure to anti-parallel β -sheet.

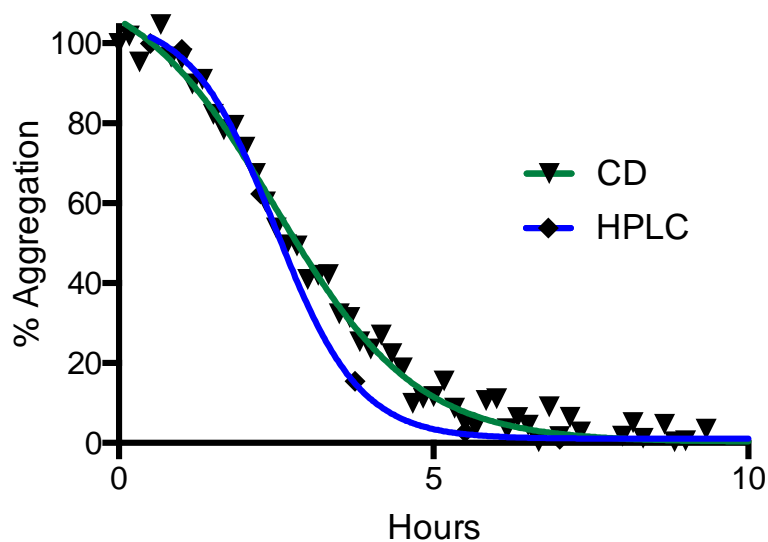


Figure 11: Overlay of Circular Dichroism and Sedimentation Analysis Kinetics for htt-ex1^{P10}-βHP. 20 μM htt-ex1^{P10}-βHP was measured from parallel reactions by sedimentation assay (Figure 7) and by CD (Figure 10). CD progression is calculated as the percentage of progress in the 204 nm ellipticity.

2.2.3 htt^{NT}Q₂₂P₁₀K₂-βHP seeds can recruit huntingtin into amyloid fibrils

One key test for functional amyloid is the ability to seed aggregation of soluble huntingtin. Seeded elongation bypasses the rate-limiting nucleation phase and allows aggregation to proceed directly into the rapid elongation phase²². However, this process requires some degree of structural homology, as htt aggregates can seed soluble htt, but less so Aβ^{22,306}. We asked whether htt-ex1^{P10}-βHP amyloid had sufficient structural homology to seed soluble htt-ex1^{P10}-Q₂₅. Based on previous results using 10-20% weight/weight seeds for seeded elongation¹⁰⁸, we found that a 20% seed of htt-ex1^{P10}-βHP is equipotent to a htt-ex1^{P10}-Q₂₅ self-seed in recruiting

soluble htt-ex1^{P10}-Q₂₅ (Figure 12). Thus, β -hairpin motifs enhance, but do not alter, pathogenic huntingtin aggregation mechanisms. Only the kinetics of amyloid formation are affected.

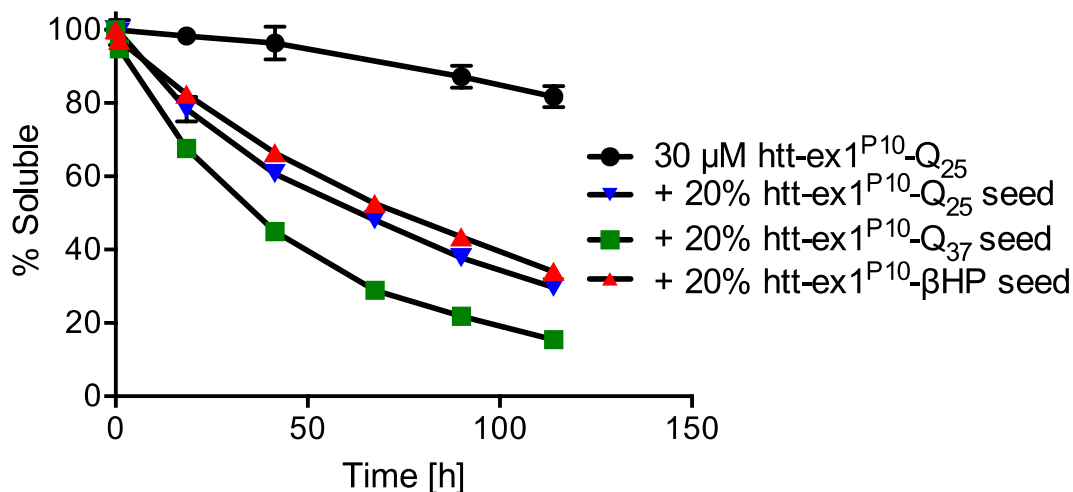


Figure 12: Seeded Elongation of htt-ex1^{P10}-Q₂₅. Time-dependent loss of solubility requires the rate limiting step of nucleus formation (Scheme 1). This step can be bypassed if exogenous amyloid aggregates with a suitable degree of sequence and structural homology are added to the soluble portion. htt-ex1^{P10}-βHP is equipotent at seeding htt-ex1^{P10}-Q₂₅ as a htt-ex1^{P10}-Q₂₅ self-seed.

2.3 DISCUSSION

Previous reports from the Wetzel laboratory established a role for β -hairpin architecture in nucleus formation of a simple polyQ model. An array of different β -hairpin encouraging motifs successfully reduced the nucleus size of K₂Q₂₃K₂ from tetrameric to monomeric ($n^* = 4$ to $n^* = 1$) with a subsequent boost to aggregation kinetics. However, these β -hairpin enhanced peptides were confined to a simple polyQ model and were not tested in the context of huntingtin exon-1. Herein we redesigned the tryptophan zipper and _D-pro-gly β -turn, two motifs to enhance β -

hairpin architecture, for use in a htt-exon1 background and for future use in *in vivo* systems. These β -hairpin enhanced huntingtin peptides, if aggregation competent, could be a useful model to determine the biological ramifications of polyQ aggregation into amyloid. These peptides may also be useful tools to disassociate absolute polyQ repeat length from aggregation propensity, which may shed light as to how mutant htt gains its toxic function. For instance, a recent paper from the La Spada laboratory claims that expanded polyQ sequences within the huntingtin protein preferentially bind to, sequester, and ultimately repress peroxisome proliferator-activated receptor delta (PPAR- δ), a critical protein for neuron survival³⁰⁷. If this type of altered protein binding is responsible for an HD phenotype, we would expect our β HP peptide, with a nominal polyQ region, to be non-toxic or well tolerated.

We present here that β -hairpin motifs constructed from only L-amino acids (which can be expressed in cells *via* standard genetic methods) retain the ability to shift the nucleus size of K₂Q₂₃K₂ from tetrameric to monomeric, resulting in a reduction of time spent in the lag phase and a boost to overall aggregation kinetics. The resulting enhancements are similar to previously employed β -hairpin encouraging motifs in other simple polyQ models. Because the hyper-amyloid construct β HP no longer requires chemical modification, it can be now be built into a htt-ex1 background, which makes it possible to probe the impact of β -hairpin enhancement of polyQ on the htt-ex1 nucleation mechanism.

The addition of the htt^{NT} segment alters the aggregation mechanism of polyQ by introducing an intermediary oligomeric phase that adds an addition step to the nucleation mechanism, therefore no longer following the Eaton-Ferrone mathematical model (steps 2-5 of Scheme 1). The simple polyQ aggregation mechanism (steps 8-9 of Scheme 1) is still functional, but is outcompeted by the significantly more competent htt^{NT}-mediated aggregation mechanisms.

It was therefore a concern that the β -hairpin enhancing substitutions, even in the context of htt^{NT}, may still favor the simple polyQ aggregation mechanism.

Using a synthetic htt^{NT}-ex1^{P10} model of htt-exon1, we show that aggregation can be drastically enhanced with the installation of β -hairpin motifs despite a modest polyQ repeat length. Aggregation kinetics, secondary structure changes, FTIR spectra, and EM morphology of htt^{NT}-ex1^{P10}- β HP all indicate that β -hairpin motifs enhance, but do not alter, the same aggregation pathways used by mutant htt-exon1.

One additional method to address whether or not the β HP motifs cooperate with an htt^{NT}-mediated aggregation mechanism is to determine whether the critical nucleus changes to non-real values. For example, the Eaton-Ferrone mathematical model returns real values for the simple polyQ peptide K₂Q₃₇K₂ ($n^* = 1$), but yields non-real values for htt-ex1^{P10}-Q₃₇ ($n^* = -1$). Similarly, the critical nucleus size of β HP also shifts from $n^* = 1$ in the simple polyQ format to $n^* = -1$ for htt^{NT}-ex1^{P10}- β HP, indicating that the β HP motifs are cooperating with the htt^{NT}-mediated mechanisms of aggregation. If the htt-ex1^{P10}- β HP peptide primarily aggregated through enhanced simple polyQ aggregation mechanisms, we would have anticipated a real value, such as $n^* = 1$. These findings support a model inclusive of β -hairpin architecture participating in htt-exon1 nucleus formation within the oligomeric phase.

Finally, we wanted to ensure that the β -hairpin enhanced peptides formed aggregates with structural likeness to typical mhtt amyloid. FTIR, EM, CD, and other biophysical tools help solidify that htt-ex1^{P10}- β HP aggregates have comparable gross morphology and secondary structure to htt-ex1^{P10}-Q₃₇, but these techniques do not address issues of finer structural likeness. As a probe into this structural likeness, we challenged htt-ex1^{P10}- β HP aggregates to seed the elongation of monomeric htt-ex1^{P10}-Q₂₃. We found the htt-ex1^{P10}- β HP aggregates were

equipotent to a htt-ex1^{P10}-Q₂₃ self seed, demonstrating that the fibril aggregates generated by htt-ex1^{P10}-βHP are structural compatible with htt-ex1^{P10}-Q₂₃. Additionally, the process of elongation and/or the seeding potential of polyQ aggregates is one proposed toxic mechanism of mhtt. This efficient seeding potential is preserved in our β-hairpin enhanced peptides; whether or not these β-hairpin enhanced peptides generate an HD phenotype *in vivo* may provide further clues to the toxic mechanism of mhtt.

Thus, the hyper-amyloid competent htt^{NT}-ex1^{P10}-βHP peptide can be used in future studies to test the toxic amyloid hypothesis *in vivo*. Because the hyper-amyloid htt^{NT}-ex1^{P10}-βHP is capable of robust aggregation, in spite of its relatively short polyQ repeat length, htt^{NT}-ex1^{P10}-βHP makes an excellent diagnostic tool to test the toxicity of amyloid. Htt^{NT}-ex1^{P10}-βHP can essentially decouple absolute polyQ repeat length from its inherent propensity to aggregate into amyloid without leading to measurable levels of monomeric β-hairpin forms of htt-ex1, as demonstrated by CD. Whether or not a hyper-amyloid peptide like htt^{NT}-ex1^{P10}-βHP is toxic in cells or animals would provide valuable insight into the nature of the toxic species of huntingtin. A more detailed understanding of the mutant huntingtin aggregation pathway and how polyQ repeat expansion causes toxicity *in vivo* is crucial to developing new lines of therapies and designing more sophisticated mechanistic-oriented drug screens.

3.0 DESIGNING HUNTINGTIN AMYLOID INHIBITORS THAT STOP HUNTINGTIN AGGREGATION AT NON-BETA OLIGOMERS

3.1 INTRODUCTION

The toxic species of expanded polyQ huntingtin is fiercely debated in the literature, as is the mechanism by which mutant huntingtin exerts its toxic gain-of-function. Several hypotheses have been put forward, including the toxic amyloid hypothesis (Section 1.3.2), the toxic oligomer hypothesis (Section 1.3.3), and a toxic monomer hypothesis (Section 1.3.4). There is currently no consensus within the field how mutant huntingtin gains toxicity, thereby delaying hypothesis-driven therapeutic drug design. A better and more detailed understanding of how expanded polyQ huntingtin generates toxicity is critical in designing effective therapies that can slow or prevent HD onset.

The toxic oligomer hypothesis states that some non- β -structure, non-amyloid, diffusible oligomer of huntingtin is the toxic species^{85,86}. In some experiments, neurons successfully forming large inclusion bodies survived better than those without inclusion body formation⁸¹. These findings have been interpreted to mean that large inclusion bodies are non-toxic or are a cellular protective response^{92,93}. Other experiments have correlated the appearance of huntingtin species with the timing of toxic events, concluding that some soluble portion of huntingtin generates toxicity⁹¹. In separate studies, a truncated huntingtin analog discovered

serendipitously (truncated at amino acid 117, which lies beyond the polyQ core), has significant inclusion formation in transgenic mice, but little detectable neurodegeneration and behavioral defects seen in other HD mice⁸⁷.

More recently, large inclusions were shown to have their own toxic effects by disrupting the nuclear membrane⁸³. Furthermore, super-resolution microscopy has shown that small amyloid-like aggregates exist outside of inclusion bodies^{42-44,308}. These small aggregates were not initially visible due to being smaller than the diffraction limits of confocal microscopy and to the intense obscuring brightness of inclusions within the same cell. The contribution of non- β huntingtin oligomers in HD is heavily debated. As with large β -structure amyloid, directly assigning a contribution of each huntingtin species is extremely difficult, due to how rapidly huntingtin adopts a multitude of forms, including monomeric, oligomeric, and small β -rich aggregates (Sahoo 2016 Manuscript Submitted). Correlative studies that rely on the timing of toxic events with the appearance of huntingtin species, while informative, need to be reevaluated in light of these recent findings.

In order to circumvent these technological limitations, we have designed amyloid-incompetent huntingtin analogs that remain as soluble non- β oligomers essentially indefinitely. Previous work from the Wetzel laboratory showed that chemical modifications of simple polyQ peptide's backbone amide nitrogen by methylation or L-Glutamine to D-Glutamine substitution was sufficient to block aggregation (Kar 2016 Manuscript Submitted). Glutamine to proline substitutions or L-glutamine to D-glutamine substitutions within simple polyQ peptides also diminish the ability of these peptides to self-aggregate²⁹². Unlike htt^{NT}-based inhibitors, these hypo-amyloid polyQ peptide designs primarily act to limit elongation.

We introduce here a series of “hypo-amyloid” simple polyQ peptides with strategically placed glutamine to proline substitutions that significantly limit aggregation *in vitro*. We then expanded the hypo-amyloid polyQ design to incorporate the htt-ex1^{P10} flanking sequences. These inhibited htt-ex1^{P10} peptides are capable of rapidly forming intermediate oligomers *via* the htt^{NT} domain, but are severely compromised in their ability to nucleate aggregation. These peptides can be feasibly expressed *in vivo* and offer new tools to test the toxic amyloid hypothesis and toxic oligomer hypothesis.

In addition to being a test of the toxic oligomer hypothesis, these hypo-amyloid peptides may also be a proof-of-principle aggregation inhibitor with potential therapeutic effects. The htt^{NT} segment plays an accessory role in aggregation by forming α -helical bundles with other htt^{NT} segments, thereby bringing together aggregation prone polyQ sequences (Section 1.4.4). Mishra *et al.* showed that “naked” htt^{NT} peptides can compete with huntingtin for oligomer formation¹⁸⁹. This process essentially dilutes the aggregation prone polyQ segments, which limits the ability of expanded polyQ huntingtin to nucleate aggregation within the intermediate oligomer phase. However, statistically some portion of pathogenic huntingtin oligomers can be expected to contain a low number of htt^{NT} inhibitors, increasing the likelihood that nucleation will occur. Additionally, pathogenic huntingtin can also overcome htt^{NT} inhibition by nucleating aggregation *via* the slower htt^{NT}-independent simple polyQ aggregation mechanism¹⁸³. Together these two “escape” mechanisms explain why amyloid nucleation is not completely stopped, but only delayed, by the simple htt^{NT} peptide inhibitor.

To combine these strategies, we designed and tested hypo-amyloid constructs containing both an htt^{NT} domain as well as a proline interrupted polyQ core. These peptides are capable of

inhibiting both the nucleation and elongation steps of huntingtin aggregation and therefore are effective aggregation inhibitors.

These hypo-amyloid peptides offer a number of valuable insights. First, they demonstrate that interruption of the polyQ core with even a single glutamine to proline substitution is sufficient to block nucleation of huntingtin. Second, due to their hypo-amyloid nature, they provide a new tool to diagnose the contribution of huntingtin oligomers on toxicity. Thirdly, their ability to inhibit aggregation has helped detail further structural detail about potential mechanisms to limit aggregation. Finally, the therapeutic effect (if any) of these hypo-amyloid peptides to slow mutant huntingtin aggregation into amyloid will provide a further confirmation of the toxic species of huntingtin.

3.2 RESULTS

3.2.1 Rational design of a competitive peptide-based inhibitor of nucleation

Peptide-based inhibitors of nucleation of aggregation and/or elongation of huntingtin amyloid fibrils are modeled after previous findings, which used chemically modified glutamine residues or glutamine to proline substitutions to limit aggregation^{183,291,292} (Kar 2016 Manuscript Submitted). Proline is a unique amino acid in that it strongly disfavors being in α -helices or β -sheet secondary structures, but can be found in ordered structures such as β -turns and as Type II poly-proline α -helices^{309,310}. A glutamine to proline substitution is predicted to lose some intra-strand hydrogen bonding required for β -hairpin formation, and may “kink” the backbone to

further destabilize β -sheet structure³¹¹. Other chemical modifications, such as D-glutamine or N α -methyl glutamine, which also disfavor β -sheet formation, were not used due to the limited potential of *in vivo* expression.

We present here the rational design of htt-ex1 analogs that contain a htt^{NT} segment, which can compete for mixed oligomer formation, a polyQ segment which may enhance oligomer formation (Sahoo 2016 Manuscript Submitted), a β -hairpin backbone, which may enhance recognition and incorporation of the inhibitor into the growing end of an amyloid fibril, and one or more glutamine to proline substitutions within the polyQ track to limit amyloid formation (Table 1).

Working with these constraints, several peptide designs were developed: A single proline substitution in the first polyQ sequence (P¹), a single proline substitution in the second polyQ sequence (P²), and a double proline substitution (P^{1,2}) (Table 1, Schematic 1). These substitutions were incorporated into both a simple polyQ format as well as huntingtin analog peptide htt^{NT}-ex1^{P10} format. The simple polyQ inhibitors (β HP-P^N) are predicted to limit elongation only, while the htt^{NT}-containing huntingtin analogs (htt-ex1^{P10}- β HP-P^N) should interfere with both the nucleation and elongation mechanisms of huntingtin. The glutamine \rightarrow proline substitution peptides also act as a control for the htt^{NT}-ex1^{P10}- β HP peptide. That is, it is possible that the addition of tryptophan, proline, and glycine residues into htt-ex1^{P10}- β HP could produce toxicity and aggregation through mechanisms other than enhanced amyloidogenesis. As a control, these hypo-amyloid htt analogs contain the same background β HP motif.

3.2.2 Glutamine to Proline substitutions block amyloidogenesis

Well placed proline substitutions in certain polyQ settings can drastically diminish the ability of simple polyQ peptides to aggregate. $K_2Q_{23}K_2$ aggregates slowly over time at high concentrations, while β -hairpin enhancing motifs drastically enhance this aggregation, as discussed in Section 2.0 (Figure 1). Despite having β -hairpin enhancing motifs, a single (β HP- P^2) or double (β HP- $P^{1,2}$) glutamine to proline substitution nearly eliminates any noticeable sedimentation, even after several hundred hours (Figure 13). In fact, these hypo-amyloid analogs aggregate slower than a peptide with a non-pathogenic repeat length, $K_2Q_{23}K_2$.

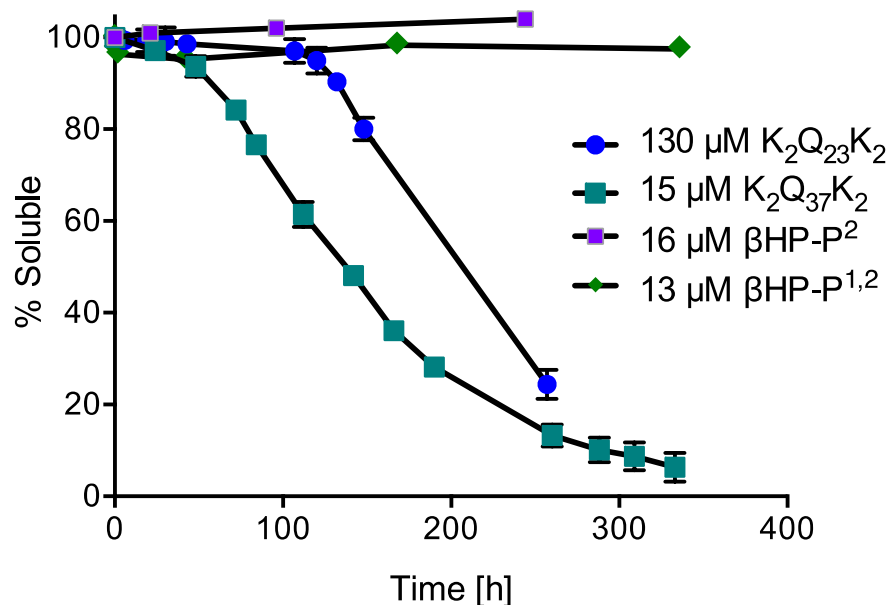


Figure 13: Sedimentation Analysis of Hypo-Amyloid Peptides. Time-dependent loss of monomeric peptide from solution upon incubation in PBS at 37 °C.

After characterizing and confirming that the simple polyQ proline substitution analogs do not sediment significantly *in vitro*, these peptides were extended to include the htt^{NT} region,

which is important for oligomerization and acceleration of the nucleation of aggregation (Section 1.4.4), and the P₁₀ region, the endogenous C-terminal flanking sequence of huntingtin (Section 1.4.5). The single proline substitution peptides, htt-ex1^{P10}-βHP-P¹ and htt-ex1^{P10}-βHP-P² aggregate very poorly, slowing losing a small fraction of soluble material (~80% remains soluble) over 400 hours at 15 and 20 μM concentrations, respectively (Figure 14). Aggregation is slowed dramatically for the proline-substituted peptides and is even slower than for a comparable non-pathogenic htt-ex1^{P10}-Q₂₅. Htt-ex1^{P10}-βHP-P^{1,2}, the double proline substitution, remains near 100% solubility for at least 400 hours (Figure 14). Circular dichroism of the hypo-amyloid peptide htt-ex1^{P10}-βHP-P² initially shows a random coil structure and persists in this state (Figure 15). Electron microscopy images of htt-ex1^{P10}-βHP-P¹, htt-ex1^{P10}-βHP-P², and htt-ex1^{P10}-βHP-P^{1,2} taken after 2,000+ hours incubation show only scattered small amorphous structures, which resemble oligomers, spheroids, or small non-β non-amyloid amorphous aggregates (Figure 16).

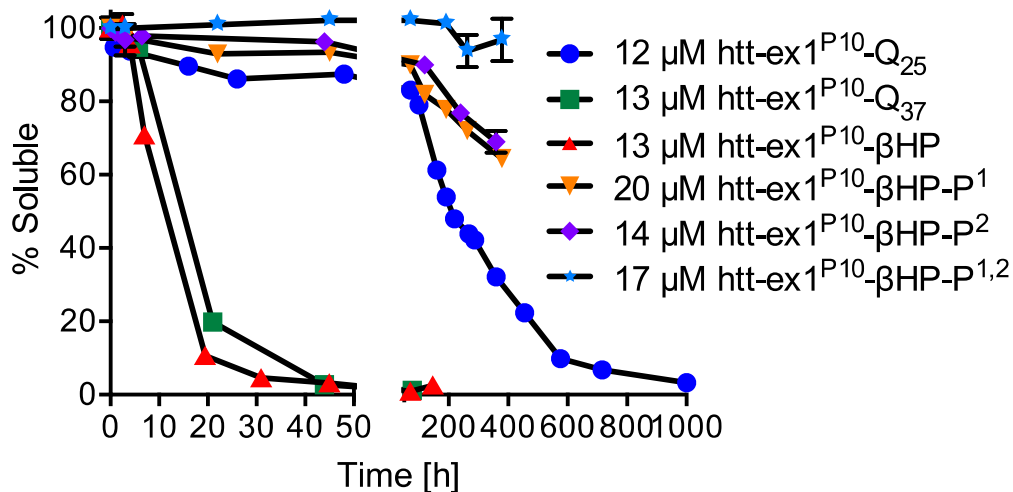


Figure 14: Sedimentation Analysis of htt-ex1^{P10} Hypo-Amyloid Peptides. Time-dependent loss of monomeric peptide from solution upon incubation in PBS at 37 °C.

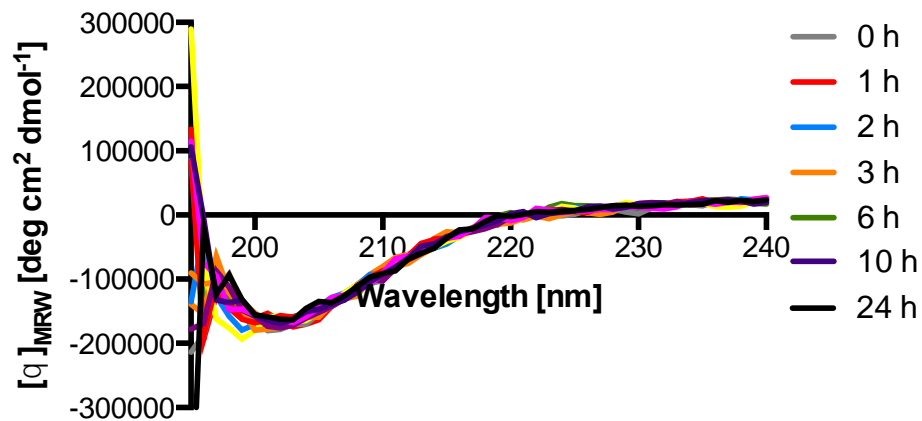


Figure 15: Circular Dichroism Traces of htt-ex1^{P10}-βHP-P². Time-dependent far-UV CD was analyzed in a 1 mm path-length cuvette using the same freshly disaggregated monomeric solution in parallel to sedimentation assays. CD time course was done in Tris buffer (50 mM Tris-Cl pH 7.5, 150 mM NaCl) at 37 °C. 25 μM htt-ex1^{P10}-βHP-P² shows a random coil structure that is unchanged over 24 hours.

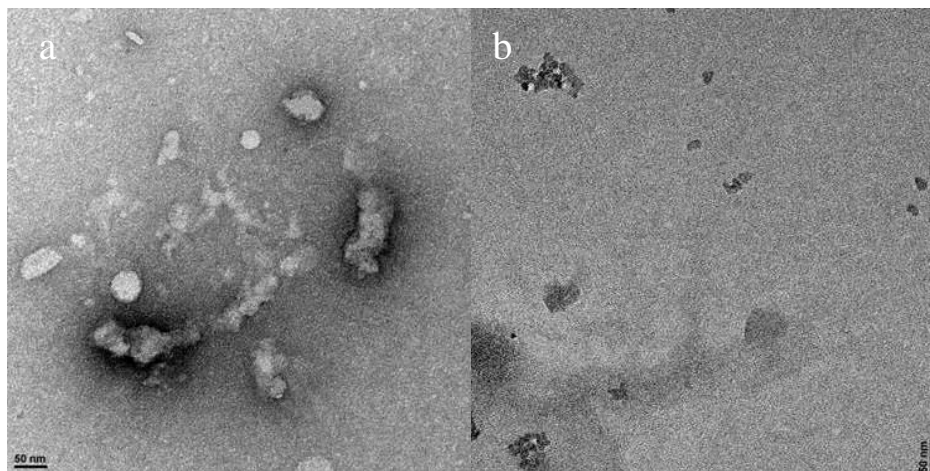


Figure 16: Electron Microscopy Images of Hypo-Amyloid htt-ex1^{P10} Peptides. (a) htt-ex1^{P10}-βHP-P² (b) htt-ex1^{P10}-βHP-P^{1,2}

3.2.3 Hypo-Amyloid huntingtin analogs as proof-of-principal polyQ aggregation inhibitors

Htt^{NT} plays a crucial role in huntingtin oligomerization and nucleation of amyloid aggregation. Previous work hinted at the potential of the htt^{NT} 17 amino acid segment to act as an inhibitor of huntingtin amyloid nucleation by competing for oligomer formation and inhibiting nucleus formation in the oligomeric phase^{189,292}. These htt^{NT} fragment inhibitors were imperfect in their ability to significantly delay synthetic htt^{NT}Q₃₀P₆K₂ aggregation, requiring molar excess to achieve a 2 or 3-fold delay in $t_{1/2}$ aggregation kinetics. Adding several molar excess repeatedly throughout the time course of htt^{NT}Q₃₀P₆K₂ aggregation only delayed aggregation modestly and incompletely. Herein we describe new, more potent inhibitors, which can be feasibly tested *in vivo* using genetic expression models.

In vitro, 10 μ M htt-ex1^{P10}-Q₃₇ aggregates to $t_{1/2}$ in 14 hours and to completion in less than 48 hours (Figure 17). Addition of 20 μ M of the inhibitor htt-ex1^{P10}- β HP-P¹ delays htt-ex1^{P10}-Q₃₇ aggregation to $t_{1/2} = 54$ hours, a 4-fold delay. Htt-ex1^{P10}- β HP-P² and htt-ex1^{P10}- β HP-P^{1,2} are even more potent, significantly delaying htt-ex1^{P10}-Q₃₇ aggregation to $t_{1/2} = 125$ hours, almost an order of magnitude (Figure 17).

Stoichiometric (Figure 18) and sub-stoichiometric (Figure 19) ratios are also effective at delaying target huntingtin aggregation. While the kinetics of htt-ex1^{P10}-Q₃₇ aggregation are delayed in each case, the final thermodynamic product remains the amyloid fibril. EM images taken after the completion of each inhibited reaction shows amyloid fibrils similar to uninhibited htt-ex1^{P10}-Q₃₇ (Figure 20).

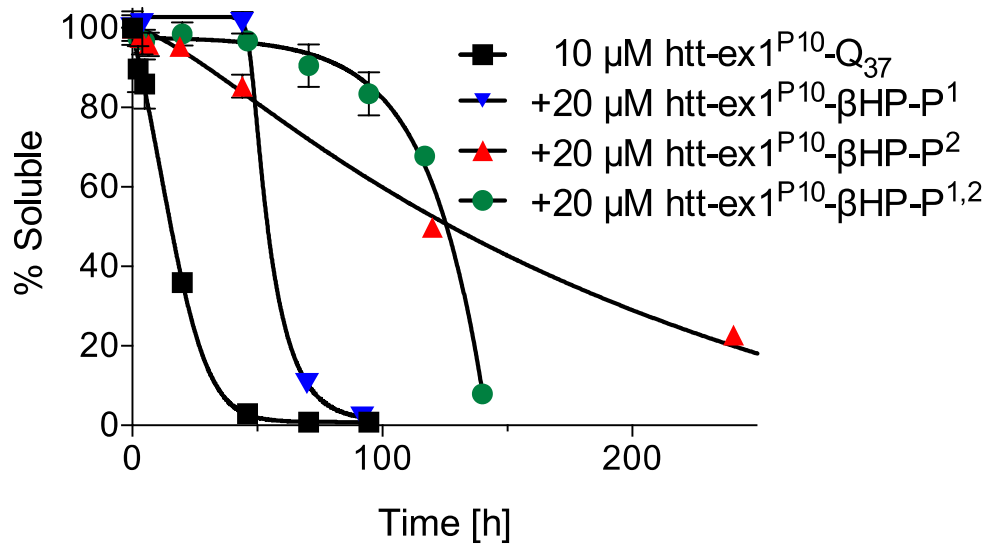


Figure 17: Sedimentation Analysis of Hypo-Amyloid Inhibition 10:20. Time-dependent loss of monomeric htt-ex1^{P10}-Q₃₇ in the presence of absence of different mid-strand Pro analogs. Freshly disaggregated peptides were incubated alone or in co-mixtures.

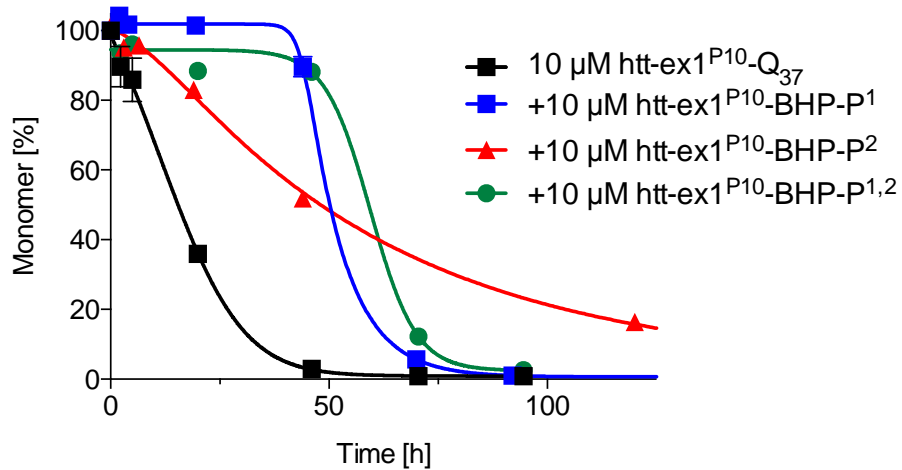


Figure 18: Sedimentation Analysis of Hypo-Amyloid Inhibition 10:10. Time-dependent loss of monomeric htt-ex1^{P10}-Q₃₇ in the presence of absence of different mid-strand Pro analogs. Freshly disaggregated peptides were incubated alone or in co-mixtures.

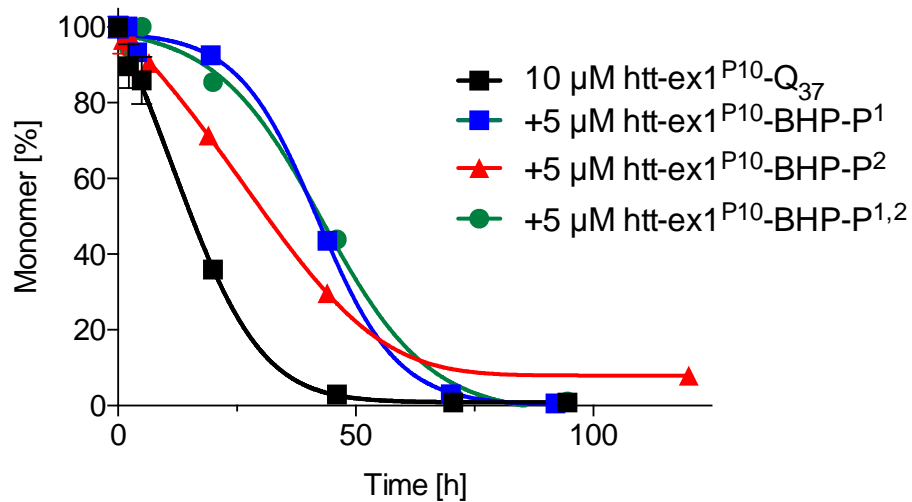


Figure 19: Sedimentation Analysis of Hypo-Amyloid Inhibition 10:5. Time-dependent loss of monomeric htt-ex1^{P10}-Q₃₇ in the presence of absence of different mid-strand Pro analogs. Freshly disaggregated peptides were incubated alone or in co-mixtures.

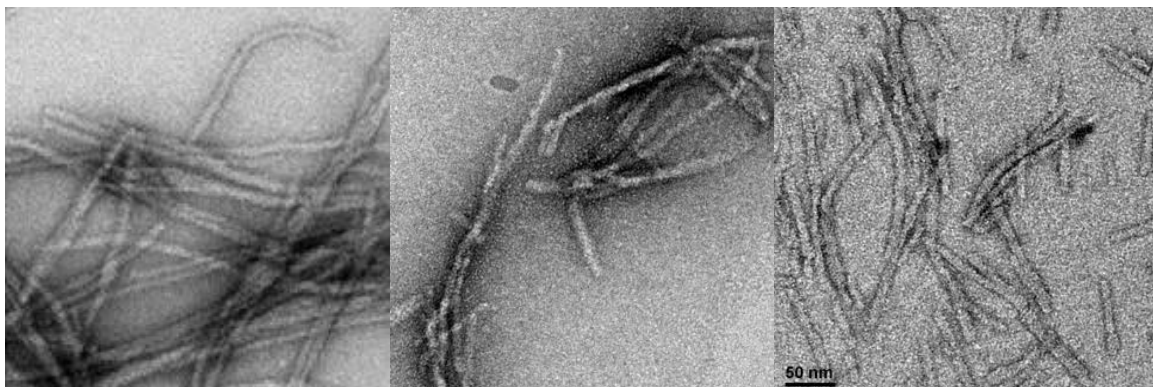


Figure 20: Electron Microscopy Images of the Hypo-Amyloid Inhibited Reaction. (a) htt-ex1¹¹⁰-Q₃₇ alone (b) htt-ex1¹¹⁰-Q₃₇ + htt-ex1¹¹⁰-βHP-P² (c) htt-ex1¹¹⁰-Q₃₇ + htt-ex1¹¹⁰-βHP-P^{1,2}

On their own, the three hypo-amyloid analogs resist aggregation for an extended period of time (Figure 14), but in the presence of their target htt-ex1^{P10}-Q₃₇, they co-aggregate in a 1:1 ratio with their target mutant huntingtin (Figure 21). Changing stoichiometry to 1:2, 1:1, or 2:1

does not effect the 1:1 parallel aggregation. To test the contribution of htt^{NT} to the inhibitory action of these hypo-amyloid analogs, we synthesized inhibitors lacking the htt^{NT} segment. These peptides have severely reduced inhibitory potency limited to the elongation phase, and no longer co-aggregate in the presence of their target (Figure 22). Thus, the htt^{NT} domain is critical to the inhibitory action of these hypo-amyloid analogs.

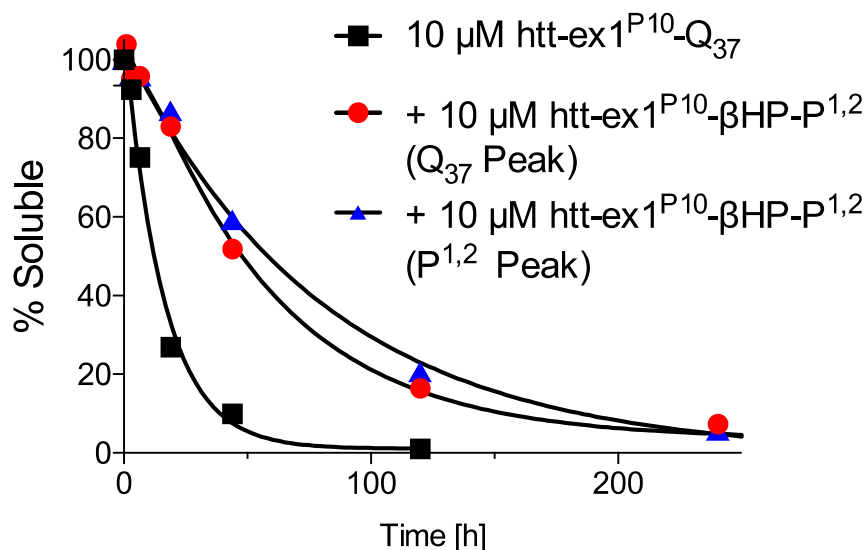


Figure 21: Co-Aggregation of the Hypo-Amyloid Peptides with its target htt-ex1^{P10}-Q₃₇. Time-dependent loss of monomeric htt-ex1^{P10}-Q₃₇ in the presence of absence of different mid-strand Pro analogs. The hypo-amyloid htt-ex1^{P10}-βHP-P^{1,2} co-aggregates with its target htt-ex1^{P10}-Q₃₇.

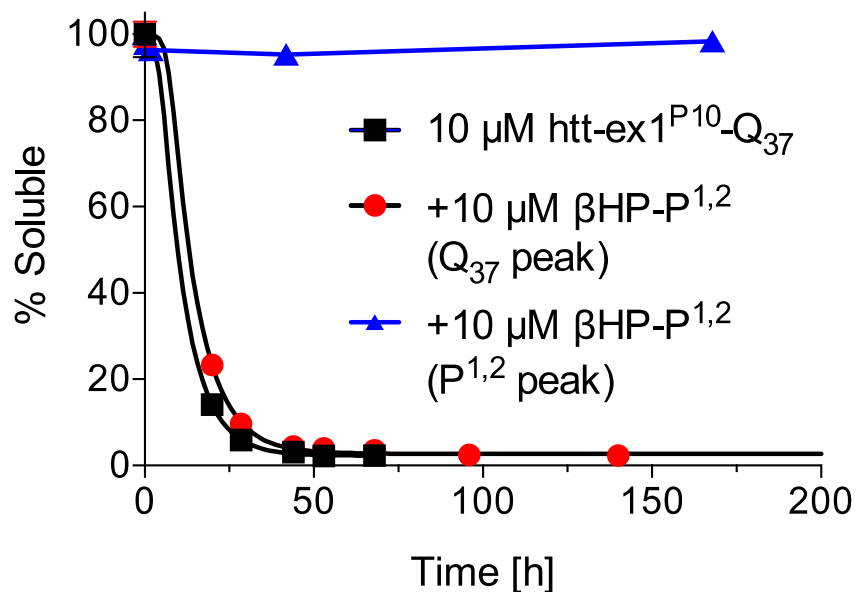


Figure 22: Lack of Inhibition or Co-Aggregation Between without htt^{NT}. Time-dependent loss of monomeric htt-ex1^{P10}-Q₃₇ in the presence of absence of different mid-strand Pro analogs.

Interestingly, the inhibitor βHP-P² was synthesized both with and without an acetylated trp-zip motif – a stronger inducer of β-hairpin formation. This stronger β-hairpin formation correlates with a stronger elongation inhibition, confirming that the ability to engage in a β-hairpin structure upon the docking of an inhibitor onto the growing edge of the fibril enhances its inhibitory power (Figure 23). When both Q₁₁ strands were blocked, such as in the βHP-P^{1,2} peptide, no inhibition of elongation took place, confirming that at least one uninterrupted polyQ face is necessary for inhibition of elongation (Figure 22).

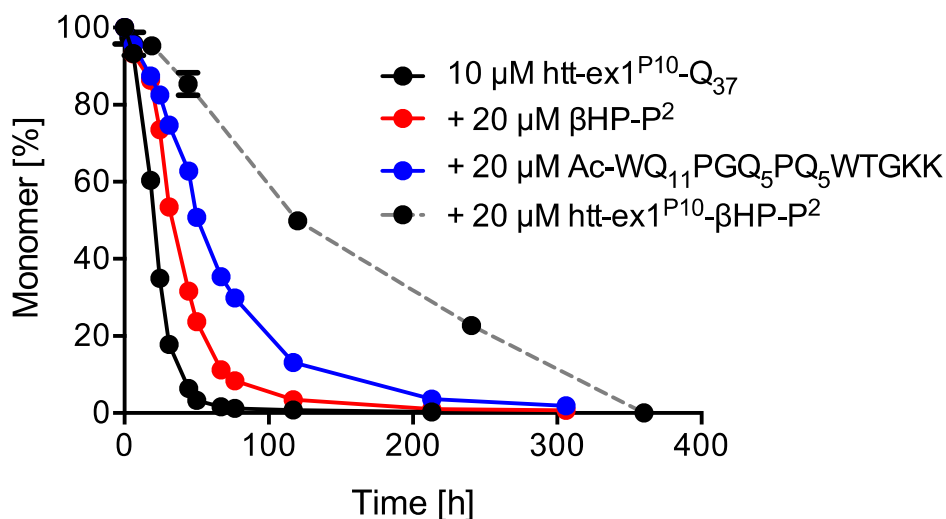


Figure 23: Stronger β HP Motifs Correlate with Stronger Inhibition. Deletion of the htt^{NT} and P_{10} segments from the elongation inhibitor $\text{htt-ex1}^{\text{P10}}\text{-}\beta\text{HP-P}^2$ results in weaker inhibition of target $\text{htt-ex1}^{\text{P10}}\text{-Q}_{37}$ ($\beta\text{HP-P}^2$). Peptides with stronger βHP encouraging motifs ($\text{Ac-WQ}_{11}\text{PGQ}_5\text{PQ}_5\text{WTGKK}$) are stronger inhibitors of elongation.

3.3 DISCUSSION

In this work, we demonstrate that disruption of the polyQ sequence using glutamine to proline substitutions in a βHP background drastically diminishes the ability of both simple polyQ peptides and $\text{htt-ex1}^{\text{P10}}$ format peptides to participate in aggregation. In the case of $\text{htt-ex1}^{\text{P10}}$ format hypo-amyloid constructs, we show that an intact htt^{NT} domain is sufficient to generate an intermediate oligomeric phase visible by EM, but subsequent amyloid formation is efficiently blocked, which is in agreement with the previously defined mechanism of htt^{NT} 's involvement in oligomer formation¹⁸³. These hypo-amyloid constructs do not gain appreciable β -structure over time and remain soluble for longer than a comparable $\text{htt-ex1}^{\text{P10}}\text{-Q}_{25}$. Because these hypo-amyloid analogs stably form non- β oligomers *in vitro*, they offer an ideal tool to circumvent

technological limitations that have prevented identification of the toxic species of huntingtin. If expressed in model organisms, toxicity (or lack thereof) of these peptides could help better understand the toxic oligomer hypothesis. In addition, with the hyper-amyloid β HP peptide from Section 2.0, we can probe the robustness of the link between repeat length and pathology, as well as test the contribution of rapid amyloid formation to disease pathology.

Sedimentation assays, EM, CD, and other biophysical tools used here strongly support a model of the proline substituted peptides forming non- β oligomers, which do not progress to amyloid. However, these techniques cannot quantitatively assign what proportion of the population exists as an oligomeric aggregate versus monomer. With these proline substituted inserts, we expect some level of monomer to remain in equilibrium with the oligomeric phase. One potential method to address this problem is the use of analytical ultracentrifugation (AUC). For instance, AUC has been previously employed to determine the molecular size distribution of htt^{NT}-containing huntingtin peptides³⁸. Quantifying the molecular size distribution for these proline-substituted peptides would more definitively determine whether these peptides' preferred conformation is oligomeric or monomeric. Secondly, one could also incorporate fluorescent labels into our peptides and determine the size distribution using fluorescence correlation spectroscopy. A final alternative experimental approach to AUC could be size exclusion chromatography (SEC), although previous attempts to determine molecular size distributions of huntingtin oligomers using this method have generated conflicting results, potentially due to either the shearing forces of SEC, from interactions between the huntingtin peptides and the column, or due to an effect of the buffers used.

We additionally show that these hypo-amyloid constructs can effectively delay aggregation of a target htt-ex1^{P10}-Q₃₇ peptide by as much as an order of magnitude. However,

htt-ex1^{P10}-Q₃₇ eventually overcomes these inhibitors to form a thermodynamically stable amyloid; only the kinetics of nucleation and aggregation are changed. During this process, the inhibitors are drawn into the growing amyloid fibril in a 1:1 ratio in a mechanism that is dependent on the presence of htt^{NT}. This data suggests a possible role of htt^{NT} in the inhibition of nucleation and/or elongation. It is unclear how htt^{NT} achieves this, though there is previous evidence to suspect that htt^{NT} plays a role in the final β -sheet structure of the amyloid, which could help stabilize the addition of monomers in a dock and lock type mechanism³¹².

Interestingly, these hypo-amyloid analogs vary in their mechanisms of inhibition depending on the position of the glutamine to proline substitution. Hypo-amyloid constructs whose substitution is near the htt^{NT} domain (htt-ex1^{P10}- β HHP-P¹ and htt-ex1^{P10}- β HHP-P^{1,2}) strongly inhibit nucleation, but have a minimal impact on delaying elongation. Conversely, glutamine to proline substitutions near the C-terminal portion of the polyQ domain (htt-ex1^{P10}- β HHP-P²) has a strong inhibition of the elongation phase, but very little effect on delaying nucleation. This can be rationalized by how the polyQ domains arrange themselves within the oligomeric phase. Residual structure from the htt^{NT} domain, which actively participates in forming α -helical coiled-coil tertiary structure, may align a portion of the polyQ domain immediately following the coiled-coil structure. Within the oligomeric phase, alignment of this portion of the polyQ domain makes rational sense as the most likely initiator of early β -sheet formation and nucleation of aggregation, and preventing β -sheet formation at this step would potentially interrupt nucleation of aggregation. Conversely, we can rationalize that the growing end of an amyloid fibril requires an uninterrupted polyQ to interact with in order to continue elongation. Thus, β HHP-P², which contains one uninterrupted Q₁₁ stretch, is a much better inhibitor of elongation than β HHP-P^{1,2}, whose longest unbroken polyQ stretch is only Q₅. However, this does not explain why htt-ex1^{P10}-

β HP-P¹ is only an inhibitor of nucleation, but seems incapable of being an inhibitor of elongation.

We have shown that these hypo-amyloid analogs provide a tool to dissect the mechanism of huntingtin aggregation. Moreover, they provide a novel means of testing the toxic amyloid hypothesis and the toxic oligomer hypothesis, if expressed in model organisms. Any toxicity associated with these hyper- or hypo-amyloid analogs can be directly linked to their inherent relative capacities for β -structured amyloid formation. It will also be interesting to see whether or not these hypo-amyloid constructs, which efficiently delay aggregation *in vitro*, have any therapeutic effect in HD model organisms. Additionally, due to the incompletely understood abilities of these hypo-amyloid peptides to preferentially inhibit either nucleation or elongation, it will be thought provoking to test whether these inhibitors have variable therapeutic effects *in vivo*.

4.0 VALIDATING & TRANSLATING BIOPHYSICAL OBSERVATIONS IN CELL MODELS

4.1 INTRODUCTION

Previous studies from Section 2.0 demonstrated the construction of a hyper-amyloid β -hairpin enhanced huntingtin analog peptide capable of rapid fibrilization, while Section 3.0 discussed hypo-amyloid huntingtin analogs that rapidly aggregate into non- β oligomers and resist further aggregation. These peptides have a number of substitutions that either enhance or severely compromise their ability to nucleate aggregation of amyloid. This makes them ideal biological tools to circumvent current technological limitations and help identify the toxic species in HD – a toxic amyloid, a toxic non- β oligomer, or other. Additionally, the hypo-amyloid constructs delay aggregation of htt-ex1^{P10}-Q37 by roughly an order of magnitude *in vitro*. These extremely potent aggregation inhibitors could provide therapeutic benefit and prevent or delay HD onset if aggregation of amyloid is the major toxic species. In order to probe the identity of the toxic species and investigate the potential therapeutic benefit of the hypo-amyloid peptides, we first utilized cell culture systems.

A number of cell culture systems can be used to model HD, of which we chose PC12 cells. Historically, PC12 cell culture has been extensively used. The PC12 cell model provides a number of benefits and can be used to screen for several cellular outcomes, such as inclusion

body formation, cytoplasmic aggregation, apoptosis initiation, and cell death. Because of their ease of culture, PC12 cells offer a convenient mammalian cell culture model. Other immortalized cell lines, such as SH-SY5Y and SThdhQ^{111/111} provide similar benefits.

In contrast to immortalized cell lines, primary cultures of neurons are more physiologically relevant in their origin, form intranuclear inclusions similar to animal models and human patients, and are more sensitive to mutant huntingtin expression than immortalized cell systems. Primary mouse and rat cortical, striatal, and hippocampal neurons have been used to better understand drug mechanisms of action, htt and mhtt lifecycle and proteostasis, and mitochondrial dynamics. For instance, work by Cattaneo *et al.* showed that cholesterol homeostasis is disturbed in HD³¹³; primary neurons were used in conjunction with SIRT2 inhibitors to modulate sterol biosynthesis, which showed promising therapeutic results³¹⁴, but were ultimately not effective in an R6/2 genetic mouse model of HD crossed for SIRT2 ablation³¹⁵. Mhtt lifecycle studies in primary neurons have revealed a pivotal role of calpain cleavage in htt protein turnover³¹⁶ (which was later corroborated in *Drosophila*³¹⁷), while others detailed a role of serine 16 phosphorylation in the accumulation of htt in the nucleus³¹⁸. A number of studies using primary neurons to study mitochondrial dysfunction have identified a number of potential therapeutic targets, such as an altered interaction between polyQ expanded htt and PPAR- δ , a nuclear hormone transcription factor critical in lipid homeostasis, glucose metabolism, energy production, and mitochondrial health³⁰⁷. Primary neuron cultures have also been used to verify aggregation inhibitors²¹², as well as test the relationship between structure-function of mhtt and neuron toxicity³⁰¹. Thus, primary neurons allow for a detailed analysis of HD phenotype in a physiologically relevant cell culture system. For these reasons, we tested the expression of our huntingtin analogs in both PC12 cells and rat primary cortical neurons.

Herein we report that expression of the hyper-amyloid htt-ex1- β HP results in cytoplasmic inclusion formation in PC12 cells as well as perinuclear and intranuclear aggregation and cell death in primary rat cortical neurons. Conversely, the hypo-amyloid htt-ex1- β HP-P² peptide does not exhibit aggregation or cell death in PC12 cells or primary rat cortical neurons. Co-expression of htt-ex1- β HP-P² mitigated both the toxicity and number of intracellular aggregates caused by htt-ex1-Q₉₄ expression. Similar to how the hypo-amyloid peptides co-aggregate with their target *in vitro*, we present evidence of colocalization between htt-ex1- β HP-P² and htt-ex1-Q₉₄ puncta in live cells, whereas htt-ex1- β HP-P² forms no puncta alone. These results collectively point towards (a) a toxic amyloid species in HD, (b) disfavor a toxic oligomer hypothesis, (c) support the mechanism of action of our hypo-amyloid aggregation inhibitors, (d) provide a rationally designed therapeutic, and (e) provide a proof-of-principle target.

4.2 RESULTS

4.2.1 Transient Transfection of the β -Hairpin Enhanced htt Analogs in PC12 cells

PC12 cells are neuroendocrine in nature and are derived from a pheochromocytoma of the rat adrenal medulla³¹⁹. PC12 cells respond to NGF by differentiating into neuron-like dopamine-synthesizing cells^{204,319}. Both neuronal-like and undifferentiated PC12 cells respond to mutant huntingtin insult by undergoing caspase 3/7 mediated apoptosis³²⁰, cell death, and visible puncta formation^{308,321,322}. PC12 cells therefore offer a convenient cell model that can be used to rapidly screen for disease-modifiers³²³.

To determine whether any toxic effect is seen in the hyper-amyloid β HP or hypo-amyloid mid-strand Pro insertion peptides, we nucleofected PC12 cells to express the htt-exon1 constructs under control of a CMV promoter (Methods). At 48 hours post-transfection, as expected, htt-ex1-Q₂₅-EGFP forms no visible puncta by fluorescence microscopy, while htt-ex1-Q₄₆-EGFP forms at least one visible punctum in $23.8 \pm 2.5\%$ of PC12 cells (Figure 24). The hyper-amyloid htt-ex1- β HP, despite only containing 22-24 glutamines, forms aggregate puncta in PC12 cells ($23.0 \pm 9.4\%$) to a similar extent as pathogenic Q₄₆. Conversely, a single proline substitution that blocks aggregation *in vitro* also suppresses aggregation in PC12 cells; htt-ex1- β HP-P² forms visible puncta in only $9.9 \pm 3.5\%$ of cells (Figure 24).

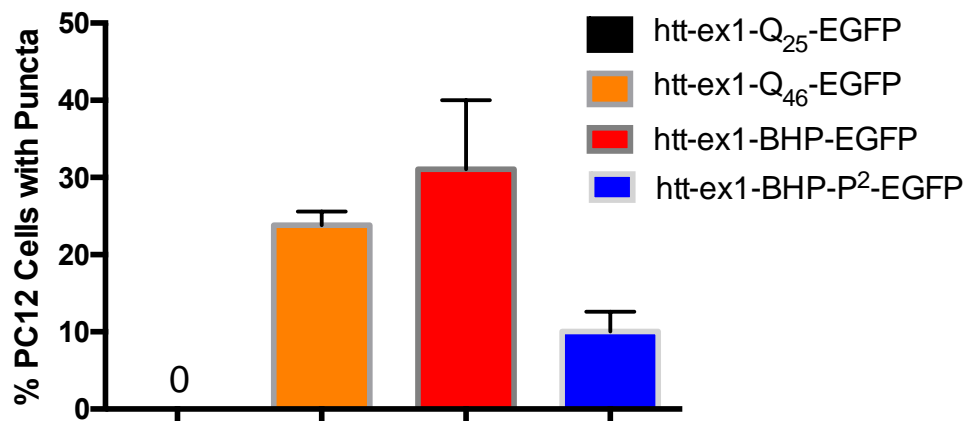


Figure 24: Percentage of PC12 Cells with Visible Puncta. PC12 cells were nucleofected with 2.0 μ g of appropriate DNA vector. PC12 cells were cultured for 48 hours, fixed, and imaged *via* fluorescence microscopy. The percentage of cells expressing the construct that were also positive for puncta are reported. n = 2, with at least 100 cells imaged per condition. Htt-ex1-Q₂₅-EGFP was completely absent of visible puncta.

In vitro, the hypo-amyloid analogs delay aggregation of pathogenic huntingtin (Section 3.0). To assess whether these constructs are able to inhibit aggregation in live cells, we co-

expressed htt-ex1-Q₉₄-EGFP alongside untagged mCherry, htt-ex1-βHP-P²-mCherry, or htt-ex1-βHP-P^{1,2}-mCherry. Htt-ex1-Q₉₄-EGFP/mCherry showed 30.3% (n = 1, >100 cells) of cells with aggregates, while htt-ex1-Q₉₄-EGFP/ htt-ex1-βHP-P^{1,2}-mCherry (20.3%, n = 1, >100 cells) and htt-ex1-Q₉₄-EGFP/ htt-ex1-βHP-P²-mCherry (15.1%, n = 1, >100 cells) showed fewer PC12 cells with visible puncta. Preliminary work using PC12 cells as a model ended after identifying their poor cell death response, even when expressing *bona fide* pathogenic huntingtin. For this reason, inclusion body formation studies were ended at n = 1.

Cell death measured by LDH release revealed no significant toxicity in any transfection scenario at 48 hours, including positive control htt-ex1-Q₄₆-EGFP. This is likely due to a number of factors, including the relatively short expression time of 48 hours, the hardiness of PC12 cells compared to more sensitive primary neurons, poor transfection efficiencies, and the limited discriminating power of ensemble-based cell death assays. To overcome these hurdles, we moved on to assess the toxicity of our constructs in primary rat cortical neurons, which can express the same plasmids for weeks. We expect primary neurons to be more sensitive to mhtt due to longer expression times leading to more time to exert toxicity and a reduced capacity to divide, as asymmetric division of damaged proteins is a coping mechanism of dealing with aggregates³²⁴. Additionally, we employed a more sensitive fluorescence based cell death assay to quantify viability on a cell-by-cell basis.

4.2.2 β -Hairpin Enhanced Huntingtin Analogs are toxic in primary rat cortical neurons.

Oligomeric huntingtin analogs are well tolerated and rescue htt-ex1-Q₉₄ associated toxicity.

Rat primary cortical neurons were isolated on E18 and nucleofected as previously described^{325,326}. At day *in vitro* (DIV) 14 and 21, neurons were fixed and imaged for aggregates and the percentage of Map2 positive neurons with visible inclusions was scored blind. Live neurons were also imaged at DIV 14 and 21 for cell viability using a NucRed 647 Dead exclusion assay. Negative control htt-ex1-Q₂₅-EGFP + mCherry ($2.5 \pm 3.9\%$) and had very few neurons with visible puncta at DIV 14 (Figure 25, 26). The positive control htt-ex1-Q₉₄-EGFP + mCherry ($87.2 \pm 10.9\%$) showed nearly all expressing neurons positive for aggregates. In sharp contrast to the polyQ repeat length dependence of aggregation above, htt-ex1- β HP-EGFP (which contains only a modest 22 glutamines) should not be sufficient to aggregate appreciably *in vivo* based on its nominal polyQ repeat length. However, because of its hyper-amyloidogenic β -hairpin enhancing motifs, $39.3 \pm 4.2\%$ of neurons expressing htt-ex1- β HP-EGFP were positive for aggregates. Expression of the proline substituted htt construct htt-ex1- β HP-P²-mCherry + EGFP, which does not aggregate appreciably beyond oligomers *in vitro*, did not show any significant puncta formation ($4.8 \pm 4.3\%$). While expression of the htt-ex1-Q₉₄-EGFP construct alone revealed widespread puncta, the htt-ex1-Q₉₄-EGFP + htt-ex1- β HP-P²-mCherry ($59.9 \pm 12.2\%$) had significantly fewer neurons with puncta (Figure 25, 26). Therefore, inclusion and aggregate formation *in vivo* are more closely associated with inherent amyloidogenesis and less dependent on absolute polyQ repeat length. The amyloid-incompetent htt analog htt-ex1- β HP-P²-mCherry, whose aggregation stalls at the non- β oligomer phase *in vitro*, was insufficient to trigger visible aggregation in primary neurons. Co-expression of htt-ex1- β HP-P²-mCherry alongside pathogenic

htt-ex1-Q₉₄-EGFP was sufficient to statistically significantly reduce puncta burden (from $87.2 \pm 10.9\%$ down to $59.9 \pm 12.2\%$)

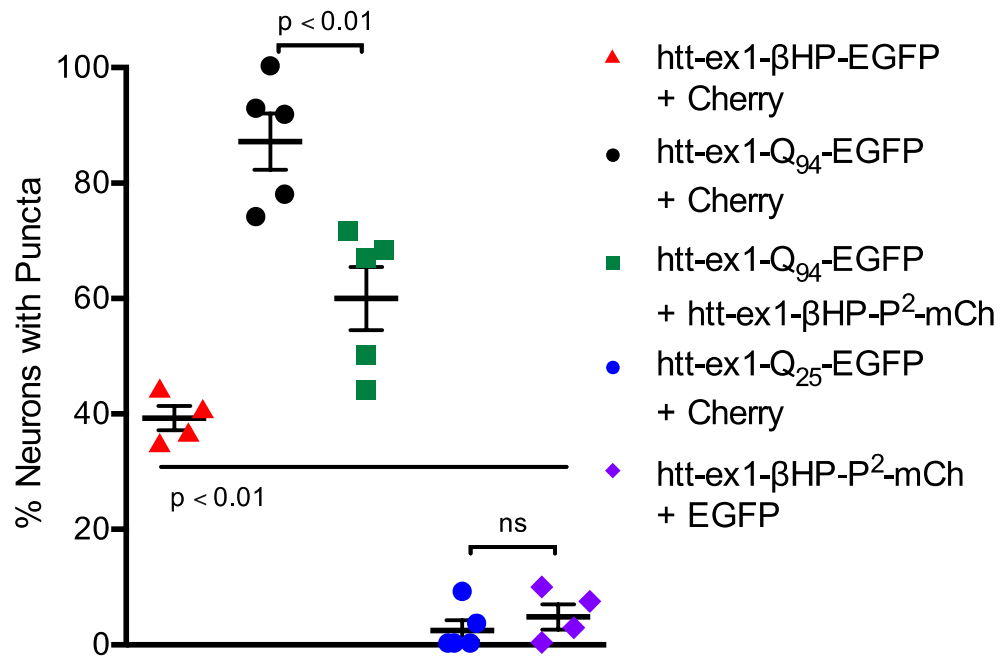


Figure 25: Percentage of Expressing Neurons Positive for Puncta. Rat primary cortical neurons were co-transfected with 1.5 + 1.5 μg DNA, cultured for 14 days, fixed and stained for Map2, and then scored blind for puncta in 4-5 independent experiments. Error bars are standard error of the mean.

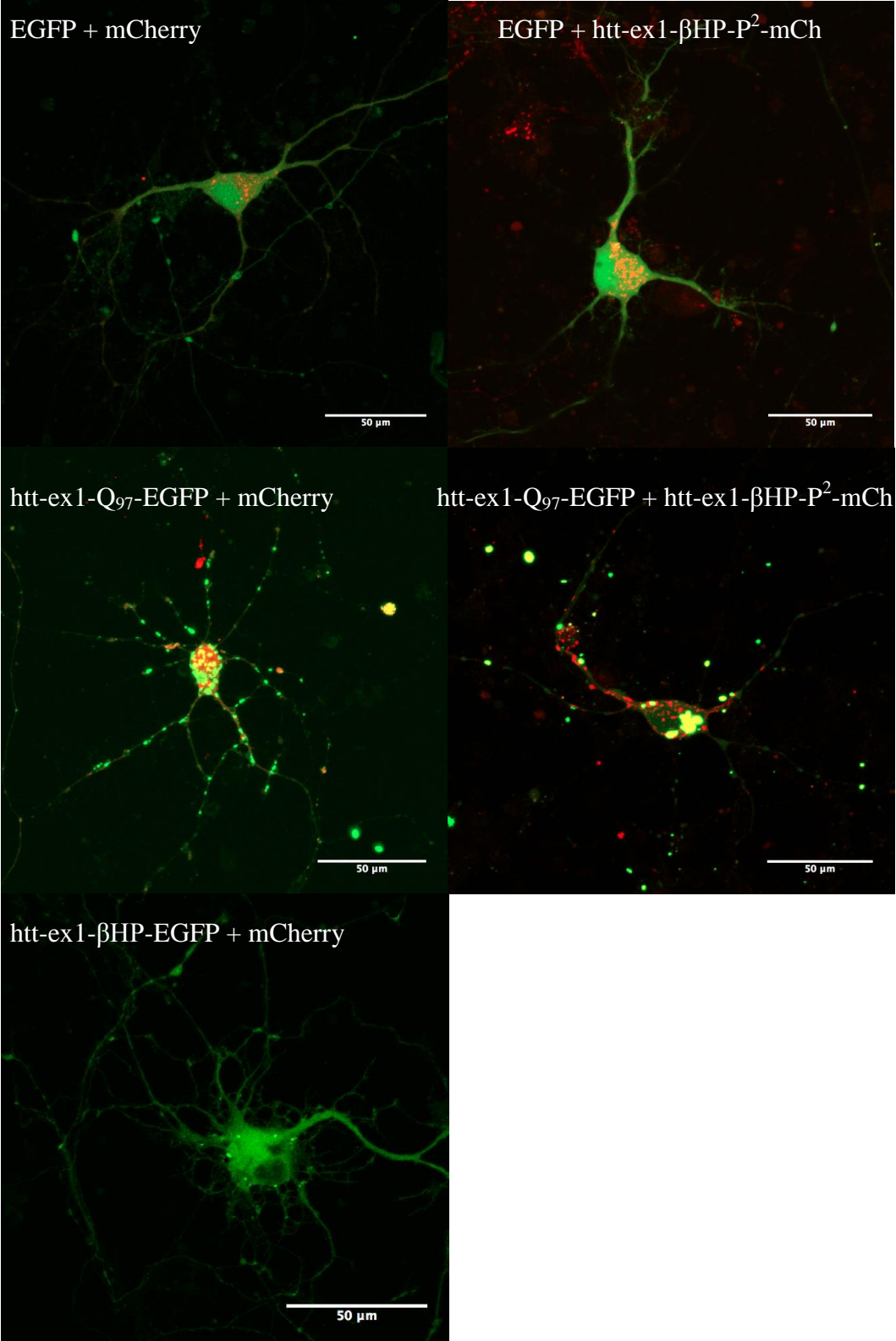


Figure 26: Representative confocal images from Figure 25 used in puncta quantification.

Using our hyper- or hypo-amyloid huntingtin analogs, we tested whether their expression alone was toxic in rat primary cortical neurons on DIV14 and 21 using a NucRed 647 Dead exclusion assay. In this assay, healthy cells reject the dye, which neurons with compromised cell membranes allow the dye to diffuse into the nucleus and bind to DNA and increase in fluorescence. As expected, htt-ex1-Q₉₄-EGFP expression is overtly toxic ($45.8 \pm 4.2\%$ viability at DIV 14 and 21) (Figures 27 & 28). The negative control htt-ex1-Q₂₅-EGFP is largely non-toxic ($84.4 \pm 4.1\%$ viability), showcasing a polyQ repeat length dependence of HD phenotype in this model. Depending on which is the toxic species in HD, we expected either the hypo-amyloid construct, which stably forms non- β oligomers *in vitro*, or the hyper-amyloid huntingtin analog, which rapidly progresses to an amyloid fibril endpoint, to be toxic. The non- β hypo-amyloid huntingtin analog htt-ex1- β HP-P²-mCherry was very well tolerated ($74.8 \pm 9.3\%$ viability) in primary neurons and had no statistically significant difference from a negative control htt-ex1-Q₂₅-EGFP. Conversely, the hyper-amyloid htt-ex1- β HP-EGFP was toxic ($47.1 \pm 7.8\%$ viability) to the same extent as our positive control htt-ex1-Q₉₄-EGFP. As an additional test of the toxic species of huntingtin, the inhibitor htt-ex1- β HP-P²-mCherry was expressed alongside htt-ex1-Q₉₄-EGFP. Htt-ex1- β HP-P²-mCherry significantly rescued the overt toxicity of htt-ex1-Q₉₄-EGFP for a 61% level of protection ($69.3 \pm 7.1\%$ viability, up from $45.8 \pm 4.2\%$) (Figure 28).

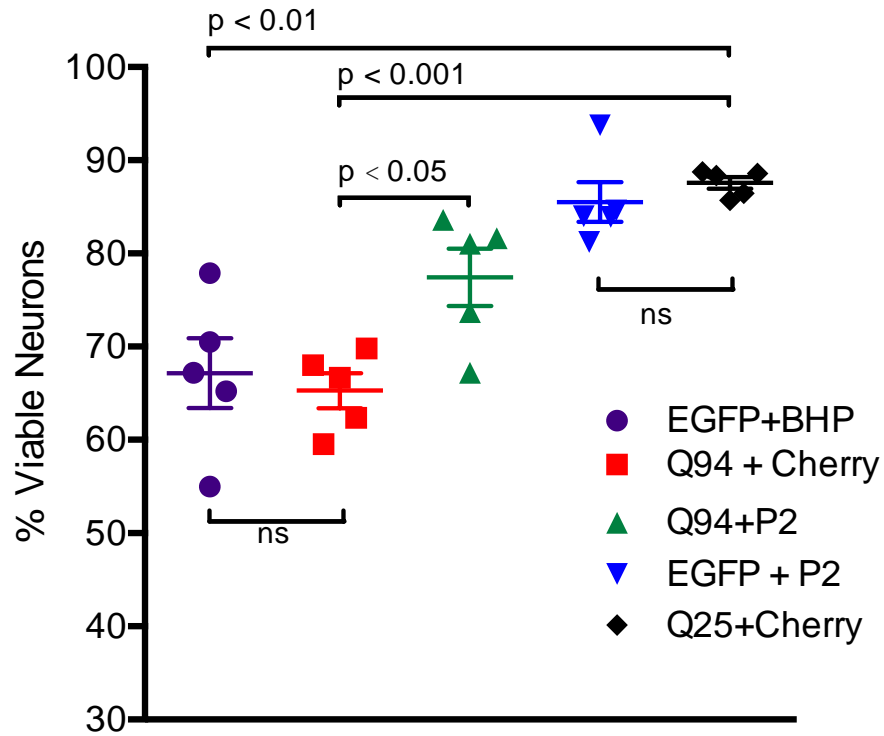


Figure 27: Viability of Neurons at DIV14. Rat primary cortical neurons were co-transfected with 1.5 + 1.5 μ g DNA and cultured for 14 days. Viability was measured in 4-5 independent experiments using a NucRed 647 Dead assay in live neurons at DIV14. Error bars are standard error of the mean.

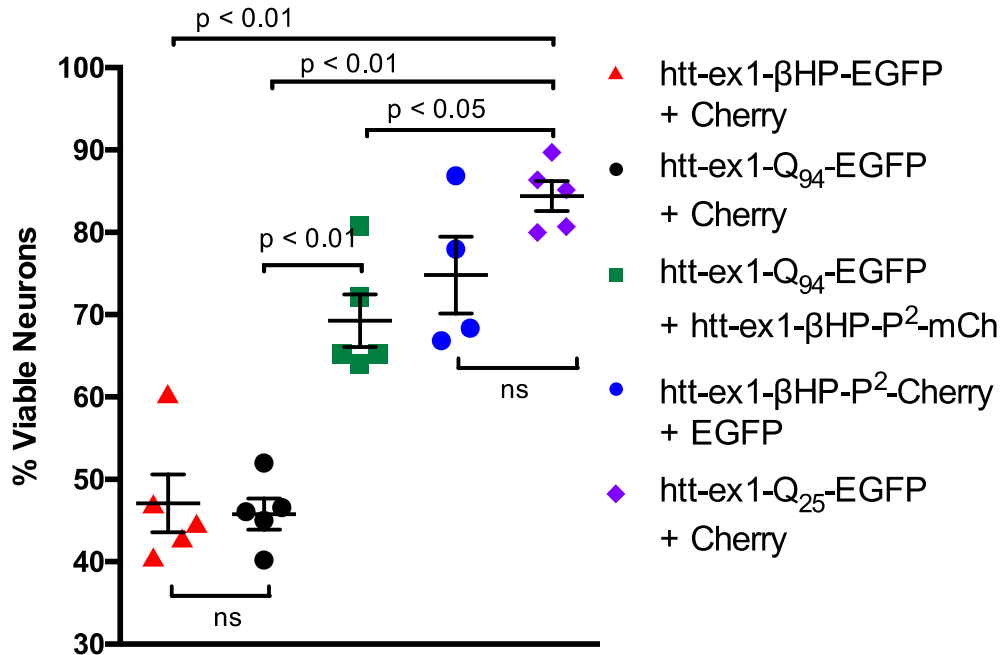


Figure 28: Viability of Neurons at DIV21. Rat primary cortical neurons were co-transfected with 1.5 + 1.5 μg DNA and cultured for 21 days. Viability was measured in 4-5 independent experiments using a NucRed 647 Dead assay in live neurons at DIV21. Error bars are standard error of the mean.

As discussed Section 3.0, the proline substituted inhibitors co-aggregate with their target huntingtin *in vitro*. To determine if this occurs in neurons, we used confocal microscopy to quantify colocalization. As expected, line intensity profiles of htt-ex1-Q₉₄-EGFP + mCherry show no correlation between the bright localized EGFP puncta of Htt-ex1-Q₉₄-EGFP and the diffuse mCherry signal (Figure 29, Pearson's correlation = 0.17 ± 0.05 for 15 random cell images). However, htt-ex1-Q₉₄-EGFP + htt-ex1-βHP-P²-mCherry co-expression shows significant overlap between bright EGFP puncta and bright mCherry puncta (Figure 30, Pearson's correlation = 0.86 ± 0.07 for 15 random cell images), illustrating that these inhibitors are able to find and co-aggregate with their huntingtin targets both *in vitro* and *in vivo*. This co-

aggregation phenomenon likely results from specific details of the inhibitor mechanism of htt-ex1- β HP-P².

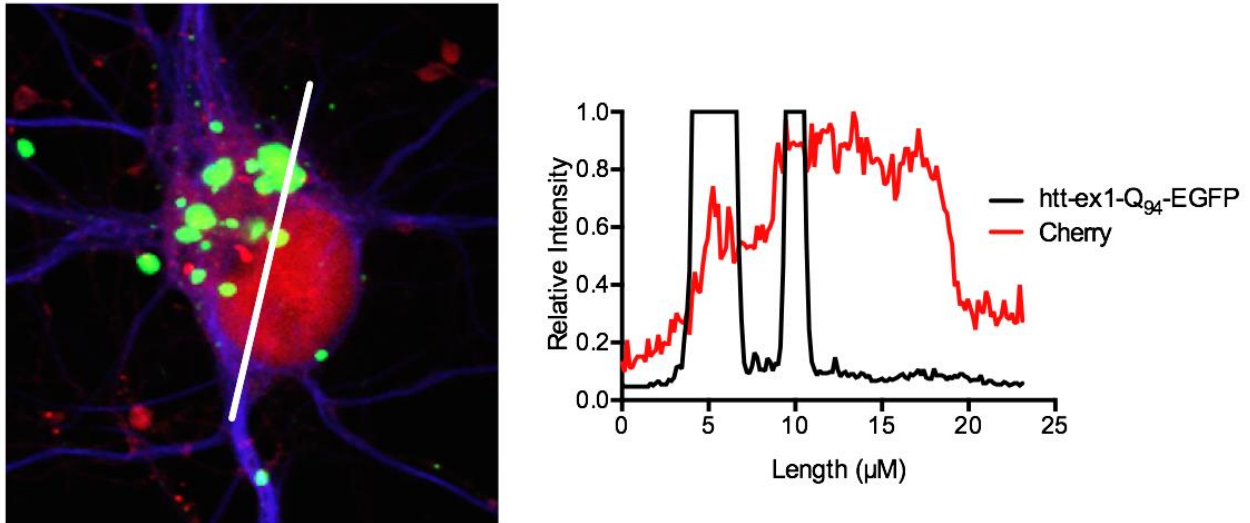


Figure 29: Example Line Trace Between htt-ex1-Q₉₄-EGFP and mCherry. Primary rat cortical neurons expressing htt-ex1-Q₉₄-EGFP and mCherry were fixed and stained for Map2 (blue) at DIV14. Fluorescence intensity line traces along a straight line path shows no obvious colocalization between the intense scattered green puncta signal and the diffuse mCherry signal. 15 cells were randomly chosen to generate one-dimensional line intensity profiles taken over 3 cultures, yielding an average Pearson's coefficient of 0.17 ± 0.05

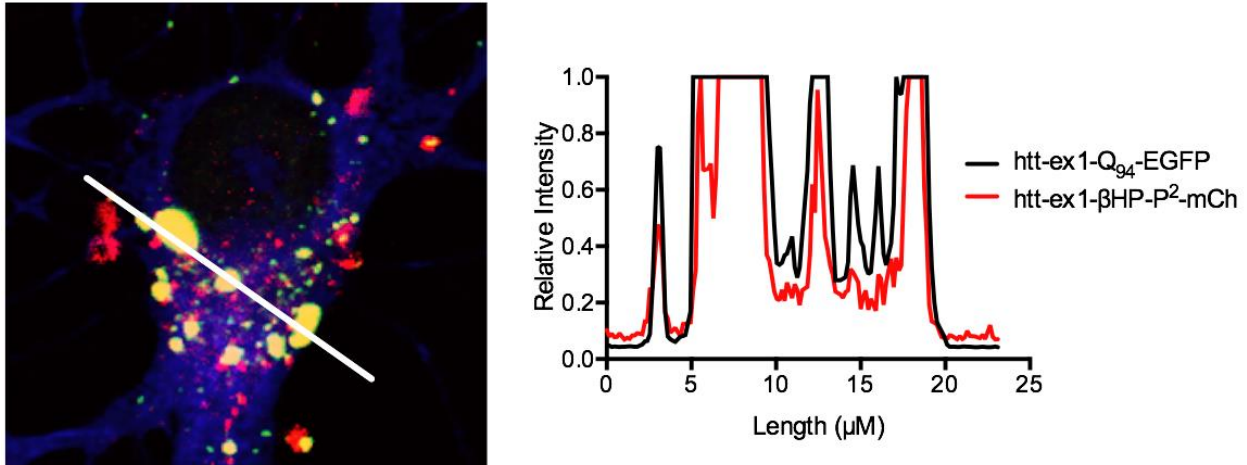


Figure 30: Example Line Trace Between htt-ex1-Q₉₄-EGFP and htt-ex1-βHP-P²-mCherry. Primary rat cortical neurons expressing htt-ex1-Q₉₄-EGFP and htt-ex1-βHP-P²-mCherry were fixed and stained for Map2 (blue) at DIV14. Fluorescence intensity line traces along a straight line path shows significant colocalization between the intense scattered green puncta signal and the intense red puncta. 15 randomly generated one-dimensional line intensity profiles were taken from a total of 15 cells over 3 cultures, yielding an average Pearson's coefficient of 0.86 ± 0.07 .

4.3 DISCUSSION

The toxic species of huntingtin is highly contested and must be resolved before therapeutics can be rationally designed. The toxic protein conformer of huntingtin has been technologically difficult to study due to the ability of huntingtin to rapidly adopt a multitude of heterogeneous conformers in solution (Sahoo 2016 Manuscript Submitted). Many studies attempting to identify the toxic conformer of huntingtin rely on the correlation between the timing of when huntingtin species appear and the onset of molecular pathologies.

To circumvent these technological limitations, we designed a series of huntingtin analogs that *in vitro* are either hyper-amyloid (Section 2.0) and rapidly nucleate aggregation into amyloid formation, or are hypo-amyloid (Section 3.0) and stall at the non- β oligomer phase. These analog proteins make ideal tools to (a) decouple absolute polyQ repeat length from aggregation and (b) parse the toxic contribution of soluble non- β oligomers. We expressed these constructs in mammalian cells and in primary rat cortical neurons to determine their capacity to generate an HD phenotype *in vivo*.

The hyper-amyloid htt-ex1- β HP, which aggregates rapidly in *in vitro* experiments, forms large puncta aggregates in both PC12 cells and primary cortical neurons. Additionally, htt-ex1- β HP-EGFP expression is associated with poor viability in primary neurons. Thus, we determined that absolute polyQ repeat length is not necessary to generate a toxic HD phenotype, but rather it is the intrinsic capacity of polyQ to aggregate into amyloid that most closely correlates with toxicity. These results have a broad impact in the interpretation of toxic models of HD, such as a toxic RNA which relies on absolute CAG repeat length, as well as other toxic models that rely on absolute polyQ repeat length. That is, the correlation between absolute CAG/polyQ repeat length and HD progression is derived from an increased propensity to aggregate into amyloid.

Conversely, the hypo-amyloid htt-ex1- β HP-P²-mCherry, which forms stable non- β oligomers *in vitro*, does not appreciably form amyloid in cells. The hypo-amyloid construct does not have any apparent toxicity and is well tolerated in both PC12 cells and primary rat neurons. Therefore, we find no evidence in favor of a toxic oligomer hypothesis by this direct test.

Finally, *in vitro*, the hypo-amyloid peptides, when added to soluble htt-ex1^{P10}-Q₃₇, delay its amyloid formation by as much as an order of magnitude (Section 3.0), while presumably leading to an intermediate build-up of mixed oligomers (Figures 17-19, 21, Scheme 1). This

mechanism involves the co-aggregation of the normally soluble hypo-amyloid analogs into the growing htt-ex1^{P10}-Q₃₇ fibril. In primary neurons, the hypo-amyloid analog htt-ex1-βHP-P²-mCherry rescues the toxic effect of htt-ex1-Q₉₄-EGFP. Thus, neurons expressing both htt-ex1-Q₉₄-EGFP + htt-ex1-βHP-P²-mCherry show fewer puncta than neurons expressing htt-ex1-Q₉₄-EGFP + mCherry. Additionally, similar to the mechanism of inhibition demonstrated *in vitro*, we find that the inhibitor htt-ex1-βHP-P²-mCherry co-aggregates with its target htt-ex1-Q₉₄-EGFP in primary neurons. Since this mechanism depends on the formation of mixed non-β oligomers with prolonged lifetimes before amyloid nucleation, these data also suggest further, indirect evidence against the toxic oligomer hypothesis.

Previous experiments utilizing super-resolution microscopy have demonstrated that the previously labeled “soluble” portion of htt in cells can be populated by small aggregated species, including small amyloid-like structures^{42,44,308}. Given the use of confocal microscopy to identify aggregation *in vivo* in this chapter, it is a salient point to remember the significant limitations of this approach. These cell studies were only able to identify the largest aggregated structures – inclusion bodies – and cannot easily differentiate between small amyloid, oligomeric, and other aggregated structures from the monomeric population. One technique that could potentially overcome this hurdle is fluorescence correlation spectroscopy (FCS). FCS could be used on live cells to estimate the molecular size distribution of fluorescently labeled particles and differentiate between monomers, small oligomers (4-20mer), and large diffusible aggregates. Additionally, inclusion bodies may also be quantified in this model. For instance, cell lysates could be centrifuged to isolate inclusion bodies, which could then be disaggregated similar to the disaggregation of chemically synthesized peptides^{77,99,293}. The solubilized inclusion bodies could then be semi-quantified by Western Blot by comparing densitometries of htt-exon1-GFP to a

recombinant GFP protein standard. In this way, we could attempt to quantify the mass of inclusion bodies present in neurons.

Together, these data strongly support the toxic amyloid hypothesis and not the toxic oligomer hypothesis. The hyper-amyloid construct generates an HD phenotype despite its nominal absolute polyQ repeat length, while the hypo-amyloid peptides are well tolerated and rescue mutant huntingtin HD phenotype, likely by sequestering and stalling mutant huntingtin in the non-toxic oligomer phase before the inevitable thermodynamically favorable amyloid aggregate overwhelms neurons.

5.0 DROSOPHILA AS A MODEL OF NEURODEGENERATION

5.1 INTRODUCTION

Several pathologies of HD, such as protein aggregation and cell death, can be conveniently modeled using *in vitro* and cell culture systems; however, more complex symptoms of HD are derived from changes in the connectivity and communication between disparate neuronal populations³²⁷, which cannot feasibly be modeled without using whole organisms. Since the discovery of the mutant CAG expansion in the *huntingtin* gene that causes HD, a number of HD animal models have been constructed, such as: *C. elegans*^{174,233}, zebrafish³²⁸, mice^{7,168}, and more recently non-human primates^{329,330}. Each model brings its own tool set, benefits, and resource constraints. Mice and other mammals have the benefit of being genetically and anatomically more related to humans than zebrafish or worms. In Huntington's disease, this becomes evident as humans and mice brains share anatomical structures, such as a striatum and cortex, which are classically the first brain regions to undergo neurodegeneration in humans. Conversely, the entire adult *C. elegans* nervous system contains only 302 neurons, which has its own benefits and draw backs.

Drosophila offer an excellent compromise between a robustness of end points, CNS anatomical homology, ease of use, and powerful genetic tools. *Drosophila* HD models are well characterized, mimic the age and polyQ-repeat dependence of HD pathophysiology in humans,

and have well defined quantitative and qualitative outcomes^{78,197,225}. *Drosophila* therefore are a powerful model that recapitulate many key aspects of HD in humans.

To take advantage of this system, we generated a series of female flies homozygous for htt-exon1 C-terminally fused with a fluorescent protein (EGFP or mCherry). We drove expression pan-neuronally using the *elav*-Gal4 promoter and analyzed age-dependent behavior phenotypes as well as lifespan. Flies expressing these huntingtin analogs mirrored the results found *in vitro* and in PC12 and primary neuron cultures: the hyper-amyloid htt-ex1-βHP is associated with locomotor and lifespan defects, while the hypo-amyloid htt-ex1-βHP-P² and htt-ex1-βHP-P^{1,2} are non-toxic. Additionally, when co-expressed alongside pathogenic htt-ex1-Q₉₄, htt-ex1-βHP-P² and htt-ex1-βHP-P^{1,2} improve lifespan and locomotor function associated with toxic htt-ex1-Q₉₄.

5.2 RESULTS

5.2.1 Constructing a *Drosophila* HD model

We generated *Drosophila* expressing our transgenes using the Gal4/UAS expression system²¹⁸, where Gal4 is a soluble protein that actively promotes genes immediately downstream from UAS promoter sequences. In this system, expression of a gene of interest can be modulated by when and where Gal4 is expressed. Placing the *Gal4* gene downstream from various regulatory elements can grant specific spatial or temporal expression patterns of the Gal4 protein., therefore conferring spatio-temporal expression of our gene of interest.

Currently, hundreds of Gal4 lines have been developed and characterized for tissue-specific expression. Of interest is the embryonic lethal abnormal visual system (*elav*) gene, which is required for *Drosophila* nervous system development and maintenance^{215,331,332}. Promoter fragments from the *elav* sequence were used to generate *elav*-Gal4, which allows for Gal4 expression in all neurons of larva and adult *Drosophila*³³³. *elav*-Gal4 is transiently expressed to a lesser extent in neuroblasts and glial cells of the *Drosophila* CNS³³⁴. The *elav*-Gal4 is commonly used in *Drosophila* models to study neurodegeneration.

A UAS element followed by the heat shock protein 70 basal promoter was placed upstream from the GOI, which is expressed in the presence of Gal4. The combined UAS-*htt* sequence is placed within a pUAS-attB vector, which contains a marker for successful gene insertion, w^+ , as well as an attB site suitable for homologous recombination³³⁵. To stably integrate our UAS-*htt* into the fly genome, there are currently dozens of *Drosophila* stocks containing *AttP* landing sites on all chromosomes available through *Genetic Services, Inc.* (Cambridge, MA). This allows for site-specific insertion to ensure minimal perturbation to the *Drosophila*'s endogenous genome. Insertion into the genome is accomplished using site selection homologous recombination *via* a ϕ C31 integrase system²¹⁴. *Drosophila* with successful integration are identified by a marker, typically w^+ , and mated with balancer chromosomes. For our studies, we selected AttP18 located at 6C12 of chromosome X, and chose the X chromosome balancer *FM0*. Insertion of our gene of interest onto the X chromosome has the benefit of using the male Y chromosome as a natural balancer during future genetic crosses. As a consequence, in order to generate homozygotes of our construct, we must use two X chromosomes, thus the need for female flies in the following experiments. AttR flies were also constructed, which underwent

the same genetic engineering process, but do not have a UAS-*htt* element for Gal4 to act on. Mating schemes to achieve co-expression and homozygous expression are found in Scheme 2.

$$\begin{array}{l}
\text{F0} \quad \frac{\sigma^{\text{♂}} [w^+]htt}{y} \text{ ;; } \text{X} \quad \frac{\text{♀} \quad +}{\text{FM0}} \text{ ;;} \\
\text{F1} \quad \frac{\text{♀} [w^+]htt}{\text{FM0}} \text{ ;; } \text{X} \quad \frac{\sigma^{\text{♂}} \text{ FM0}}{y} \text{ ;;} \\
\text{F2} \quad \frac{\text{♀} [w^+]htt}{\text{FM0}} \text{ ;; } \text{X} \quad \frac{\sigma^{\text{♂}} [w^+]htt}{y} \text{ ;;} \\
\text{F3} \quad \frac{\text{♀} [w^+]htt}{[w^+]htt} \text{ ;; } \text{X} \quad \frac{\sigma^{\text{♂}} \quad +}{y} ; \frac{elav-Gal4, [w^+]}{\text{CyO}} ; \\
\text{F4} \quad \frac{\text{♀} [w^+]htt}{[w^+]htt} \text{ ;; } \text{X} \quad \frac{\sigma^{\text{♂}} [w^+]htt}{y} ; \frac{+}{\text{CyO}} ; \\
\text{F5} \quad \frac{\text{♀} [w^+]htt}{[w^+]htt} ; \frac{+}{\text{CyO}} ; \text{X} \quad \frac{\sigma^{\text{♂}} \quad +}{y} ; \frac{elav-Gal4, [w^+]}{elav-Gal4, [w^+]} ; \\
\text{F6} \quad \frac{\sigma^{\text{♂}} [w^+]htt}{y} ; \frac{elav-Gal4, [w^+]}{\text{CyO}} ; \text{X} \quad \frac{\text{♀} [w^+]htt}{[w^+]htt} \text{ ;;} \\
\text{F7} \quad \frac{\text{♀} [w^+]htt}{[w^+]htt} ; \frac{elav-Gal4, [w^+]}{+} ;
\end{array}$$

Scheme 2: *Drosophila* mating scheme

5.2.2 Hyper-amyloid huntingtin analogs, and not hypo-amyloid analogs, have locomotor and lifespan defects.

To quantify HD phenotype in our *Drosophila* model, we employed a Rapid Iterative Negative Geotaxis assay (RING) to measure locomotor function²²⁶, which challenges flies to climb a maximum of 5 vertical centimeters in 8 seconds. Additionally, we recorded death events every 2 days while changing media to measure lifespan. Occasionally, flies may become trapped between the wall of the vial and the media, the media may become overly wet and drown flies, or flies may become tangled in the cotton tops of the vials. In these instances, the fly deaths were ruled as non-natural and those events were not included in the final lifespan tallies.

Homozygous female flies expressing our huntingtin analogs under *elav*-Gal4 control were aged at 29 C post-eclosion (Day 0). Wild type *AttR* were used as controls that underwent the genetic engineering process. These flies contain the pUAS-attB-IVS^{8/9} backbone vector and UAS promoter sequence inserted into AttP18, *elav*-Gal4 on chromosome 2, but lack any *htt* gene associated with the UAS promoter sequence to be expressed. *The AttR control and htt-ex1-Q25-EGFP* showed normal locomotor function with age (Figure 31). *Htt-ex1-Q46-EGFP* flies, featuring a polyQ repeat length in the same range as most HD patients, exhibit a moderately accelerated decrease in RING performance with age. Furthermore, *htt-ex1-Q94-EGFP* flies, featuring a polyQ repeat length comparable to very aggressive juvenile HD in humans, show a severe drop in performance at all ages tested. Starkly breaking this trend of increased polyQ repeat length on disease, the *htt-ex1-βHP-mCherry* flies have severely and statistically

significantly compromised locomotor function at nearly all ages, with severity ranging between *htt-ex1-Q₄₆-EGFP* and *htt-ex1-Q₉₄-EGFP* (Figure 31).

However, a single (*htt-ex1-βHP-P²-mCherry*) or double (*htt-ex1-βHP-P^{1,2}-mCherry*) proline substitution, which stalls aggregation *in vitro* at the non-β oligomer form *in vitro*, is sufficient to block the toxic effect of the β-hairpin enhancing motifs (Figure 31).

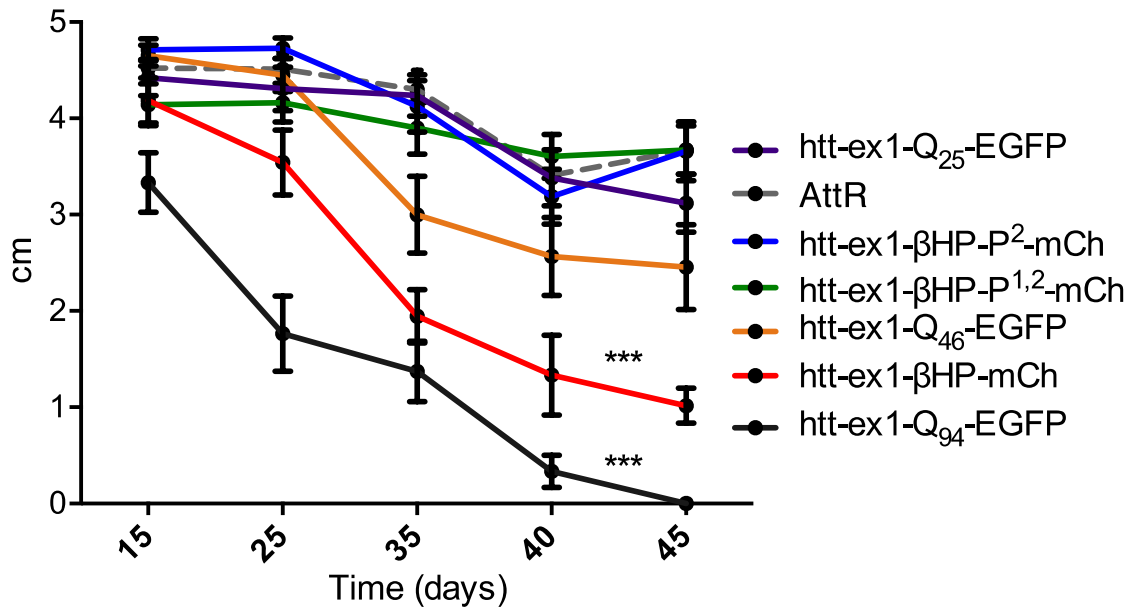


Figure 31: Rapid Iterative Negative Geotaxis (RING) Assay Testing Locomotor Function. Flies were challenged with a RING test at various ages. A total of at least 30 flies and three technical repeats with 10 flies per vial were used per condition. A two-way ANOVA using Bonferroni's multiple comparisons test was used to determine statistical significant *versus* *htt-ex1-Q₂₅*. *** $p < 0.001$, error bars are standard error of the mean.

The same polyQ repeat length dependent trend was observed for longevity, with *htt-ex1-Q₂₅-EGFP* flies exhibiting normal longevity (median survival 68 days) comparable to that of *AttR* control flies. *htt-ex1-Q₄₆-EGFP* flies have moderate lifespan defects (52 days) and *htt-ex1-*

Q94-EGFP flies show severely reduced longevity (36 days) (Figure 32). Our *htt-ex1-Q94-EGFP* lifespans are on par with other HD *Drosophila* lines, which tend to include ~128-150 glutamine repeats, and result in a median lifespan of 20-45 days (down from ~65-80 days for Q0, Q15, or white+ flies aged at 25 C or 29 C)^{225,306}. As expected, polyQ repeat length inversely correlates with HD severity in our model. Again breaking the polyQ repeat threshold of disease, *htt-ex1-βHP-mCherry* exhibits significantly shortened lifespan (56 days, Figure 32). *htt-ex1-βHP-mCherry* severity is roughly on par with *htt-ex1-Q46-EGFP*. Thus, as in the primary neuron experiments, pathology is less associated with absolute polyQ content, and more associated with the demonstrated ability of each protein to support amyloid formation.

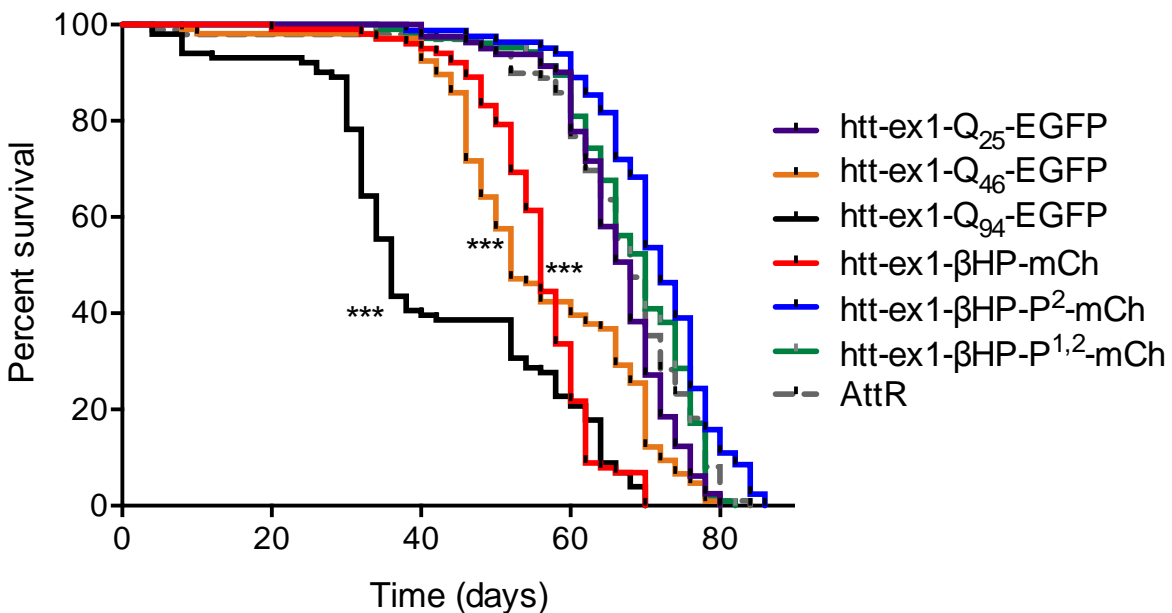


Figure 32: Lifespan Analysis of *Drosophila*. Survival curves of flies aged at 29 °C after eclosion. Dead flies were counted and removed every 2 days. A log-rank Mantel-Cox comparison of survival curves was used to determine the statistical significant *versus* *htt-ex1-Q25-EGFP* flies. *** $p < 0.0001$.

Conversely, both the *htt-ex1-βHP-P²-mCherry* and *htt-ex1-βHP-P^{1,2}-mCherry* flies have uncompromised lifespan (70 days, Figure 32), which is consistent with their uncompromised locomotion (Figure 31). Thus, hypo-amyloid *htt-ex1* analogs are well tolerated, while the hyper-amyloid peptide *htt-ex1-βHP-mCherry* exhibits severe HD phenotype.

5.2.3 Hypo-amyloid huntingtin analogs rescue *htt-ex1-Q₉₄* associated toxicity

To confirm the inhibitory effects of the mid-strand proline versions of *htt-ex1-βHP* *in vitro* (Figures 17-20) and in primary neurons (Figures 25-30), we generated *Drosophila* co-expression models. Four expression-balanced lines were constructed, each containing one copy of *htt-ex1-Q₉₄-EGFP* plus a second alternate copy of either *htt-ex1-Q₉₄-EGFP*, *htt-ex1-Q₂₅-EGFP*, *htt-ex1-βHP-P²-mCherry*, or *htt-ex1-βHP-P^{1,2}-mCherry*.

The lifespan of the *htt^{Q₉₄}/htt^{Q₂₅}* flies (36 days) was indistinguishable from that of the *htt^{Q₉₄}/htt^{Q₉₄}* flies (36 days) (Figure 33), both exhibiting reduced longevity from that of control flies. Likewise, we found that the *htt^{Q₉₄}/htt^{Q₂₅}* flies exhibited an age-dependent decline in locomotor function nearly as severe as that of the *htt^{Q₉₄}/htt^{Q₉₄}* flies described above (Figure 34). In contrast, flies expressing a combination of *htt-ex1-Q₉₄* and either of the two mid-strand proline-substituted analogs exhibit normal locomotion and improved longevity. The age-dependent locomotion observed for the *htt^{Q₉₄}/htt^{P²}* and *htt^{Q₉₄}/htt^{P^{1,2}}* flies is comparable to that of control flies and dramatically improved from *htt^{Q₉₄}/htt^{Q₂₅}* and *htt^{Q₉₄}/htt^{Q₉₄}* flies (Figure 34). Lifetimes of *htt^{Q₉₄}/htt^{P²}* (52 days) and *htt^{Q₉₄}/htt^{P^{1,2}}* flies (54 days) were also remarkably improved compared to *htt^{Q₉₄}/htt^{Q₉₄}* (36 days) or *htt^{Q₉₄}/htt^{Q₂₅}* (36 days) (Figure 33). This is equivalent to a ~40% rescue with respect to the normal median longevity of ~68 days in *AttR* or

htt-ex1-Q25-EGFP flies. Thus, co-expression of a mid-strand Pro analog of *htt-ex1-βHP* drastically abrogates the toxic effects of mutant *htt-ex1*.

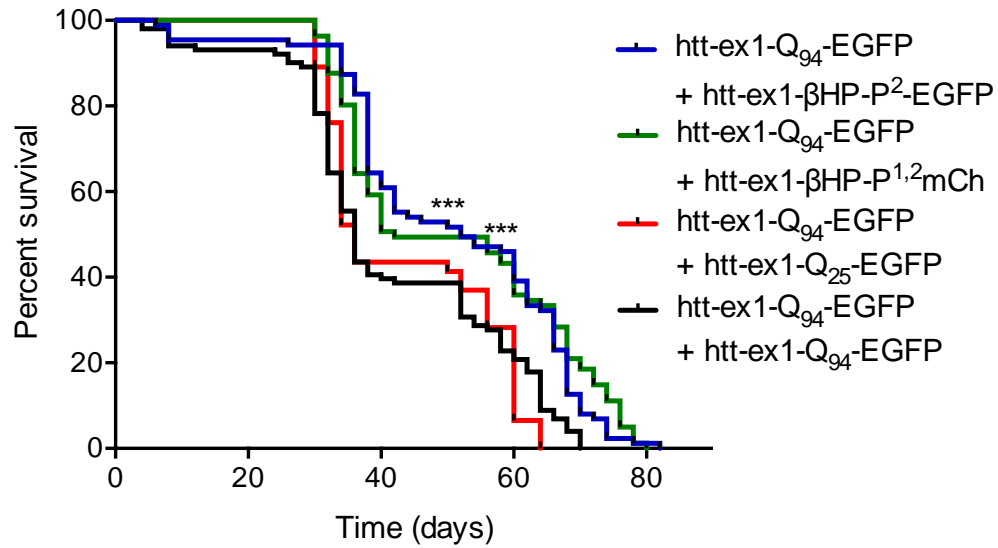


Figure 33: Lifespan Rescue Analysis of Rescue HD *Drosophila*. Survival curves of flies aged at 29 °C after eclosion. Dead flies were counted and removed every 2 days. A log-rank Mantel-Cox comparison of survival curves was used to determine the statistical significant *versus* *htt-ex1-Q₉₄/htt-ex1-Q₂₅*. *** p < 0.0001.

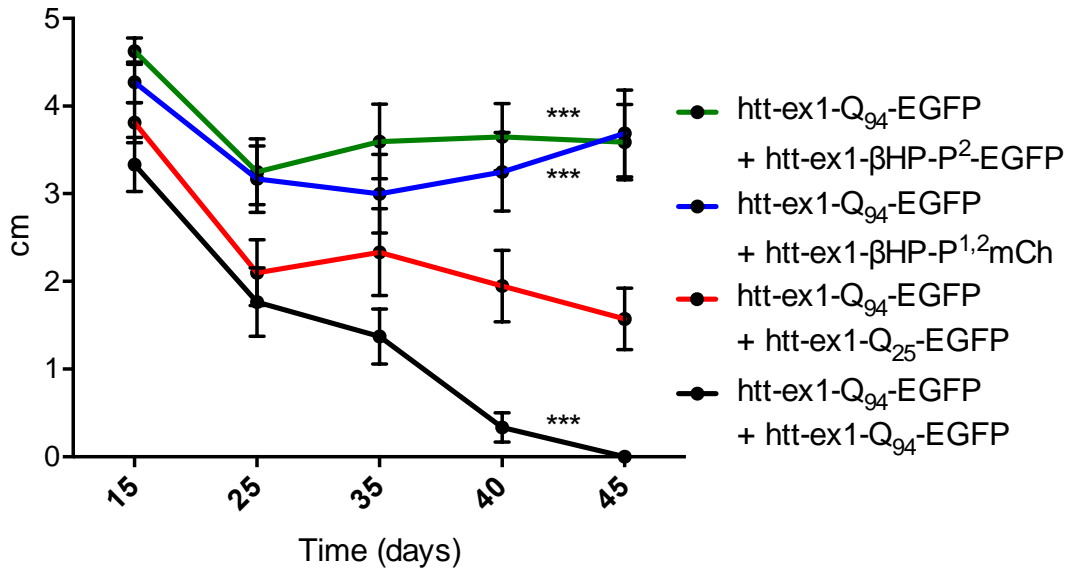


Figure 34: Locomotor Rescue of Rescue HD *Drosophila*. Flies were challenged with a RING test at various ages. A total of at least 30 flies and three technical repeats with 10 flies per vial were used per condition. A two-way ANOVA using Bonferroni's multiple comparisons test was used to determine statistical significant *versus* htt-ex1-Q₉₄/htt-ex1-Q₂₅. *** p < 0.001, error bars are standard error of the mean.

5.3 DISCUSSION

The mechanism by which mhtt gains toxic function is controversial and is a central roadblock in designing hypothesis driven therapeutics. Herein we present data from whole animal *Drosophila* expressing hyper- and hypo-amyloid htt-ex1 analog constructs. These data are consistent with the results from primary neurons, PC12 cell culture, and *in vitro* biophysics. We find that the absolute polyQ repeat length is less important than its amyloidogenicity – a protein's inherent propensity to misfold and aggregate into amyloid.

In constructing our *Drosophila* model controls (homozygous Q25, Q46, Q97), we identified a system in which pathologically relevant repeat lengths, such as Q46, give a robust HD phenotype. *Drosophila* expressing htt-ex1-Q₄₆-EGFP showed an age-dependent decline in locomotor capacity as well as a decrease in median lifespan. At the time of this work, and to our knowledge, there are no other animal models showing lifespan and behavioral defects using polyQ repeat lengths near that of the typical human HD patient (polyQ = 37-50). Our findings may be due to a number of factors, including (a) potentially increased expression using homozygotes (b) potentially increased translation by incorporating a splicing intronic sequence IVS^{8/9} (c) a large ‘n’ value, granting high statistical power in our statistical analysis, and (d) robust and highly reproducible assays, such as the RING assay for locomotion. These htt-ex1-Q₄₆-EGFP fly models could be used as a more biologically relevant model to screen for disease modifying drugs that may be effective enough to limit htt-ex1-Q₄₆ toxicity (a polyQ repeat length similar to most human HD patients), but note excessively aggressive htt-ex1-Q₉₄.

A second unique observation that came from our control flies was the identification of poor allele specificity in determining HD progression in animal models. Previous reports suggest that humans homozygous for the mutant huntingtin allele have a similar age-of-onset of disease to their heterozygous counterparts³³⁶. We found that homozygous Q97/Q97 *Drosophila* showed no statistically significant difference in median lifespan versus heterozygous Q97/Q25 strains. However, the heterozygous Q97/Q25 flies did perform moderately better in locomotor assays. Our results are consistent with the literature, suggesting that homozygosity of the mutant *htt* allele does not significantly affect age-of-onset compared to heterozygotes, but homozygous carriers may have more severe symptoms, which is recapitulated in our locomotion RING assays.

As in primary neuron cultures, *Drosophila* expressing the hyper-amyloid htt-ex1-βHP exhibit HD-like phenotypes characterized by locomotor defects and shortened lifespans. It is possible that htt-ex1-βHP gains its toxic function from a mechanism other than by enhancing nucleation of aggregation into amyloid, but this process would require some other attribute not shared with htt-ex1-Q₂₅. Amyloid formation is the only known process that connects the βHP enhanced peptide to mhtt. This culmination of data supporting a toxic HD-like phenotype associated with a hyper-amyloid construct further strengthens polyQ aggregation into amyloid as the toxic species in HD.

In sharp contrast, the hypo-amyloid htt constructs, htt-ex1-βHP-P² and htt-ex1-βHP-P^{1,2}, which are incapable of forming amyloid and only ever progress to non-β oligomers *in vitro*, are well tolerated when expressed in *Drosophila*. Furthermore, the presence of these mid-strand Pro insertion substitutions can delay aggregation of htt-ex1^{P10}-Q₃₇ into amyloid *in vitro*. In neurons co-expressing pathogenic htt-ex1-Q₉₄ alongside htt-ex1-βHP-P², we showed that the glutamine to proline substituted peptides delay the emergence of visible aggregates and cytotoxicity associated with htt-ex1-Q₉₄. Similarly, *Drosophila* expressing htt-ex1-βHP-P² or htt-ex1-βHP-P^{1,2} alongside htt-ex1-Q₉₄ have significantly improved lifespans and locomotion versus htt-ex1-Q₉₄ alone. Collectively these data do not support a toxic oligomer model of HD. In fact, sequestering htt-ex1-Q₉₄ into soluble oligomers and delaying the emergence of amyloid represents a potential therapeutic approach. For example, Frydman *et al.* recently reported the delayed emergence of a multitude of small amyloid-like htt aggregates following the formation of an inclusion body, which may very well represent a major turning point for a given cell's fate

Although our *in vitro* data strongly support that htt-ex1-βHP rapidly fibrillizes while htt-ex1-βHP-P² or htt-ex1-βHP-P^{1,2} aggregate to – and stall at – relatively soluble oligomers, we have not confirmed that these protein conformations are populated when expressed *in vivo*. The technological limitations of quantifying protein conformations in living systems are extremely challenging. However, FCS could be used on fresh brain lysates to estimate molecular size distributions of fluorescently labeled proteins - this method would rely on the assumption that lysing neurons would not significantly impact the aggregated states of huntingtin. Alternatively, the massive aggregates trapped in inclusion bodies could be better quantified by taking *Drosophila* brain lysates and centrifuging to isolate the inclusion bodies. These could then be disaggregated similar to the disaggregation of chemically synthesized peptides^{77,99,293}, resuspended, and semi-quantified by Western Blot using an anti-GFP detection of htt-ex1-GFP compared to a recombinant GFP protein standard.

In future experiments, this *Drosophila* model may also be used to gain a more detailed timeline of when pathology happens and when anti-aggregation inhibitors perform their therapeutic benefit. By placing the inhibitory protein (htt-ex1-βHP-P² or htt-ex1-βHP-P^{1,2}) downstream from an inducible promoter, such as a tetracycline³³⁷, we could vary the age at which therapeutic intervention begins. By doing this, we would potentially identify how effective anti-aggregation inhibitors remain when given later in life. If anti-aggregation inhibitors exert a significant portion of their therapeutic benefits only by delaying very early aggregation events, we would expect later-in-life intervention to be less effective. However, if these anti-aggregation inhibitors have continuous therapeutic effects by limiting ongoing or subsequent amyloid aggregation, they may be beneficial even after some level of amyloid has formed. Identifying the stage of disease progression at which anti-aggregation inhibitors lose their benefits is especially

relevant when considering anti-aggregation therapies in human HD patients, many of whom are pre- or post-symptomatic.

All together, these results suggest that the amyloid aggregation pathway is most associated with HD toxicity and is therefore the best target for the development of novel therapeutic interventions. Additionally, we demonstrate a proof-of-principle benefit using an amyloid inhibition approach that suggests a number of possible therapeutic approaches.

6.0 CONCLUSIONS

6.1 EVIDENCE SUPPORTING A BETA-STRUCTURED AMYLOID HUNTINGTIN TOXIC SPECIES

The toxic species of polyQ expanded huntingtin could potentially be any number of different protein conformers: a β -sheet rich amyloid (Section 1.3.2), a non- β oligomer (Section 1.3.3), an aberrantly folded monomer (Section 1.3.4), some other protein classification, or a toxic RNA (Section 1.4.1). Previous attempts to determine the toxic contribution of each protein conformer were plagued by the technological limitations of identifying individual protein conformers within complex heterogeneous mixtures *in vitro* or in cells. For instance, portions of cells that were once thought to be a homogenous population of soluble huntingtin, either monomeric or oligomeric, were recently identified to also contain small amyloid-like fibrils⁴⁴. Currently, there are no techniques to feasibly parse through the toxic contribution of each protein conformer *in vivo*. Microscopy, spectroscopy, and biochemical techniques rely on the correlation between the timing of appearance of different huntingtin species and the timing of cellular pathology. Recent work in the Wetzel laboratory has shown that mutant huntingtin can rapidly adopt a large distribution of molecular weight sizes *in vitro* and *in vivo* (Sahoo Manuscript Submitted). While correlative studies can be useful, they have so far been limited in their ability to identify a toxic conformer of huntingtin from a complex heterogeneous mixture.

To circumvent this technological limitation, we installed a series of amino acid substitutions within a huntingtin exon1 peptide to enhance htt's aggregation potential into amyloid. These aggregation enhancers were based on previously described modifications from the Wetzel laboratory that enhance intramolecular β -hairpin formation¹⁰⁸, the proposed intramolecular fold involved in nucleation of aggregation of polyQ proteins. These peptides have accelerated nucleation kinetics as a result of shifting the critical nucleus from an intermolecular tetramer ($n^* = 4$) to a more efficient intramolecular monomer ($n^* = 1$). These results strongly supported a role for intramolecular β -hairpin architecture in the nucleation of simple polyQ aggregation into amyloid.

Herein we describe similar β -hairpin enhancing motifs in the context of a synthetic htt-exon1-like peptide *in vitro* or full htt-exon1 *in vivo*. We show that β -hairpin architecture plays a role in htt^{NT}-mediated nucleation of amyloid. These htt-ex1- β HP peptides have accelerated aggregation kinetics and form morphologically similar amyloid-like fibrils to htt-ex1^{P10}-Q₃₇, while no longer aggregating through a simple polyQ mechanism. Therefore, these β -hairpin enhanced analogs help clarify some questions about the molecular mechanism of nucleation within huntingtin oligomers and also make an ideal molecular tool to test the toxic amyloid hypothesis of HD. Their ability to decouple their amyloid aggregation propensity apart from their absolute polyQ repeat length makes them an extremely valuable tool. For instance, a recent paper from the La Spada laboratory claims that expanded polyQ sequences within the huntingtin protein preferentially bind to, sequester, and ultimately repress peroxisome proliferator-activated receptor delta (PPAR- δ , a critical protein for neuron survival) in a polyQ repeat length dependent manner³⁰⁷. If this type of altered protein-protein binding were responsible for an HD phenotype, we would have expected our β HP peptide, with a nominal polyQ region, to be non-toxic or well

tolerated. Instead, the β HP peptide, which does not have an expanded polyQ domain and differs from benign htt-ex1-Q₂₃ mainly in its propensity to aggregation into amyloid, generates an HD phenotype in both cell and animal models. Thus, the toxic nature of the β HP brings into question several proposed mechanisms of mhtt toxicity, including polyQ-repeat dependent alterations in protein-protein binding, as well as a toxic conformer that is non-amyloid.

When expressed in mammalian PC12 cells and in rat primary cortical neurons, the hyper-amyloid htt-ex1- β HP analog is associated with aggregation into perinuclear and/or intranuclear puncta, similar to the HD phenotype of neurons expressing expanded pathogenic mhtt in other animal models and in human HD patient brains. Despite its low nominal absolute polyQ repeat length of 22-24, expression of htt-ex1- β HP not only aggregates into puncta, but is also detrimental to the viability of neurons, similar to the HD phenotype associated with a *bona fide* pathogenic htt-ex1-Q₉₄ in these model systems. When expressed in the CNS of *Drosophila*, the hyper-amyloid htt-ex1- β HP shortens lifespans and has a severe impact on the age-dependent decrease in locomotor functionality. These β HP expressing flies, which have a nominal polyQ repeat length but enhanced propensity to aggregate into amyloid, have an HD phenotype about as severe as htt-ex1-Q₄₆, a polyQ repeat length on par with the typical human HD patient.

Thus, in *in vitro*, cell experiments, primary neuron cultures, and animal models, the htt-ex1- β HP analog uniformly aggregates beyond what would be predicted by its absolute polyQ repeat length. Furthermore, htt-ex1- β HP unequivocally generates a toxic HD phenotype in cell experiments, primary cortical neuron cultures, and *Drosophila*. These data are strongly in support of the toxic amyloid hypothesis and suggest that the inherent tendency of an expanded polyQ protein to aggregate, and not necessarily its absolute polyQ repeat length, is most closely associated with HD phenotype. These results ultimately give us better structural insights into the

aggregation mechanisms of polyQ proteins. In this work, we have seen a strong correlation between (a) enhanced intramolecular β -hairpin folding of the polyQ domain, (b) enhanced propensity to nucleate aggregation of amyloid, and (c) a resulting HD phenotype whose severity far outpaces what would be predicted based solely on the β HP peptide's nominal polyQ repeat length. Thus, these results support a toxic amyloid model in Huntington's disease and provide structural insights into a candidate drug target.

6.2 EVIDENCE SUPPORTING A SOLUBLE NON-BETA, NON-AMYLOID HUNTINGTIN TOXIC SPECIES

As discussed above, the toxic mechanism of how expanded polyQ huntingtin protein causes Huntington's disease is unknown. Several lines of evidence that support the toxic oligomer hypothesis rely on flawed antibody experiments that claim to identify a particular toxic fold of huntingtin (discussed in Section 1.3.3) or rely on the correlation of timing of incompletely visualized molecular events. Namely, these studies relied on the timing of the appearance of inclusion bodies to determine whether aggregation into amyloid has begun. Recent experiments using super-resolution microscopy or fluorescence correlation spectroscopy have identified the presence of small amyloid-like aggregates within what was previously thought to be a homogeneous pool of monomeric or oligomeric huntingtin^{42-44,308} (Sahoo 2016 Manuscript Submitted). Additionally, large inclusion bodies have been found to have their own toxic effects⁸³. Given these new results, there is a need for fresh interpretations of regarding whether monomers or non- β oligomers of huntingtin contribute to HD. This has been a major technological hurdle due to the technological limitations of identifying specific protein

conformers in complex heterogeneous solution, let alone the individual toxic contribution each one may exert. At this time, directly observing the flux of different protein conformers *in vivo* and assigning them a given toxicity is not yet feasible.

In addition to the toxic oligomer hypothesis, a toxic monomer form of huntingtin cannot be completely ruled out, though its likelihood is increasingly improbable for a number of reasons. A toxic monomer conformation of htt would presumably require secondary structure, for which we see no evidence of using circular dichroism at early time points, even with β -hairpin enhanced analogs (Figure 10, 15). Given the relative sensitivity of CD, a toxic structured monomer, if it exists, would need to populate an undetectable proportion of the htt ensemble. Fluorescence correlation spectroscopy studies have demonstrated that monomeric polyglutamine peptides predominantly populate collapsed structures, whose diffusion time (τ_D) increases monotonically with increasing polyQ repeat length, showing no evidence for dramatic structural changes in solution with increasing chain length¹⁰⁹. Other studies relying on antibodies to determine altered monomeric conformations of htt³³⁸ have been explained as a linear lattice effect, where expanded polyQ domains present an increased number of binding sites that allow increased affinity of antibody binding⁹⁸. Thus, a toxic monomer of htt cannot be completely ruled out, but is increasingly unlikely.

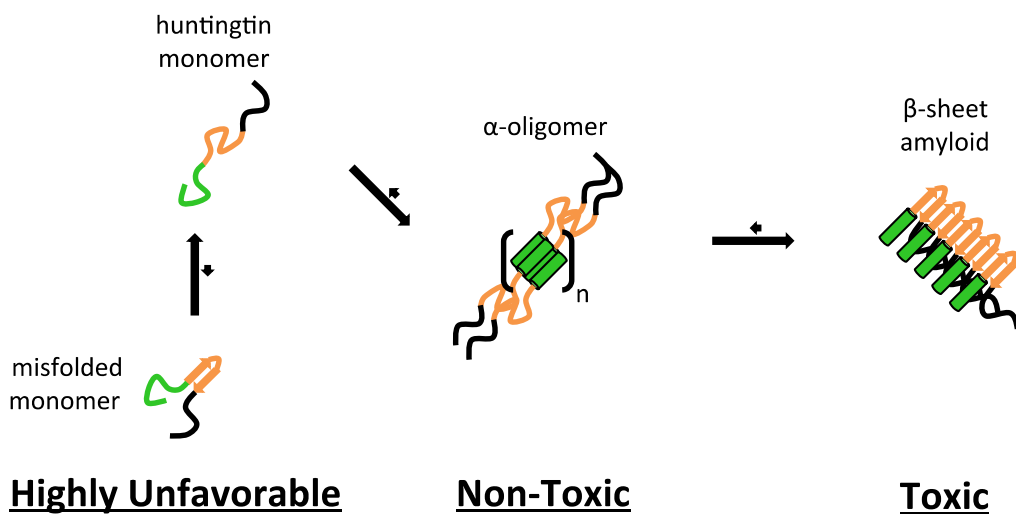
To circumvent previously met technological limitations and to test the toxic oligomer hypothesis, we designed hypo-amyloid huntingtin analog peptides that stably adopt a non- β oligomeric form *in vitro*. Even after several thousand hours of incubation (even longer than a typical lifetime of *Drosophila*) and at concentrations higher than would be found physiologically, these hypo-amyloid peptides resist amyloid formation with the only structures visible by EM being small amorphous oligomers that have no detectible β -structure by CD.

These peptides therefore offer a novel tool to determine the toxic contribution that non- β oligomers have on HD.

When expressed in PC12 mammalian cells or in primary rat cortical neurons, we did not observe any significant aggregation into large puncta, nor did we observe any cytotoxicity associated with these peptides. Furthermore, when expressed in the CNS of *Drosophila*, fly lifespans are statistically identical to wild type or negative control htt-ex1-Q₂₅ flies. The hypo-amyloid expressing flies also did not show any decrease in locomotor activity when aged, which was drastic in the hyper-amyloid and htt-ex1-Q₉₄ flies. Thus, in both cell and animal models, we find no evidence to support toxicity associated with these hypo-amyloid htt peptides.

We cannot rule out that the proline substituted peptides htt-ex1- β HP-P² and htt-ex1- β HP-P^{1,2} are non-toxic for reasons other than their reduced amyloidogenicity. For example, if the toxicity of non- β oligomers is somehow dependent on unbroken stretches of polyQ, glutamine to proline substitutions may compromise that integrity. Furthermore, a glutamine to proline substitution may alter huntingtin's capacity to explore certain types of oligomer conformations, some of which may be more inherently toxic than others.

Collectively, these data demonstrate that the non- β oligomers formed by these hypo-amyloid analogs are well tolerated and likely do not represent a toxic conformer of huntingtin. Therefore, we strongly propose that future avenues exploring therapeutic strategies should target the aggregation pathway into amyloid, which is found to be uniformly toxic in our studies.



Scheme 3: Representation of the Toxic Species of Huntingtin

6.3 THE POTENTIAL OF TARGETING AGGREGATION FOR DISEASE-MODIFYING THERAPIES

Small molecules or peptides identified from high throughput screens ultimately showed poor efficacy in preventing HD symptoms in animal models (Section 1.3.1 and 1.3.4). Many of the small molecule compounds were found to have generic colloidal properties, which can show promising anti-aggregation properties in some *in vitro* screens, but may not be able to specifically inhibit aggregation of amyloid at safe concentrations in the complex environment of the cell. Previously used screening systems have been flawed due to an incomplete understanding of the htt-ex1 aggregation mechanism and how it is altered by subtle structural changes. Screens that take the full mechanism of htt aggregation into account (for instance not using htt derived from GST-cleavage that destroys a portion of the htt^{NT} domain) may be able to

find viable and efficacious small molecule amyloid inhibitors. As an alternative strategy, this work aims to take a rational approach to design hypothesis-driven inhibitors of aggregation. These inhibitors therefore can provide further mechanistic insight into the aggregation mechanisms of huntingtin. This approach also allows us to take an evidence-based system to understand the basis for how these and future aggregation inhibitors might work.

In vitro, the hypo-amyloid peptides potently inhibit the aggregation of target htt-ex1-Q₃₇ by nearly an order of magnitude in a 2:1 stoichiometry. These inhibitors, which do not aggregate into large fibrils on their own, co-aggregate with htt-ex1-Q₃₇ in a 1:1 ratio, showcasing their efficient incorporation in growing amyloid fibrils. We show that the ability of the inhibitor to co-aggregate and contribute to fibril elongation is not entirely driven by the polyQ core domain as previously thought, but is also highly dependent on the presence of htt^{NT}.

Curiously, the placement of the glutamine to proline substitution has a defining impact on the mechanism of inhibition. Hypo-amyloid constructs whose glutamine to proline substitution is near the htt^{NT} domain (htt-ex1^{P10}-βHP-P¹ and htt-ex1^{P10}-βHP-P^{1,2}) strongly inhibit nucleation, but have a minimal impact on delaying elongation. Conversely, the glutamine to proline substitution near the C-terminal portion of the polyQ domain (htt-ex1^{P10}-βHP-P²) has a strong inhibition of the elongation phase, but very little effect on delaying nucleation. These effects can be rationalized by how the polyQ domains arrange themselves within the structures of the oligomer or the amyloid nucleus. Residual structure from the htt^{NT} domain, which actively participates in forming α-helical coiled-coil tertiary structure, may align a portion of the polyQ domain immediately following the coiled-coil structure. In the oligomeric phase, alignment of the polyQ domain immediately C-terminal from the htt^{NT} domain makes rational sense as the most likely initiator of early β-sheet formation and nucleation of aggregation, and preventing β-

sheet formation in this step (i.e. P¹ glutamine to proline substitution) would potentially interrupt nucleation of aggregation. Conversely, we can rationalize that the growing end of an amyloid fibril requires a clean, uninterrupted polyQ to interact with in order to continue elongation. Thus, β HP-P², which contains one uninterrupted Q₁₁ stretch, is a much better inhibitor of elongation than β HP-P^{1,2}, whose longest unbroken stretch is only Q₅. We also showed that the htt^{NT} domain plays a role in the inhibition of elongation of htt-ex1 amyloid, since mid-strand proline versions of the β HP polyQ peptide are ineffective inhibitors if they lack the htt^{NT} segment (Figures 21, 22, 23). It may be that the growing amyloid fibril prefers to interact with a combined htt^{NT}-polyQ segment (possible with htt- β HP-P²) and that glutamine to proline substitution near the htt^{NT} domain (such as with htt- β HP-P¹) limits this interaction to just the more C-terminal polyQ portion. These interesting results highlight some of the mechanistic insights gained from using rationally derived inhibitors of aggregation.

When expressed alongside pathogenic mutant huntingtin in mammalian PC12 cells and in primary rat cortical neurons, these hypo-amyloid constructs delay the emergence of large aggregates and significantly improve viability. We used confocal microscopy to determine the cellular distribution of these proteins. On its own, the hypo-amyloid peptides exhibit an even distribution and appear soluble throughout the cytoplasm of the cell (of which confocal microscopy cannot distinguish between monomers or small oligomers), while htt-ex1-Q₉₄ aggregates into an intense puncta pattern. When expressed together, the hypo-amyloid peptide forms puncta that colocalize with the intense puncta of htt-ex1-Q₉₄. This colocalization strongly agrees with the co-aggregation mechanism seen between these two proteins *in vitro*. Furthermore, when co-expressed in *Drosophila*, these hypo-amyloid constructs greatly reduced

the age-dependent decline in locomotion associated with htt-ex1-Q₉₇ expression and also improved the lifespan in HD flies.

In summary, these hypo-amyloid peptides are potent inhibitors of expanded polyQ huntingtin aggregation both *in vitro* and *in vivo*. The anti-aggregation effects are also met with improved viability and a dampened HD phenotype in cell and animal models. All in all, we provide evidence that these aggregation-inhibiting hypo-amyloid peptides provide a therapeutic benefit by delaying amyloid formation likely by sequestering pathogenic huntingtin into non-toxic oligomers. Not only are these data a further confirmation of the toxic amyloid hypothesis and a contradiction to the toxic oligomer hypothesis, they also represent a proof-of-principle of a therapeutic approach featuring an anti-amyloid inhibitor. Furthermore, potentially even more potent inhibitors could be developed based on these studies, though delivery of these peptides or their successors to neurons in the CNS will be a challenge.

Lipinski's rule of five attempts to crudely estimate whether a molecule has favorable drug properties and includes: (1) No more than 5 hydrogen bond donors, (2) No more than 10 hydrogen bond acceptors, (3) A molecular mass of less than 500 daltons, and (4) a partition coefficient in water not greater than 5, although there are certainly many exceptions to these rules. While these rules generally predict important drug properties, such as their absorption, distribution, metabolism, and excretion, they do not address the drug's activity. As such, this may be one of several reasons for the failure of many small molecule screens, whose methodology might not yet be sophisticated enough to fully incorporate proper huntingtin targets. It may be unfeasible to demand a small molecule with limited hydrogen bonding potential to interact with large relatively featureless 2-dimensional surfaces, such as the polyglutamine domain of huntingtin. Instead, this thesis proposes an alternative to blind screens

of small molecules by focusing on rationally designed aggregation inhibitors that can make sufficient contacts with huntingtin.

However, this approach comes at a significant cost, in that delivery of these hypo-amyloid aggregation inhibitors, which are roughly >5,000 Da in size, to affected neurons in HD patients will be technologically difficult. Cell penetrating peptide sequences may allow passage from the general circulation past the cell membrane³³⁹, but these sequences to date tend to have their own cytotoxicity, are inefficient, would add to the size of the peptide, may generally become sequestered in intracellular organelles, and would not address the need to bypass the blood-brain barrier³⁴⁰.

One alternative approach is the genetic delivery of DNA or RNA coding for these hypo-amyloid peptides. Recent advances in AAV technology have made delivery of RNAi oligonucleotides to the CNS of rats possible, which may be capable of silencing *htt* expression³⁴¹. AAV serotype 9, when injected intrajugularly, efficiently crosses the blood brain barrier and transduces both neurons and glia throughout the CNS in multiple mouse models. The largest *htt*-exon1 versions of our hypo-amyloid inhibitors are less than 100 amino acids in length, or less than 300 base pairs when coded by DNA or RNA. This makes them easily within the range of being carried by AAV vectors as DNA or RNA constructs to be expressed. Future avenues in the genetic delivery of these peptides to mice or humans may be one exciting direction worth pursuing.

BIBLIOGRAPHY

1. Knowles, T. P. J., Vendruscolo, M. & Dobson, C. M. The amyloid state and its association with protein misfolding diseases. *Nat. Rev. Mol. Cell Biol.* **15**, 384–96 (2014).
2. Fargo, K. Alzheimer's Association Report: 2014 Alzheimers disease facts and figures. *Alzheimer's Dement.* **10**, e47–e92 (2014).
3. Olshansky, S. J. *et al.* A potential decline in life expectancy in the United States in the 21st century. *N. Engl. J. Med.* **352**, 1138–1145 (2005).
4. Hardy, J. & Selkoe, D. J. The Amyloid Hypothesis of Alzheimer ' s Disease : Progress and Problems on the Road to Therapeutics. *Science (80-.).* **297**, 353–357 (2002).
5. Hurtig, H. I. *et al.* Alpha-synuclein cortical Lewy bodies correlate with dementia in Parkinson's disease. *Neurology* **54**, 1916–21 (2000).
6. Scherzinger, E. *et al.* Huntingtin-encoded polyglutamine expansions form amyloid-like protein aggregates in vitro and in vivo. *Cell* **90**, 549–558 (1997).
7. Mangiarini, L. *et al.* Exon I of the HD gene with an expanded CAG repeat is sufficient to cause a progressive neurological phenotype in transgenic mice. *Cell* **87**, 493–506 (1996).
8. Davies, S. W. *et al.* Formation of neuronal intranuclear inclusions underlies the neurological dysfunction in mice transgenic for the HD mutation. *Cell* **90**, 537–548 (1997).
9. Prusiner, S. B. Novel proteinaceous infectious particles cause scrapie. *Science* **216**, 136–144 (1982).
10. Büeler, H. *et al.* Mice devoid of PrP are resistant to scrapie. *Cell* **73**, 1339–1347 (1993).
11. Gertz, M. a, Dispenzieri, A. & Sher, T. Pathophysiology and treatment of cardiac amyloidosis. *Nat. Rev. Cardiol.* **12**, 91–102 (2015).
12. Paulsson, J. F., Andersson, A., Westermark, P. & Westermark, G. T. Intracellular amyloid-like deposits contain unprocessed pro-islet amyloid polypeptide (proIAPP) in beta cells of transgenic mice overexpressing the gene for human IAPP and transplanted human islets. *Diabetologia* **49**, 1237–1246 (2006).

13. Gibbs, C. J., Amyx, H. L., Bacote, A., Masters, C. L. & Gajdusek, D. C. Oral transmission of kuru, Creutzfeldt-Jakob disease, and scrapie to nonhuman primates. *J. Infect. Dis.* **142**, 205–208 (1980).
14. Will, R. G. *et al.* A new variant of Creutzfeldt-Jakob disease in the UK. *Lancet* **347**, 921–925 (1996).
15. Johnson, R. T. & Gibbs Jr, C. J. Creutzfeldt-Jakob disease and related transmissible spongiform encephalopathies. *N. Engl. J. Med.* **339**, 1994–2004 (1998).
16. Belay, E. D. & Schonberger, L. B. Variant Creutzfeldt-Jakob disease and bovine spongiform encephalopathy. *Clin. Lab. Med.* **22**, 849–862 (2002).
17. Knight, R. The relationship between new variant Creutzfeldt-Jakob disease and bovine spongiform encephalopathy. *Vox Sang.* **76**, 203–208 (1999).
18. Llewelyn, C. A. *et al.* Possible transmission of variant Creutzfeldt-Jakob disease by blood transfusion. *Lancet* **363**, 417–421 (2004).
19. Jaunmuktane, Z. *et al.* Evidence for human transmission of amyloid- β pathology and cerebral amyloid angiopathy. *Nature* **525**, 247–50 (2015).
20. Nelson, R. & Eisenberg, D. Recent atomic models of amyloid fibril structure. *Curr. Opin. Struct. Biol.* **16**, 260–265 (2006).
21. Hoop, C. L. *et al.* Huntingtin exon 1 fibrils feature an interdigitated β -hairpin-based polyglutamine core. *Proc. Natl. Acad. Sci.* **113**, 201521933 (2016).
22. O’Nuallain, B., Williams, A. D., Westermark, P. & Wetzel, R. Seeding Specificity in Amyloid Growth Induced by Heterologous Fibrils. *J. Biol. Chem.* **279**, 17490–17499 (2004).
23. Huntington, G. On chorea. *J. Neuropsychiatry Clin. Neurosci.* **15**, 109–112 (2003).
24. Huntington, T. *et al.* A novel gene containing a trinucleotide repeat that is expanded and unstable on Huntington’s disease chromosomes. The Huntington’s Disease Collaborative Research Group. *Cell* **72**, 971–983 (1993).
25. Fisher, E. R. & Hayden, M. R. Multisource ascertainment of Huntington disease in Canada: Prevalence and population at risk. *Mov. Disord.* **29**, 105–114 (2014).
26. Walker, F. O. Huntington’s disease. **369**, 218–228 (2007).
27. Orr, H. T. & Zoghbi, H. Y. Trinucleotide Repeat Disorders. *Annu. Rev. Neurosci.* **30**, 575–621 (2007).
28. Siomi, M. C. *et al.* FXR1, an autosomal homolog of the fragile X mental retardation gene. *EMBO J.* **14**, 2401–2408 (1995).

29. Riordan, J. R. *et al.* Identification of the cystic fibrosis gene: cloning and characterization of complementary DNA. *Science* **245**, 1066–73 (1989).
30. Ross, C. a *et al.* Huntington disease: natural history, biomarkers and prospects for therapeutics. *Nat. Rev. Neurol.* **10**, 204–16 (2014).
31. Dumas, E. M. *et al.* Visual Working Memory Impairment in Premanifest Gene-Carriers and Early Huntington ' s Disease. **1**, 97–106 (2012).
32. Ross, C. a. & Tabrizi, S. J. Huntington's disease: From molecular pathogenesis to clinical treatment. *Lancet Neurol.* **10**, 83–98 (2011).
33. Swarnkar, S. *et al.* Ectopic expression of the striatal-enriched GTPase Rhes elicits cerebellar degeneration and an ataxia phenotype in Huntington's disease. *Neurobiol Dis* **82**, 66–77 (2015).
34. Landles, C. *et al.* Proteolysis of mutant huntingtin produces an exon 1 fragment that accumulates as an aggregated protein in neuronal nuclei in huntington disease. *J. Biol. Chem.* **285**, 8808–8823 (2010).
35. Sathasivam, K. *et al.* Aberrant splicing of HTT generates the pathogenic exon 1 protein in Huntington disease. *Proc. Natl. Acad. Sci. U. S. A.* **110**, 2366–70 (2013).
36. Gipson, T. a, Neueder, A., Wexler, N. S., Bates, G. P. & Housman, D. E. Aberrantly spliced HTT , a new player in Huntington's disease pathogenesis. *RNA Biol.* **10**, 1–6 (2013).
37. Weiss, A. *et al.* Sensitive biochemical aggregate detection reveals aggregation onset before symptom development in cellular and murine models of Huntington ' s disease. 846–858 (2008). doi:10.1111/j.1471-4159.2007.05032.x
38. Jayaraman, M. *et al.* Slow amyloid nucleation via a-helix-rich oligomeric intermediates in short polyglutamine-containing huntingtin fragments. *J. Mol. Biol.* **415**, 881–899 (2012).
39. Poirier, M. a. *et al.* Huntingtin spheroids and protofibrils as precursors in polyglutamine fibrilization. *J. Biol. Chem.* **277**, 41032–41037 (2002).
40. DiFiglia, M. *et al.* Aggregation of huntingtin in neuronal intranuclear inclusions and dystrophic neurites in brain. *Science* **277**, 1990–1993 (1997).
41. Wetzel, R. Physical chemistry of polyglutamine: Intriguing tales of a monotonous sequence. *J. Mol. Biol.* **421**, 466–490 (2012).
42. Duim, W., Chen, B., Frydman, J. & Moerner, W. E. Sub-Diffraction Imaging of Huntingtin Protein Aggrgates by Fluorescence Blink-Microscopy and Atomic Force Microscopy. **12**, 2387–2390 (2012).

43. Duim, W. C., Jiang, Y., Shen, K., Frydman, J. & Moerner, W. E. Super-Resolution Fluorescence of Huntingtin Reveals Growth of Globular Species into Short Fibers and Coexistence of Distinct Aggregates. (2014).
44. Sahl, S. J. *et al.* Delayed emergence of subdiffraction- sized mutant huntingtin fibrils following inclusion body formation. *Q. Rev. Biophys.* 1–13 (2015). doi:10.1017/S0033583515000219
45. Scherzinger, E. *et al.* Self-assembly of polyglutamine-containing huntingtin fragments into amyloid-like fibrils: implications for Huntington's disease pathology. *Proc. Natl. Acad. Sci. U. S. A.* **96**, 4604–4609 (1999).
46. Frost, B. & Diamond, M. I. Prion-like mechanisms in neurodegenerative diseases. *Nat. Rev. Neurosci.* **11**, 155–9 (2009).
47. Yang, W., Dunlap, J. R., Andrews, R. B. & Wetzel, R. Aggregated polyglutamine peptides delivered to nuclei are toxic to mammalian cells. *Hum. Mol. Genet.* **11**, 2905–2917 (2002).
48. Vidal, R., Caballero, B., Couve, a & Hetz, C. Converging pathways in the occurrence of endoplasmic reticulum (ER) stress in Huntington's disease. *Curr. Mol. Med.* **11**, 1–12 (2011).
49. Labbadia, J. & Morimoto, R. I. Huntington's disease: Underlying molecular mechanisms and emerging concepts. *Trends Biochem. Sci.* **38**, 378–385 (2013).
50. Labbadia, J. *et al.* Altered chromatin architecture underlies progressive impairment of the heat shock response in mouse models of Huntington disease. *J. Clin. Invest.* **121**, 3306–3319 (2011).
51. Ortega, Z. & Lucas, J. J. Ubiquitin-proteasome system involvement in Huntington's disease. *Front. Mol. Neurosci.* **7**, 1–11 (2014).
52. Martin, D. D. O., Ladha, S., Ehrnhoefer, D. E. & Hayden, M. R. Autophagy in Huntington disease and huntingtin in autophagy. *Trends Neurosci.* **38**, 26–35 (2015).
53. Younes, L. *et al.* Regionally selective atrophy of subcortical structures in prodromal HD as revealed by statistical shape analysis. *Hum. Brain Mapp.* **35**, 792–809 (2014).
54. Shirendeb, U. P. *et al.* Mutant Huntingtin's interaction with mitochondrial protein Drp1 impairs mitochondrial biogenesis and causes defective axonal transport and synaptic degeneration in Huntington's disease. *Hum. Mol. Genet.* **21**, 406–420 (2012).
55. Chandra, A., Johri, A. & Beal, M. F. Prospects for neuroprotective therapies in prodromal Huntington's disease. *Mov. Disord.* **29**, 285–293 (2014).

56. Nithianantharajah, J. & Hannan, A. J. Dysregulation of synaptic proteins, dendritic spine abnormalities and pathological plasticity of synapses as experience-dependent mediators of cognitive and psychiatric symptoms in Huntington's disease. *Neuroscience* **251**, 66–74 (2013).
57. Ochaba, J. *et al.* Potential function for the Huntingtin protein as a scaffold for selective autophagy. *Proc. Natl. Acad. Sci.* **111**, 16889–16894 (2014).
58. Fang, Q. *et al.* Brain-specific proteins decline in the cerebrospinal fluid of humans with Huntington disease. *Mol. Cell. Proteomics* **8**, 451–66 (2009).
59. Wild, E. J. *et al.* Quantification of mutant huntingtin protein in cerebrospinal fluid from Huntington's disease patients. *J. Clin. Invest.* **125**, 1–8 (2015).
60. Uhlen, M. *et al.* Tissue-based map of the human proteome. *Science (80-.)*. **347**, 1260419–1260419 (2015).
61. White, J. K. *et al.* Huntingtin is required for neurogenesis and is not impaired by the Huntington's disease CAG expansion. *Nat. Genet.* **17**, 404–10 (1997).
62. Dragatsis, I., Levine, M. S. & Zeitlin, S. Inactivation of Hdh in the brain and testis results in progressive neurodegeneration and sterility in mice. *Nat. Genet.* **26**, 300–306 (2000).
63. Macdonald, M. E. *et al.* Targeted inactivation of the mouse Huntington's disease gene homolog Hdh. in *Cold Spring Harb. Symp. Quant. Biol.* **61**, 627–638 (1996).
64. Dragatsis, I., Efstratiadis, A. & Zeitlin, S. Mouse mutant embryos lacking huntingtin are rescued from lethality by wild-type extraembryonic tissues. *Development* **125**, 1529–1539 (1998).
65. Nguyen, G. D., Molero, A. E., Gokhan, S. & Mehler, M. F. Functions of Huntingtin in Germ Layer Specification and Organogenesis. *PLoS One* **8**, 1–17 (2013).
66. Cattaneo, E. *et al.* Loss of normal huntingtin function: New developments in Huntington's disease research. *Trends Neurosci.* **24**, 182–188 (2001).
67. Mayford, M., Wang, J., Kandel, E. R. & O'Dell, T. J. CaMKII regulates the frequency-response function of hippocampal synapses for the production of both LTD and LTP. *Cell* **81**, 891–904 (1995).
68. Tsien, J. Z. *et al.* Subregion- and cell type-restricted gene knockout in mouse brain. *Cell* **87**, 1317–1326 (1996).
69. Braubach, P. *et al.* Altered Ca²⁺ signaling in skeletal muscle fibers of the R6 / 2 mouse, a model of Huntington's disease. 393–413 (2014). doi:10.1085/jgp.201411255
70. Mielcarek, M. *et al.* HDAC4-Myogenin Axis As an Important Marker of HD-Related Skeletal Muscle Atrophy. *PLOS Genet.* **11**, e1005021 (2015).

71. Mielcarek, M. *et al.* Dysfunction of the CNS-Heart Axis in Mouse Models of Huntington's Disease. *PLoS Genet.* **10**, e1004550 (2014).
72. Keiser, M. S., Kordasiewicz, H. B. & McBride, J. L. Gene suppression strategies for dominantly inherited neurodegenerative diseases: lessons from Huntington's disease and spinocerebellar ataxia. *Hum. Mol. Genet.* 1–12 (2015). doi:10.1093/hmg/ddv442
73. Zuccato, C., Valenza, M. & Cattaneo, E. Molecular Mechanisms and Potential Therapeutical Targets in Huntington ' s Disease. *Physiol Rev* **90**, 905–981 (2010).
74. Palidwor, G. A. *et al.* Detection of alpha-rod protein repeats using a neural network and application to huntingtin. *PLoS Comput. Biol.* **5**, (2009).
75. Shirasaki, D. I. *et al.* Network organization of the huntingtin proteomic interactome in mammalian brain. *Neuron* **75**, 41–57 (2012).
76. Chen, S., Berthelie, V., Yang, W. & Wetzel, R. Polyglutamine aggregation behavior in vitro supports a recruitment mechanism of cytotoxicity. *J. Mol. Biol.* **311**, 173–82 (2001).
77. Kar, K., Jayaraman, M., Sahoo, B., Kodali, R. & Wetzel, R. Critical nucleus size for disease-related polyglutamine aggregation is repeat-length dependent. *Nat. Struct. Mol. Biol.* **18**, 328–336 (2011).
78. Marsh, J. L. *et al.* Expanded polyglutamine peptides alone are intrinsically cytotoxic and cause neurodegeneration in *Drosophila*. *Hum. Mol. Genet.* **9**, 13–25 (2000).
79. Perutz, M. F. & Windle, A. H. Cause of neural death in neurodegenerative diseases attributable to expansion of glutamine repeats. *Nature* **412**, 143–144 (2001).
80. Eigen, M. Prionics or the kinetic basis of prion diseases. *Biophys. Chem.* **63**, (1996).
81. Arrasate, M., Mitra, S., Schweitzer, E. S., Segal, M. R. & Finkbeiner, S. Inclusion body formation reduces levels of mutant huntingtin and the risk of neuronal death. *Nature* **431**, 805–810 (2004).
82. Arrasate, M. & Finkbeiner, S. Automated microscope system for determining factors that predict neuronal fate. *Proc. Natl. Acad. Sci. U. S. A.* **102**, 3840–3845 (2005).
83. Liu, K. *et al.* Disruption of the nuclear membrane by perinuclear inclusions of mutant huntingtin causes cell-cycle re-entry and striatal cell death in mouse and cell models of Huntington ' s disease. **24**, 1602–1616 (2015).
84. Sahoo, B., Drombosky, K. W. & Wetzel, R. Fluorescence Correlation Spectroscopy: A Tool to Study Protein Oligomerization and Aggregation In Vitro and In Vivo. *Methods Mol. Biol.* **1345**, 291–8 (2016).

85. Truant, R., Atwal, R. S., Desmond, C., Munsie, L. & Tran, T. Huntington's disease: Revisiting the aggregation hypothesis in polyglutamine neurodegenerative diseases. *FEBS J.* **275**, 4252–4262 (2008).
86. Nucifora, L. G. *et al.* Identification of novel potentially toxic oligomers formed in vitro from mammalian-derived expanded huntingtin exon-1 protein. *J. Biol. Chem.* **287**, 16017–16028 (2012).
87. Slow, E. J. *et al.* Absence of behavioral abnormalities and neurodegeneration in vivo despite widespread neuronal huntingtin inclusions. *Proc. Natl. Acad. Sci. U. S. A.* **102**, 11402–11407 (2005).
88. Klement, I. A. *et al.* Ataxin-1 Nuclear Localization and Aggregation. *Cell* **95**, 41–53 (1998).
89. Saudou, F., Finkbeiner, S., Devys, D. & Greenberg, M. E. Huntingtin acts in the nucleus to induce apoptosis but death does not correlate with the formation of intranuclear inclusions. *Cell* **95**, 55–56 (1998).
90. Fox, J. H. *et al.* The mTOR kinase inhibitor Everolimus decreases S6 kinase phosphorylation but fails to reduce mutant huntingtin levels in brain and is not neuroprotective in the R6/2 mouse model of Huntington's disease. *Mol. Neurodegener.* **5**, 26 (2010).
91. Nath, S., Munsie, L. N. & Truant, R. A huntingtin-mediated fast stress response halting endosomal trafficking is defective in Huntington's disease. *Hum. Mol. Genet.* **24**, 450–462 (2014).
92. Ross, C. a & Poirier, M. a. Opinion: What is the role of protein aggregation in neurodegeneration? *Nat. Rev. Mol. Cell Biol.* **6**, 891–898 (2005).
93. Ravikumar, B. & Rubinsztein, D. C. Role of autophagy in the clearance of mutant huntingtin: A step towards therapy? *Mol. Aspects Med.* **27**, 520–527 (2006).
94. Takahashi, T. *et al.* Soluble polyglutamine oligomers formed prior to inclusion body formation are cytotoxic. *Hum. Mol. Genet.* **17**, 345–356 (2008).
95. Leitman, J. *et al.* ER stress-induced eIF2-alpha phosphorylation underlies sensitivity of striatal neurons to pathogenic huntingtin. *PLoS One* **9**, (2014).
96. Schaffar, G. *et al.* Cellular Toxicity of Polyglutamine Expansion Proteins Mechanism of Transcription Factor Deactivation. *Mol. Cell* **15**, 95–105 (2004).
97. Sharma, D., Sharma, S., Pasha, S. & Brahmachari, S. K. Peptide models for inherited neurodegenerative disorders: Conformation and aggregation properties of long polyglutamine peptides with and without interruptions. *FEBS Lett.* **456**, 181–185 (1999).

98. Bennett, M. J. *et al.* A linear lattice model for polyglutamine in CAG-expansion diseases. *Proc. Natl. Acad. Sci. U. S. A.* **99**, 11634–11639 (2002).
99. Jayaraman, M., Thakur, A., Kar, K., Kodali, R. & Wetzel, R. Assays for studying nucleated aggregation of polyglutamine proteins. *Sci. York* **53**, 246–254 (2012).
100. Trottier, Y. *et al.* Polyglutamine expansion as a pathological epitope in Huntington's disease and four dominant cerebellar ataxias. *Nature* **378**, 403–406 (1995).
101. Miller, J. *et al.* Identifying polyglutamine protein species in situ that best predict neurodegeneration. *Nat. Chem. Biol.* **7**, 925–34 (2011).
102. Klein, F. A. C. *et al.* Pathogenic and Non-pathogenic Polyglutamine Tracts Have Similar Structural Properties: Towards a Length-dependent Toxicity Gradient. *J. Mol. Biol.* **371**, 235–244 (2007).
103. Owens, G. E., New, D. M., West, A. P. & Bjorkman, P. J. Anti-PolyQ Antibodies Recognize a Short PolyQ Stretch in Both Normal and Mutant Huntingtin Exon 1. *J. Mol. Biol.* **427**, 2507–19 (2015).
104. Gordon-Smith, D. J., Carbajo, R. J., Stott, K. & Neuhaus, D. Solution studies of chymotrypsin inhibitor-2 glutamine insertion mutants show no interglutamine interactions. *Biochem. Biophys. Res. Commun.* **280**, 855–60 (2001).
105. Masino, L. & Pastore, A. Glutamine repeats: structural hypotheses and neurodegeneration. *Biochem Soc T* **30**, 548–551 (2002).
106. Altschuler, E. L., Hud, N. V, Mazrimas, J. a & Rupp, B. Random coil conformation for extended polyglutamine stretches in aqueous soluble monomeric peptides. *J. Pept. Res.* **50**, 73–75 (1997).
107. Chen, S., Ferrone, F. a & Wetzel, R. Huntington's disease age-of-onset linked to polyglutamine aggregation nucleation. *Proc. Natl. Acad. Sci. U. S. A.* **99**, 11884–11889 (2002).
108. Kar, K. *et al.* B-Hairpin-Mediated Nucleation of Polyglutamine Amyloid Formation. *J. Mol. Biol.* **425**, 1183–1197 (2013).
109. Crick, S. L., Jayaraman, M., Frieden, C., Wetzel, R. & Pappu, R. V. Fluorescence correlation spectroscopy shows that monomeric polyglutamine molecules form collapsed structures in aqueous solutions. *Proc. Natl. Acad. Sci. U. S. A.* **103**, 16764–9 (2006).
110. Kegel, K. B. *et al.* Huntingtin is present in the nucleus, interacts with the transcriptional corepressor C-terminal binding protein, and represses transcription. *J. Biol. Chem.* **277**, 7466–7476 (2002).

111. Ismailoglu, I. *et al.* Huntingtin protein is essential for mitochondrial metabolism, bioenergetics and structure in murine embryonic stem cells. *Dev. Biol.* **391**, 230–240 (2014).
112. Kar, K., Arduini, I., Drombosky, K. W., Van Der Wel, P. C. a & Wetzel, R. D-polyglutamine amyloid recruits l-polyglutamine monomers and kills cells1. Kar, K., Arduini, I., Drombosky, K. W., Van Der Wel, P. C. a & Wetzel, R. D-polyglutamine amyloid recruits l-polyglutamine monomers and kills cells. *J. Mol. Biol.* **426**, 816–829 (20. *J. Mol. Biol.* **426**, 816–829 (2014).
113. Olzscha, H. *et al.* Amyloid-like aggregates sequester numerous metastable proteins with essential cellular functions. *Cell* **144**, 67–78 (2011).
114. Nucifora, F. C. *et al.* Interference by huntingtin and atrophin-1 with cbp-mediated transcription leading to cellular toxicity. *Science* **291**, 2423–2428 (2001).
115. Hageman, J. *et al.* A DNAJB Chaperone Subfamily with HDAC-Dependent Activities Suppresses Toxic Protein Aggregation. *Mol. Cell* **37**, 355–369 (2010).
116. Månsson, C. *et al.* DNAJB6 is a peptide-binding chaperone which can suppress amyloid fibrillation of polyglutamine peptides at substoichiometric molar ratios. *Cell Stress Chaperones* **19**, 227–239 (2014).
117. Ormsby, A. R., Ramdzan, Y. M., Mok, Y. F., Jovanoski, K. D. & Hatters, D. M. A platform to view huntingtin exon 1 aggregation flux in the cell reveals divergent influences from chaperones hsp40 and hsp70. *J. Biol. Chem.* **288**, 37192–37203 (2013).
118. Qi, L. *et al.* The Role of Chaperone-Mediated Autophagy in Huntingtin Degradation. *PLoS One* **7**, 1–16 (2012).
119. Fujimoto, M. *et al.* Active HSF1 significantly suppresses polyglutamine aggregate formation in cellular and mouse models. *J. Biol. Chem.* **280**, 34908–34916 (2005).
120. Shahmoradian, S. H. *et al.* TRiC's tricks inhibit huntingtin aggregation. *Elife* **2013**, 1–17 (2013).
121. Tam, S. *et al.* The chaperonin TRiC blocks a huntingtin sequence element that promotes the conformational switch to aggregation. *Nat. Struct. Mol. Biol.* **16**, 1279–1285 (2009).
122. Robertson, A. L. *et al.* Small heat-shock proteins interact with a flanking domain to suppress polyglutamine aggregation. *Proc. Natl. Acad. Sci. U. S. A.* **107**, 10424–10429 (2010).
123. Tue, N. T., Shimaji, K., Tanaka, N. & Yamaguchi, M. Effect of β -crystallin on protein aggregation in drosophila. *J. Biomed. Biotechnol.* **2012**, (2012).
124. Miller, V. M. *et al.* CHIP suppresses polyglutamine aggregation and toxicity in vitro and in vivo. *J. Neurosci.* **25**, 9152–9161 (2005).

125. Yu, A. *et al.* Protein aggregation can inhibit clathrin-mediated endocytosis by chaperone competition. *Proc. Natl. Acad. Sci. U. S. A.* **111**, E1481–90 (2014).
126. Coffee, B. *et al.* Incidence of Fragile X Syndrome by Newborn Screening for Methylated FMR1 DNA. *Am. J. Hum. Genet.* **85**, 503–514 (2009).
127. Fu, Y. H. *et al.* Variation of the CGG repeat at the fragile X site results in genetic instability: resolution of the Sherman paradox. *Cell* **67**, 1047–1058 (1991).
128. Ashley, C. T., Wilkinson, K. D., Reines, D. & Warren, S. T. FMR1 protein: conserved RNP family domains and selective RNA binding. *Science* **262**, 563–566 (1993).
129. Delatycki, M. B., Williamson, R. & Forrest, S. M. Friedreich ataxia: an overview. *J. Med. Genet.* **37**, 1–8 (2000).
130. Sakamoto, N. *et al.* Sticky DNA: Self-association properties of long GAA ?? TTC repeats in R ?? R ?? Y triplex structures from Friedreich’s ataxia. *Mol. Cell* **3**, 465–475 (1999).
131. Thornton, C. A. Myotonic dystrophy. *Neurol. Clin.* **32**, 705–719 (2014).
132. Sicot, G. & Gomes-Pereira, M. RNA toxicity in human disease and animal models: From the uncovering of a new mechanism to the development of promising therapies. *Biochim. Biophys. Acta - Mol. Basis Dis.* **1832**, 1390–1409 (2013).
133. Sicot, G., Gourdon, G. & Gomes-Pereira, M. Myotonic dystrophy, when simple repeats reveal complex pathogenic entities: New findings and future challenges. *Hum. Mol. Genet.* **20**, 116–123 (2011).
134. Osborne, R. J. R. J. & Thornton, C. A. RNA-dominant diseases. *Hum. Mol. Genet.* **15**, (2006).
135. Jiang, H., Mankodi, A., Swanson, M. S., Moxley, R. T. & Thornton, C. A. Myotonic dystrophy type 1 is associated with nuclear foci of mutant RNA, sequestration of muscleblind proteins and deregulated alternative splicing in neurons. *Hum. Mol. Genet.* **13**, 3079–3088 (2004).
136. Mankodi, A., Lin, X., Blaxall, B. C., Swanson, M. S. & Thornton, C. A. Nuclear RNA foci in the heart in myotonic dystrophy. *Circ. Res.* **97**, 1152–1155 (2005).
137. Figura, G., Koscianska, E. & Krzyzosiak, W. J. In Vitro Expansion of CAG, CAA, and Mixed CAG/CAA Repeats. *Int. J. Mol. Sci.* **16**, 18741–51 (2015).
138. Gao, R. *et al.* Instability of expanded CAG/CAA repeats in spinocerebellar ataxia type 17. *Eur. J. Hum. Genet.* **16**, 215–22 (2008).
139. Kim, J.-M. *et al.* Importance of low-range CAG expansion and CAA interruption in SCA2 Parkinsonism. *Arch. Neurol.* **64**, 1510–8 (2007).

140. Nielsen, T. T. *et al.* ATXN2 with intermediate-length CAG/CAA repeats does not seem to be a risk factor in hereditary spastic paraplegia. *J. Neurol. Sci.* **321**, 100–102 (2012).
141. McMurray, C. T. Mechanisms of trinucleotide repeat instability during human development. *Nat. Rev. Genet.* **11**, 786–799 (2010).
142. Mirkin, S. M. Expandable DNA repeats and human disease. *Nature* **447**, 932–40 (2007).
143. Kovtun, I. V & McMurray, C. T. Features of trinucleotide repeat instability in vivo. *Cell Res.* **18**, 198–213 (2008).
144. Debacker, K. *et al.* Histone deacetylase complexes promote trinucleotide repeat expansions. *PLoS Biol.* **10**, (2012).
145. Iyer, R. R., Pluciennik, A., Rosche, W. A., Sinden, R. R. & Wells, R. D. DNA polymerase III proofreading mutants enhance the expansion and deletion of triplet repeat sequences in Escherichia coli. *J. Biol. Chem.* **275**, 2174–2184 (2000).
146. Petruska, J., Hartenstine, M. J. & Goodman, M. F. Analysis of strand slippage in DNA polymerase expansions of CAG/CTG triplet repeats associated with neurodegenerative disease. *J. Biol. Chem.* **273**, 5204–5210 (1998).
147. Sobczak, K. & Krzyzosiak, W. J. CAG repeats containing CAA interruptions form branched hairpin structures in spinocerebellar ataxia type 2 transcripts. *J. Biol. Chem.* **280**, 3898–3910 (2005).
148. Bates, G. *et al.* Title - Huntington ' s disease – a primer. 1–52
149. Bates, G. Huntingtin aggregation and toxicity in Huntington ' s disease. *Lancet* **361**, 1642–1644 (2003).
150. Orr, H. T. Are Polyglutamine Diseases Expanding? *Neuron* **70**, 377–378 (2011).
151. Shiraishi, R., Tamura, T., Sone, M. & Okazawa, H. Systematic Analysis of Fly Models with Multiple Drivers Reveals Different Effects of Ataxin-1 and Huntingtin in Neuron Subtype-Specific Expression. 1–25 (2014). doi:10.1371/journal.pone.0116567
152. Al-Ramahi, I. *et al.* CHIP protects from the neurotoxicity of expanded and wild-type ataxin-1 and promotes their ubiquitination and degradation. *J. Biol. Chem.* **281**, 26714–26724 (2006).
153. Aguiar, J. *et al.* Ubiquitous expression of human SCA2 gene under the regulation of the SCA2 self promoter cause specific Purkinje cell degeneration in transgenic mice. *Neurosci. Lett.* **392**, 202–206 (2006).
154. Huynh, D. P., Figueroa, K., Hoang, N. & Pulst, S. M. Nuclear localization or inclusion body formation of ataxin-2 are not necessary for SCA2 pathogenesis in mouse or human. TL - 26. *Nat. Genet.* **26 VN - r**, 44–50 (2000).

155. Masino, L. Polyglutamine and neurodegeneration: structural aspects. *Protein Pept Lett* **11**, 239–248 (2004).
156. Ellisdon, A. M., Thomas, B. & Bottomley, S. P. The two-stage pathway of ataxin-3 fibrillogenesis involves a polyglutamine-independent step. *J. Biol. Chem.* **281**, 16888–16896 (2006).
157. Li, X., Liu, H., Fischhaber, P. L. & Tang, T.-S. Toward therapeutic targets for SCA3: Insight into the role of Machado–Joseph disease protein ataxin-3 in misfolded proteins clearance. *Prog. Neurobiol.* (2015). doi:10.1016/j.pneurobio.2015.06.004
158. Yang, H. *et al.* Aggregation of polyglutamine-expanded ataxin-3 sequesters its specific interacting partners into inclusions: Implication in a loss-of-function pathology. *Sci. Rep.* **4**, 6410 (2014).
159. Takahashi, M. *et al.* Cytoplasmic Location of α 1A Voltage-Gated Calcium Channel C-Terminal Fragment (Cav2.1-CTF) Aggregate Is Sufficient to Cause Cell Death. *PLoS One* **8**, 1–11 (2013).
160. Vinatier, G., Corsi, J.-M., Mignotte, B. & Gaumer, S. Quantification of Ataxin-3 and Ataxin-7 aggregates formed in vivo in *Drosophila* reveals a threshold of aggregated polyglutamine proteins associated with cellular toxicity. *Biochem. Biophys. Res. Commun.* 3–8 (2015). doi:10.1016/j.bbrc.2015.07.071
161. Guyenet, S. J. *et al.* Proteolytic Cleavage of Ataxin-7 Promotes SCA7 Retinal Degeneration and Neurological Dysfunction. 1–32 (2015).
162. Yang, H. *et al.* Aggregation of polyglutamine-expanded ataxin 7 protein specifically sequesters ubiquitin-specific protease 22 and deteriorates its deubiquitinating function in the Spt-Ada-Gcn5-acetyltransferase (SAGA) complex. *J. Biol. Chem.* **290**, 21996–22004 (2015).
163. Katsuno, M. *et al.* Testosterone reduction prevents phenotypic expression in a transgenic mouse model of spinal and bulbar muscular atrophy. *Neuron* **35**, 843–854 (2002).
164. Kelp, A. *et al.* A Novel Transgenic Rat Model for Spinocerebellar Ataxia Type 17 Recapitulates Neuropathological Changes and Supplies In Vivo Imaging Biomarkers. *J. Neurosci.* **33**, 9068–9081 (2013).
165. Schilling, G. *et al.* Nuclear accumulation of truncated atrophin-1 fragments in a transgenic mouse model of drpla. *Neuron* **24**, 275–286 (1999).
166. Sato, A. *et al.* Adenovirus-mediated expression of mutant DRPLA proteins with expanded polyglutamine stretches in neuronally differentiated PC12 cells. Preferential intranuclear aggregate formation and apoptosis. *Hum. Mol. Genet.* **8**, 997–1006 (1999).

167. Sato, T. *et al.* Transgenic mice harboring a full-length human mutant DRPLA gene exhibit age-dependent intergenerational and somatic instabilities of CAG repeats comparable with those in DRPLA patients. *Hum. Mol. Genet.* **8**, 99–106 (1999).
168. Slow, E. J. *et al.* Selective striatal neuronal loss in a YAC128 mouse model of Huntington disease. *Hum. Mol. Genet.* **12**, 1555–1567 (2003).
169. E. Rincon-Limas, D., Jensen, K. & Fernandez-Funez, P. Drosophila Models of Proteinopathies: the Little Fly that Could. *Curr. Pharm. Des.* **18**, 1108–1122 (2012).
170. Poletti, a *et al.* Transient expression of the 5alpha-reductase type 2 isozyme in the rat brain in late fetal and early postnatal life. *Endocrinology* **139**, 2171–2178 (1998).
171. Garcia-Falgueras, A. *et al.* The role of the androgen receptor in CNS masculinization. *Brain Res.* **1035**, 13–23 (2005).
172. Catterall, W. A. Structure and regulation of voltage-gated Ca²⁺ channels. *Annu. Rev. Cell Dev. Biol.* **16**, 521–555 (2000).
173. Tzvetkov, N. & Breuer, P. Josephin domain-containing proteins from a variety of species are active de-ubiquitination enzymes. *Biol. Chem.* **388**, 973–978 (2007).
174. Satyal, S. H. *et al.* Polyglutamine aggregates alter protein folding homeostasis in *Caenorhabditis elegans*. *Proc. Natl. Acad. Sci. U. S. A.* **97**, 5750–5 (2000).
175. Ordway, J. M. *et al.* Ectopically expressed CAG repeats cause intranuclear inclusions and a progressive late onset neurological phenotype in the mouse. *Cell* **91**, 753–763 (1997).
176. Thakur, A. K. *et al.* Polyglutamine disruption of the huntingtin exon1 N-terminus triggers a complex aggregation mechanism. *October* **16**, 380–389 (2009).
177. Bhattacharyya, A. M., Thakur, A. K. & Wetzel, R. Polyglutamine Aggregation Nucleation: Thermodynamics of a Highly Unfavorable Protein Folding Reaction. *Proc. Natl. Acad. Sci. U. S. A.* **102**, 15400–15405 (2005).
178. Ferrone, F. Analysis of protein aggregation kinetics. *Methods Enzymol.* **309**, 256–74 (1999).
179. Thakur, A. K. & Wetzel, R. Mutational analysis of the structural organization of polyglutamine aggregates. *Proc. Natl. Acad. Sci. U. S. A.* **99**, 17014–17019 (2002).
180. Pearce, M. M., Spartz, E. J., Hong, W., Luo, L. & Kopito, R. R. Prion-like transmission of neuronal huntingtin aggregates to phagocytic glia in *Drosophila*. *Submitt. Manuscr.* **6**, 1–11 (2015).
181. Cicchetti, F. *et al.* Mutant huntingtin is present in neuronal grafts in huntington disease patients. *Ann. Neurol.* **76**, 31–42 (2014).

182. Cisbani, G. & Cicchetti, F. Review: The fate of cell grafts for the treatment of Huntington's disease: the post-mortem evidence. *Neuropathol. Appl. Neurobiol.* **40**, 71–90 (2014).
183. Jayaraman, M. *et al.* Kinetically competing huntingtin aggregation pathways control amyloid polymorphism and properties. *Biochemistry* **51**, 2706–2716 (2012).
184. Chen, S., Berthelie, V., Hamilton, J. B., O'Nuallain, B. & Wetzel, R. Amyloid-like features of polyglutamine aggregates and their assembly kinetics. *Biochemistry* **41**, 7391–7399 (2002).
185. Bagriantsev, S. N., Kushnirov, V. V. & Liebman, S. W. Analysis of Amyloid Aggregates Using Agarose Gel Electrophoresis. *Methods Enzymol.* **412**, 33–48 (2006).
186. Sivanandam, V. N. *et al.* The aggregation-enhancing huntingtin N-terminus is helical in amyloid fibrils. *J. Am. Chem. Soc.* **133**, 4558–4566 (2011).
187. Kelley, N. W. *et al.* The Predicted Structure of the Headpiece of the Huntingtin Protein and Its Implications on Huntingtin Aggregation. *J. Mol. Biol.* **388**, 919–927 (2009).
188. Mishra, R. *et al.* Serine phosphorylation suppresses huntingtin amyloid accumulation by altering protein aggregation properties. *J. Mol. Biol.* **424**, 1–14 (2012).
189. Mishra, R. *et al.* Inhibiting the nucleation of amyloid structure in a huntingtin fragment by targeting α -helix-rich oligomeric intermediates. *J. Mol. Biol.* **415**, 900–917 (2012).
190. Kim, M. W., Chelliah, Y., Kim, S. W., Otwinowski, Z. & Bezprozvanny, I. Secondary Structure of Huntingtin Amino-Terminal Region. *Structure* **17**, 1205–1212 (2009).
191. Williamson, T. E., Vitalis, A., Crick, S. L. & Pappu, R. V. Modulation of Polyglutamine Conformations and Dimer Formation by the N-Terminus of Huntingtin. *J. Mol. Biol.* **396**, 1295–1309 (2010).
192. Caron, N. S., Desmond, C. R., Xia, J. & Truant, R. Polyglutamine domain flexibility mediates the proximity between flanking sequences in huntingtin. *Proc. Natl. Acad. Sci. U. S. A.* **110**, 14610–5 (2013).
193. Bhattacharyya, A. *et al.* Oligoproline effects on polyglutamine conformation and aggregation. *J. Mol. Biol.* **355**, 524–535 (2006).
194. Sahoo, B., Singer, D., Kodali, R., Zuchner, T. & Wetzel, R. Aggregation behavior of chemically synthesized, full-length huntingtin exon1. *Biochemistry* **53**, 3897–3907 (2014).
195. Sieradzan, K. a *et al.* Huntington's disease intranuclear inclusions contain truncated, ubiquitinated huntingtin protein. *Exp. Neurol.* **156**, 92–99 (1999).

196. Barbaro, B. a. *et al.* Comparative study of naturally occurring huntingtin fragments in *Drosophila* points to exon 1 as the most pathogenic species in Huntington's disease. *Hum. Mol. Genet.* **24**, 913–925 (2014).
197. Romero, E. *et al.* Suppression of Neurodegeneration and Increased Neurotransmission Caused by Expanded Full-Length Huntingtin Accumulating in the Cytoplasm. *Neuron* **57**, 27–40 (2008).
198. Huang, B. *et al.* Scalable Production in Human Cells and Biochemical Characterization of Full-Length Normal and Mutant Huntingtin. *PLoS One* **10**, e0121055 (2015).
199. Roethlein, C. *et al.* Architecture of polyglutamine-containing fibrils from time resolved fluorescence decay. *J. Biol. Chem.* (2014). doi:10.1074/jbc.M114.581991
200. Miettinen, M. S., Monticelli, L., Nedumpully-Govindan, P., Knecht, V. & Ignatova, Z. Stable polyglutamine dimers can contain β -Hairpins with interdigitated side chains-but not α -helices, β -nanotubes, β -pseudohelices, or steric zippers. *Biophys. J.* **106**, 1721–8 (2014).
201. Legleiter, J. *et al.* Mutant huntingtin fragments form oligomers in a polyglutamine length-dependent manner in Vitro and in Vivo. *J. Biol. Chem.* **285**, 14777–14790 (2010).
202. Burke, K. a., Godbey, J. & Legleiter, J. Assessing mutant huntingtin fragment and polyglutamine aggregation by atomic force microscopy. *Methods* **53**, 275–284 (2011).
203. Burke, K. a., Kauffman, K. J., Umbaugh, C. S., Frey, S. L. & Legleiter, J. The interaction of polyglutamine peptides with lipid membranes is regulated by flanking sequences associated with huntingtin. *J. Biol. Chem.* **288**, 14993–15005 (2013).
204. Lim, R. R., Bloomfield, M. R., Johnson, a M. & Allen, J. M. Dopamine concentrations in PC12 cells following neuronal differentiation induced by NGF or VIP. *Biochem. Soc. Trans.* **23**, 46S (1995).
205. Kazantsev, a, Preisinger, E., Dranovsky, a, Goldgaber, D. & Housman, D. Insoluble detergent-resistant aggregates form between pathological and nonpathological lengths of polyglutamine in mammalian cells. *Proc. Natl. Acad. Sci. U. S. A.* **96**, 11404–11409 (1999).
206. Zhang, Q. C. *et al.* A compact β model of huntingtin toxicity. *J. Biol. Chem.* **286**, 8188–8196 (2011).
207. Aiken, C. T., Tobin, A. J. & Schweitzer, E. S. A cell-based screen for drugs to treat Huntington's disease. *Neurobiol. Dis.* **16**, 546–555 (2004).
208. Ellison, S. M. *et al.* Dose-dependent neuroprotection of VEGF165 in Huntington's disease striatum. *Mol. Ther.* **21**, 1862–75 (2013).

209. Rüb, U. *et al.* Huntington's disease (HD): Degeneration of select nuclei, widespread occurrence of neuronal nuclear and axonal inclusions in the brainstem. *Brain Pathol.* **24**, 247–260 (2014).
210. Nguyen, H. P. *et al.* Behavioral abnormalities precede neuropathological markers in rats transgenic for Huntington's disease. *Hum. Mol. Genet.* **15**, 3177–3194 (2006).
211. Tsvetkov, A. S. *et al.* Proteostasis of polyglutamine varies among neurons and predicts neurodegeneration. *Nat. Chem. Biol.* **9**, 586–92 (2013).
212. Sontag, E. M. *et al.* Methylene Blue Modulates Huntingtin Aggregation Intermediates and Is Protective in Huntington's Disease Models. *J. Neurosci.* **32**, 11109–11119 (2012).
213. Adams, M. D. The Genome Sequence of *Drosophila melanogaster*. *Science (80-.)*. **287**, 2185–2195 (2000).
214. Groth, A. C., Fish, M., Nusse, R. & Calos, M. P. Construction of Transgenic *Drosophila* by Using the Site-Specific Integrase from Phage ϕ C31. *Genetics* **166**, 1775–1782 (2004).
215. Robinow, S. & White, K. Characterization and spatial distribution of the ELAV protein during *Drosophila melanogaster* development. *J. Neurobiol.* **22**, 443–61 (1991).
216. Godin, J. D., Poizat, G., Hickey, M. a, Maschat, F. & Humbert, S. Mutant huntingtin-impaired degradation of beta-catenin causes neurotoxicity in Huntington's disease. *EMBO J.* **29**, 2433–2445 (2010).
217. Brand, a H. & Perrimon, N. Targeted gene expression as a means of altering cell fates and generating dominant phenotypes. *Development* **118**, 401–415 (1993).
218. Duffy, J. B. GAL4 system in *Drosophila*: a fly geneticist's Swiss army knife. *Genesis* **34**, 1–15 (2002).
219. Mishra, M. & Knust, E. Analysis of the *Drosophila* Compound Eye with Light and Electron Microscopy. **935**, 201–205 (2013).
220. Green, E. & Giorgini, F. Choosing and using *Drosophila* models to characterize modifiers of Huntington's disease. 739–745 (2012). doi:10.1042/BST20120072
221. Desai, U. A. *et al.* Biologically active molecules that reduce polyglutamine aggregation and toxicity. *Hum. Mol. Genet.* **15**, 2114–2124 (2006).
222. Doumanis, J., Wada, K., Kino, Y., Moore, A. W. & Nukina, N. RNAi screening in *Drosophila* cells identifies new modifiers of mutant huntingtin aggregation. *PLoS One* **4**, (2009).
223. Zhang, S., Binari, R., Zhou, R. & Perrimon, N. A genomewide RNA interference screen for modifiers of aggregates formation by mutant huntingtin in *drosophila*. *Genetics* **184**, 1165–1179 (2010).

224. Lee, W.-C. M., Yoshihara, M. & Littleton, J. T. Cytoplasmic aggregates trap polyglutamine-containing proteins and block axonal transport in a *Drosophila* model of Huntington's disease. *Proc. Natl. Acad. Sci. U. S. A.* **101**, 3224–3229 (2004).
225. Weiss, K. R., Kimura, Y., Lee, W. M. & Littleton, J. T. Huntingtin Aggregation Kinetics and Their Disease Model. **190**, 581–600 (2012).
226. Gargano, J. W., Martin, I., Bhandari, P. & Grotewiel, M. S. Rapid iterative negative geotaxis (RING): A new method for assessing age-related locomotor decline in *Drosophila*. *Exp. Gerontol.* **40**, 386–395 (2005).
227. Jackson, G. R. *et al.* Polyglutamine-expanded human huntingtin transgenes induce degeneration of *Drosophila* photoreceptor neurons. *Neuron* **21**, 633–642 (1998).
228. Steffan, J. S. *et al.* Histone deacetylase inhibitors arrest polyglutamine-dependent neurodegeneration in *Drosophila*. *Nature* **413**, 739–743 (2001).
229. Kaltenbach, L. S. *et al.* Huntingtin interacting proteins are genetic modifiers of neurodegeneration. *PLoS Genet.* **3**, 689–708 (2007).
230. Schulte, J., Sepp, K. J., Wu, C., Hong, P. & Littleton, J. T. High-content chemical and rna screens for suppressors of neurotoxicity in a huntington's disease model. *PLoS One* **6**, (2011).
231. Park, J. *et al.* RAS-MAPK-MSK1 pathway modulates ataxin 1 protein levels and toxicity in SCA1. *Nature* **498**, 325–31 (2013).
232. Parker, J. A. *et al.* Expanded polyglutamines in *Caenorhabditis elegans* cause axonal abnormalities and severe dysfunction of PLM mechanosensory neurons without cell death. *Proc. Natl. Acad. Sci. U. S. A.* **98**, 13318–23 (2001).
233. Morley, J. F., Brignull, H. R., Weyers, J. J. & Morimoto, R. I. The threshold for polyglutamine-expansion protein aggregation and cellular toxicity is dynamic and influenced by aging in *Caenorhabditis elegans*. *Proc. Natl. Acad. Sci. U. S. A.* **99**, 10417–22 (2002).
234. Sampaio, C., Borowsky, B. & Reilmann, R. Clinical Trials in Huntington ' s Disease : Interventions in Early Clinical Development and Newer Methodological Approaches Therapeutic Interventions in Clinical Development. *Mov. Disord.* **29**, 1419–1428 (2014).
235. Gura, T. Hope in Alzheimer's fight emerges from unexpected places. *Nat. Med.* **14**, 894 (2008).
236. Zhang, X. *et al.* A potent small molecule inhibits polyglutamine aggregation in Huntington's disease neurons and suppresses neurodegeneration in vivo. *Proc. Natl. Acad. Sci. U. S. A.* **102**, 892–897 (2005).

237. Chopra, V. *et al.* A small-molecule therapeutic lead for Huntington's disease: preclinical pharmacology and efficacy of C2-8 in the R6/2 transgenic mouse. *Proc. Natl. Acad. Sci. U. S. A.* **104**, 16685–9 (2007).
238. Wang, N., Lu, X.-H., Sandoval, S. V & Yang, X. W. An Independent Study of the Preclinical Efficacy of C2-8 in the R6/2 Transgenic Mouse Model of Huntington's Disease. *J. Huntingtons. Dis.* **2**, 443–451 (2013).
239. Hockly, E. *et al.* Evaluation of the benzothiazole aggregation inhibitors riluzole and PGL-135 as therapeutics for Huntington's disease. *Neurobiol. Dis.* **21**, 228–236 (2006).
240. Feng, B. Y. *et al.* Small-molecule aggregates inhibit amyloid polymerization. *Nat. Chem. Biol.* **4**, 197–9 (2008).
241. Ehrnhoefer, D. E. *et al.* Green tea (-)-epigallocatechin-gallate modulates early events in huntingtin misfolding and reduces toxicity in Huntington's disease models. *Hum. Mol. Genet.* **15**, 2743–2751 (2006).
242. Dev, K. K. *et al.* Brain sphingosine-1-phosphate receptors: Implication for FTY720 in the treatment of multiple sclerosis. *Pharmacol. Ther.* **117**, 77–93 (2008).
243. Brinkmann, V. *et al.* The immune modulator FTY720 targets sphingosine 1-phosphate receptors. *J. Biol. Chem.* **277**, 21453–21457 (2002).
244. Ali, R., Nicholas, R. S. J. & Muraro, P. A. Drugs in development for relapsing multiple sclerosis. *Drugs* **73**, 625–650 (2013).
245. Meno-Tetang, G. M. L. *et al.* Physiologically Based Pharmacokinetic Modeling of FTY720 in Rats After Oral and Intravenous Doses. *Drug Metab. Dispos.* **34**, 1480–1487 (2006).
246. Di Menna, L. *et al.* Fingolimod protects cultured cortical neurons against excitotoxic death. *Pharmacol. Res.* **67**, 1–9 (2013).
247. Di Pardo, A. *et al.* FTY720 (fingolimod) is a neuroprotective and disease-modifying agent in cellular and mouse models of huntington disease. *Hum. Mol. Genet.* **23**, 2251–2265 (2014).
248. Xiao, G., Fan, Q., Wang, X. & Zhou, B. Huntington disease arises from a combinatory toxicity of polyglutamine and copper binding. *Proc Natl Acad Sci U S A* **110**, 14995–15000 (2013).
249. Mason, R. P. *et al.* Glutathione peroxidase activity is neuroprotective in models of Huntington's disease. *Nat. Genet.* **45**, 1249–54 (2013).
250. Rosas, H. D. *et al.* Alterations in brain transition metals in Huntington disease: an evolving and intricate story. *Arch. Neurol.* **69**, 887–93 (2012).

251. Zainelli, G. M., Ross, C. A., Troncoso, J. C. & Muma, N. A. Transglutaminase cross-links in intranuclear inclusions in Huntington disease. *J. Neuropathol. Exp. Neurol.* **62**, 14–24 (2003).
252. Karpuj, M. V *et al.* Transglutaminase aggregates huntingtin into nonamyloidogenic polymers, and its enzymatic activity increases in Huntington's disease brain nuclei. *Proc. Natl. Acad. Sci. U. S. A.* **96**, 7388–7393 (1999).
253. Prundean, A., Youssov, K., Humbert, S., Bonneau, D. & Verny, C. A phase II, open-label evaluation of cysteamine tolerability in patients with Huntington's disease. *Mov. Disord.* **30**, 288–289 (2015).
254. Karpuj, M. V *et al.* Prolonged survival and decreased abnormal movements in transgenic model of Huntington disease, with administration of the transglutaminase inhibitor cystamine. *Nat. Med.* **8**, 143–149 (2002).
255. Dedeoglu, A. *et al.* Therapeutic Effects of Cystamine in a Murine Model of Huntington's Disease. *J. Neurosci.* **22**, 8942–8950 (2002).
256. Wang, X. *et al.* Cerebral PET imaging and histological evidence of transglutaminase inhibitor cystamine induced neuroprotection in transgenic R6/2 mouse model of Huntington's disease. *J. Neurol. Sci.* **231**, 57–66 (2005).
257. Raamsdonk, J. M. Van, Murphy, Z., Slow, E. J., Leavitt, B. R. & Hayden, M. R. Selective degeneration and nuclear localization of mutant huntingtin in the YAC128 mouse model of Huntington disease. **14**, 3823–3835 (2005).
258. Seeger, T. F. *et al.* Immunohistochemical localization of PDE10A in the rat brain. *Brain Res.* **985**, 113–126 (2003).
259. Hebb, A. L. O., Robertson, H. A. & Denovan-Wright, E. M. Striatal phosphodiesterase mRNA and protein levels are reduced in Huntington's disease transgenic mice prior to the onset of motor symptoms. *Neuroscience* **123**, 967–981 (2004).
260. Katona, I. & Freund, T. F. Endocannabinoid signaling as a synaptic circuit breaker in neurological disease. *Nat. Med.* **14**, 923–30 (2008).
261. Giamp??, C. *et al.* Inhibition of the striatal specific phosphodiesterase PDE10A ameliorates striatal and cortical pathology in R6/2 mouse model of Huntington's disease. *PLoS One* **5**, (2010).
262. Gonzalez, V. *et al.* Deep brain stimulation for Huntington's disease: long-term results of a prospective open-label study. *J Neurosurg* **121**, 114–122 (2014).
263. López-Sendón Moreno, J. L., García-Caldentey, J., Regidor, I., Álamo, M. Del & García de Yébenes, J. A 5-year follow-up of deep brain stimulation in Huntington's disease. *Parkinsonism Relat. Disord.* **20**, 260–261 (2014).

264. Walter, G. M. *et al.* High-throughput screen of natural product extracts in a yeast model of polyglutamine proteotoxicity. *Chem. Biol. Drug Des.* **83**, 440–449 (2014).
265. Heiser, V. *et al.* Identification of benzothiazoles as potential polyglutamine aggregation inhibitors of Huntington's disease by using an automated filter retardation assay. *Proc. Natl. Acad. Sci. U. S. A.* **99 Suppl 4**, 16400–6 (2002).
266. Huang, J. *et al.* Finding new components of the target of rapamycin (TOR) signaling network through chemical genetics and proteome chips. *Proc. Natl. Acad. Sci. U. S. A.* **101**, 16594–9 (2004).
267. Sarkar, S. *et al.* Small molecules enhance autophagy and reduce toxicity in Huntington's disease models. *Nat. Chem. Biol.* **3**, 331–338 (2007).
268. Schipper-Krom, S. *et al.* Dynamic recruitment of active proteasomes into polyglutamine initiated inclusion bodies. *FEBS Lett.* **588**, 151–159 (2014).
269. Juenemann, K. *et al.* Expanded polyglutamine-containing N-terminal huntingtin fragments are entirely degraded by mammalian proteasomes. *J. Biol. Chem.* **288**, 27068–27084 (2013).
270. Harper, S. Q. *et al.* RNA interference improves motor and neuropathological abnormalities in a Huntington's disease mouse model. *Proc. Natl. Acad. Sci. U. S. A.* **102**, 5820–5825 (2005).
271. Rodriguez-Lebron, E., Denovan-Wright, E. M., Nash, K., Lewin, A. S. & Mandel, R. J. Intrastriatal rAAV-mediated delivery of anti-huntingtin shRNAs induces partial reversal of disease progression in R6/1 Huntington's disease transgenic mice. *Mol. Ther.* **12**, 618–633 (2005).
272. Wang, Y., Liu, W., Wada, E. & Murata, M. Clinico-pathological rescue of a model mouse of Huntington's disease by siRNA. **53**, 241–249 (2005).
273. Machida, Y. *et al.* rAAV-mediated shRNA ameliorated neuropathology in Huntington disease model mouse. *Biochem. Biophys. Res. Commun.* **343**, 190–197 (2006).
274. Skotte, N. H. *et al.* Allele-Specific Suppression of Mutant Huntingtin Using Antisense Oligonucleotides: Providing a Therapeutic Option for All Huntington Disease Patients. *PLoS One* **9**, e107434 (2014).
275. Zhang, S., Feany, M. B., Saraswati, S., Littleton, J. T. & Perrimon, N. Inactivation of *Drosophila* Huntingtin affects long-term adult functioning and the pathogenesis of a Huntington's disease model. *Dis. Model. Mech.* **2**, 247–266 (2009).
276. Drouet, V. *et al.* Sustained effects of nonallele-specific huntingtin silencing. *Ann. Neurol.* **65**, 276–285 (2009).

277. Urnov, F. D., Rebar, E. J., Holmes, M. C., Zhang, H. S. & Gregory, P. D. Genome editing with engineered zinc finger nucleases. *Nat. Publ. Gr.* **11**, 636–646 (2010).
278. Bibikova, M. *et al.* Stimulation of homologous recombination through targeted cleavage by chimeric nucleases. *Mol. Cell. Biol.* **21**, 289–297 (2001).
279. Kim, Y. G., Cha, J. & Chandrasegaran, S. Hybrid restriction enzymes: zinc finger fusions to Fok I cleavage domain. *Proc. Natl. Acad. Sci. U. S. A.* **93**, 1156–1160 (1996).
280. Garriga-canut, M., Agustín-pavón, C., Herrmann, F., Sánchez, A. & Dierssen, M. Synthetic zinc finger repressors reduce mutant huntingtin expression in the brain of R6 / 2 mice. **109**, (2012).
281. An, M. C. *et al.* Polyglutamine Disease Modeling: Epitope Based Screen for Homologous Recombination using CRISPR/Cas9 System. *PLoS Curr.* **6**, 1–19 (2014).
282. Arribat, Y. *et al.* A Huntingtin Peptide Inhibits PolyQ-Huntingtin Associated Defects. *PLoS One* **8**, 1–14 (2013).
283. Nagai, Y. *et al.* Inhibition of polyglutamine protein aggregation and cell death by novel peptides identified by phage display screening. *J. Biol. Chem.* **275**, 10437–10442 (2000).
284. Popiel, H. A., Nagai, Y., Fujikake, N. & Toda, T. Protein transduction domain-mediated delivery of QBP1 suppresses polyglutamine-induced neurodegeneration in vivo. *Mol. Ther.* **15**, 303–309 (2007).
285. Kazantsev, A. *et al.* A bivalent Huntingtin binding peptide suppresses polyglutamine aggregation and pathogenesis in *Drosophila*. *Nat. Genet.* **30**, 367–376 (2002).
286. Alberti, S., Halfmann, R., King, O., Kapila, A. & Lindquist, S. A Systematic Survey Identifies Prions and Illuminates Sequence Features of Prionogenic Proteins. *Cell* **137**, 146–158 (2009).
287. Kayatekin, C. *et al.* Prion-like proteins sequester and suppress the toxicity of huntingtin exon 1. *Proc. Natl. Acad. Sci. U. S. A.* 1–6 (2014). doi:10.1073/pnas.1412504111
288. Mielcarek, M. *et al.* HDAC4 does not act as a protein deacetylase in the postnatal murine brain in vivo. *PLoS One* **8**, 1–10 (2013).
289. Mielcarek, M. *et al.* HDAC4 Reduction: A Novel Therapeutic Strategy to Target Cytoplasmic Huntingtin and Ameliorate Neurodegeneration. *PLoS Biol.* **11**, (2013).
290. Ripaud, L. *et al.* Overexpression of Q-rich prion-like proteins suppresses polyQ cytotoxicity and alters the polyQ interactome. 1–6 (2014). doi:10.1073/pnas.1421313111
291. Lanning, J. D., Hawk, A. J., Derryberry, J. & Meredith, S. C. Chaperone-like N-methyl peptide inhibitors of polyglutamine aggregation. *Biochemistry* **49**, 7108–7118 (2010).

292. Thakur, A. K., Yang, W. & Wetzel, R. Inhibition of polyglutamine aggregate cytotoxicity by a structure-based elongation inhibitor. *FASEB J.* **18**, 923–925 (2004).
293. O’Nuallain, B. *et al.* Kinetics and Thermodynamics of Amyloid Assembly Using a High-Performance Liquid Chromatography-Based Sedimentation Assay. *Methods Enzymol.* **413**, 34–74 (2006).
294. Carter, R. J. *et al.* Characterization of progressive motor deficits in mice transgenic for the human Huntington’s disease mutation. *J. Neurosci.* **19**, 3248–3257 (1999).
295. Ratovitski, T. *et al.* Mutant huntingtin N-terminal fragments of specific size mediate aggregation and toxicity in neuronal cells. *J. Biol. Chem.* **284**, 10855–10867 (2009).
296. Matsuyama, Z. *et al.* Molecular features of the CAG repeats of spinocerebellar ataxia 6 (SCA6). *Hum. Mol. Genet.* **6**, 1283–1287 (1997).
297. McNeil, S. M. *et al.* Reduced penetrance of the Huntington’s disease mutation. *Hum. Mol. Genet.* **6**, 775–779 (1997).
298. Rubinsztein, D. C. *et al.* Phenotypic characterization of individuals with 30-40 CAG repeats in the Huntington disease (HD) gene reveals HD cases with 36 repeats and apparently normal elderly individuals with 36-39 repeats. *Am. J. Hum. Genet.* **59**, 16–22 (1996).
299. Kier, B. L., Shu, I., Eidenschink, L. a & Andersen, N. H. Stabilizing capping motif for beta-hairpins and sheets. *Proc. Natl. Acad. Sci. U. S. A.* **107**, 10466–10471 (2010).
300. Soc, S. H. J. A. C., Stanger, H. E. & Gellman, S. H. Rules for Antiparallel B-sheet Design: D-Pro-Gly is Superior to L-Asn-Gly for B-Hairpin Nucleation. **120**, 4236–4237 (1998).
301. Poirier, M. a., Jiang, H. & Ross, C. a. A structure-based analysis of huntingtin mutant polyglutamine aggregation and toxicity: Evidence for a compact beta-sheet structure. *Hum. Mol. Genet.* **14**, 765–774 (2005).
302. Santiveri, C. M., León, E., Rico, M. & Jiménez, M. A. Context-dependence of the contribution of disulfide bonds to beta-hairpin stability. *Chem. A Eur. J.* **14**, 488–499 (2008).
303. Pace, C. N. & Scholtz, J. M. A helix propensity scale based on experimental studies of peptides and proteins. *Biophys. J.* **75**, 422–427 (1998).
304. Fujiwara, K., Toda, H. & Ikeguchi, M. Dependence of alpha-helical and beta-sheet amino acid propensities on the overall protein fold type. *BMC Struct. Biol.* **12**, 18 (2012).
305. Ferdinando Fiumara, Luana Fioriti, Eric R. Kandel, W. a. H. Essential role of coiled-coils for aggregation and activity of Q/N- rich prions and polyQ proteins. **143**, 1121–1135 (2012).

306. Ren, P.-H. *et al.* Cytoplasmic penetration and persistent infection of mammalian cells by polyglutamine aggregates. *Nat. Cell Biol.* **11**, 219–225 (2009).
307. Dickey, A. S. *et al.* PPAR- δ is repressed in Huntington's disease, is required for normal neuronal function and can be targeted therapeutically. *Nat. Med.* 1–11 (2015). doi:10.1038/nm.4003
308. Sahl, S. J., Weiss, L. E., Duim, W. C., Frydman, J. & Moerner, W. E. Cellular inclusion bodies of mutant huntingtin exon 1 obscure small fibrillar aggregate species. *Sci. Rep.* **2**, 895 (2012).
309. Richardson, J. S. & Richardson, D. C. Natural beta-sheet proteins use negative design to avoid edge-to-edge aggregation. *Proc. Natl. Acad. Sci. U. S. A.* **99**, 2754–2759 (2002).
310. Minor, D. L. & Kim, P. S. Measurement of the beta-sheet-forming propensities of amino acids. *Nature* **367**, 660–663 (1994).
311. Wouters, M. A. & Curmi, P. M. G. An analysis of side chain interactions and pair correlations within antiparallel β -sheets: The differences between backbone hydrogen-bonded and non-hydrogen-bonded residue pairs. *Proteins Struct. Funct. Genet.* **22**, 119–131 (1995).
312. Hoop, C. L. *et al.* Polyglutamine Amyloid Core Boundaries and Flanking Domain Dynamics in Huntingtin Fragment Fibrils Determined by Solid-State Nuclear Magnetic Resonance. *Biochemistry* **53**, 6653–6666 (2014).
313. Sipione, S. *et al.* Early transcriptional profiles in huntingtin-inducible striatal cells by microarray analyses. *Hum. Mol. Genet.* **11**, 1953–65 (2002).
314. Luthi-Carter, R. *et al.* SIRT2 inhibition achieves neuroprotection by decreasing sterol biosynthesis. *Proc. Natl. Acad. Sci. U. S. A.* **107**, 7927–7932 (2010).
315. Bobrowska, A., Donmez, G., Weiss, A., Guarente, L. & Bates, G. SIRT2 ablation has no effect on tubulin acetylation in brain, cholesterol biosynthesis or the progression of Huntington's disease phenotypes in vivo. *PLoS One* **7**, e34805 (2012).
316. Southwell, A. L. *et al.* Perturbation with intrabodies reveals that calpain cleavage is required for degradation of huntingtin exon 1. *PLoS One* **6**, (2011).
317. Menzies, F. M. *et al.* Calpain inhibition mediates autophagy-dependent protection against polyglutamine toxicity. *Cell Death Differ.* **22**, 433–444 (2014).
318. Havel, L. S. *et al.* Preferential accumulation of N-terminal mutant huntingtin in the nuclei of striatal neurons is regulated by phosphorylation. *Hum. Mol. Genet.* **20**, 1424–1437 (2011).

319. Greene, L. A., Tischlert, A. S. & Kuffler, S. W. Establishment of a noradrenergic clonal line of rat adrenal pheochromocytoma cells which respond to nerve growth factor (sympathetic neurons/cell culture/catecholamines/differentiation/neurites). *Cell Biol.* **73**, 2424–2428 (1976).
320. Martín-Flores, N. *et al.* RTP801 Is Involved in Mutant Huntingtin-Induced Cell Death. *Mol. Neurobiol.* (2015). doi:10.1007/s12035-015-9166-6
321. Li, S. H., Cheng, a L., Li, H. & Li, X. J. Cellular defects and altered gene expression in PC12 cells stably expressing mutant huntingtin. *J. Neurosci.* **19**, 5159–5172 (1999).
322. Apostol, B. L. *et al.* A cell-based assay for aggregation inhibitors as therapeutics of polyglutamine-repeat disease and validation in *Drosophila*. *Proc. Natl. Acad. Sci. U. S. A.* **100**, 5950–5955 (2003).
323. Varma, H. *et al.* Selective inhibitors of death in mutant huntingtin cells. *Nat Chem Biol* **3**, 99–100 (2007).
324. Bufalino, M. R. & van der Kooy, D. The aggregation and inheritance of damaged proteins determines cell fate during mitosis. *Cell Cycle* **13**, 1201–7 (2014).
325. Jacob, T. C., Moss, S. J. & Jurd, R. GABA(A) receptor trafficking and its role in the dynamic modulation of neuronal inhibition. *Nat. Rev. Neurosci.* **9**, 331–343 (2008).
326. Jacob, T. C. *et al.* Gephyrin regulates the cell surface dynamics of synaptic GABAA receptors. *J. Neurosci.* **25**, 10469–10478 (2005).
327. McColgan, P. *et al.* Selective vulnerability of Rich Club brain regions is an organizational principle of structural connectivity loss in Huntington’s disease. *Brain* **138**, 3327–3344 (2015).
328. Flinn, L., Breaud, S., Lo, C., Ingham, P. W. & Bandmann, O. Zebrafish as a new animal model for movement disorders. *J. Neurochem.* **106**, 1991–1997 (2008).
329. Yang, S.-H. *et al.* Towards a transgenic model of Huntington’s disease in a non-human primate. *Nature* **453**, 921–4 (2008).
330. Wang, C. E. *et al.* Accumulation of N-terminal mutant huntingtin in mouse and monkey models implicated as a pathogenic mechanism in Huntington’s disease. *Hum. Mol. Genet.* **17**, 2738–2751 (2008).
331. Robinow, S. & White, K. The locus elav of *Drosophila melanogaster* is expressed in neurons at all developmental stages. *Dev. Biol.* **126**, 294–303 (1988).
332. Yao, K. M. & White, K. Neural specificity of elav expression: defining a *Drosophila* promoter for directing expression to the nervous system. *J. Neurochem.* **63**, 41–51 (1994).

333. Luo, L., Joyce Liao, Y., Jan, L. Y. & Jan, Y. N. Distinct morphogenetic functions of similar small GTPases: Drosophila Drac1 is involved in axonal outgrowth and myoblast fusion. *Genes Dev.* **8**, 1787–1802 (1994).
334. Berger, C., Renner, S., Lüer, K. & Technau, G. M. The commonly used marker ELAV is transiently expressed in neuroblasts and glial cells in the Drosophila embryonic CNS. *Dev. Dyn.* **236**, 3562–3568 (2007).
335. Bischof, J., Maeda, R. K., Hediger, M., Karch, F. & Basler, K. An optimized transgenesis system for Drosophila using germ-line-specific phiC31 integrases. *Proc. Natl. Acad. Sci. U. S. A.* **104**, 3312–7 (2007).
336. Squitieri, F. *et al.* Homozygosity for CAG mutation in Huntington disease is associated with a more severe clinical course. *Brain* **126**, 946–955 (2003).
337. Stebbins, M. J. *et al.* Tetracycline-inducible systems for Drosophila. *Proc. Natl. Acad. Sci. U. S. A.* **98**, 10775–10780 (2001).
338. Peters-Libeu, C. *et al.* Disease-associated polyglutamine stretches in monomeric huntingtin adopt a compact structure. *J. Mol. Biol.* **421**, 587–600 (2012).
339. Rydberg, H. a, Matson, M., Åmand, H. L., Esbjö, E. K. & Norde, B. Effects of Tryptophan Content and Backbone Spacing on the Uptake Efficiency of Cell-Penetrating Peptides. (2012).
340. Lalatsa, A., Schatzlein, A. G. & Uchegbu, I. F. Strategies to deliver peptide drugs to the brain. *Mol. Pharm.* **11**, 1081–1093 (2014).
341. Dufour, B. D., Smith, C. A., Clark, R. L., Walker, T. R. & McBride, J. L. Intrajugular vein delivery of AAV9-RNAi prevents neuropathological changes and weight loss in Huntington's disease mice. *Mol Ther* **22**, 797–810 (2014).